Univerzita Karlova v Praze
Přírodovědecká fakulta

Studijní program: Geologie

Studijní obor: Geologie

Bc. Ondřej Krátký

Distribution of trace elements in carbonatites using in-situ techniques, with focus on REE

Distribuce stopových prvků v karbonatitech pomocí in-situ metod, se zvláštním zřetelem k REE

Diplomová práce

Vedoucí práce: Dr.sc.nat. Tomáš Magna

Praha 2017

Prohlašuji, že jsem závěrečnou práci zpracoval samostatně a že jsem uvedl všechny použité informační zdroje a literaturu. Tato práce ani její podstatná část nebyla předložena k získání jiného nebo stejného akademického titulu.

V Praze, 13. 5. 2017

Ondřej Krátký

Acknowledgments

I would like to thank to my supervisor Tomáš Magna for his guidance, help and patience and for the many hours we spent discussing carbonatites and various other topics. Then I must thank to Vladislav Rapprich for his help and ideas on the field of petrography and mineralogy. Also, to Jitka Míková for her help with LA-ICPMS analyses and the Glitter software, which both were completely new to me, to Lukáš Ackerman for his ideas about geochemistry, to Martin Racek about his excellent guidance at EPMA machine and his ideas, to Vojtěch Janoušek for his consultation about distribution coefficients and to Michaela Vašinová Gallinová for making the pellet used as in-house standard. Last but not the least, I must thank to my parents and to my girlfriend for supporting me in geology and believing in me. This work was funded from GAČR 15-08583S.

Abstrakt

Karbonatity představují unikátní a záhadné horniny nejasného původu se specifickou mineralogií a geochemickými vlastnostmi. Převážně jsou tvořeny kalcitem magmatického původu a dalšími karbonátovými minerály (Le Bas, 1987) a zároveň mají nízký obsah SiO_2 (Le Maitre, 2002). Původ těchto zvláštních magmat stále nebyl vyjasněn, přesto však představují důležité "okno" do procesů, jenž se odehrávají v zemském plášti. Karbonatity jsou považovány buď za zbytkové taveniny z frakcionovaného nephelinitu nebo melilitu (Gittins 1989; Gittins and Jago 1998), za nemísivou frakci CO_2-saturované silikátové taveniny (Freestone a Hamilton 1980; Amundsen 1987; Kjarsgaard a Hamilton 1988, 1989; Brooker a Hamilton 1990; Kjarsgaard a Peterson 1991; Church a Jones 1995; Lee a Wyllie 1997; Dawson 1998; Halama a kol. 2005; Brooker a Kjarsgaard 2011), nebo za primární taveniny, které byly generovány z CO_2-bohatého peridotitu skrze proces částečného tavení (Wallace and Green 1988; Sweeney 1994; Harmer and Gittins 1998; Harmer et al. 1998; Ying et al. 2004).

Množství prvků vzácných zemin (REE) je v karbonatitech vždy vysoké, jelikož karbonatitová tavenina dokáže rozpouštět tyto prvky snadněji, než tavenina silikátová (Nelson a kol. 1988). Karbonatitová tavenina také dokáže ve velké míře rozpouštět Sr, Ba, P a hlavně Zr aNb, které (společně s REE) dokáží z některých karbonatitů učinit ekonomické zdroje těchto prvků.

V této práci jsou dvě karbonatitová tělesa, společně s asociovanými alkalickými a silikátovými horninami, – Samalpatti a Sevattur z Tamil Nadu v Indii, studována za účelem získání lepší představy o distribuci stopových prvků v karbonatitech. K tomu to účelu byl použit hmotový spektrometr s indukčně vázaným plazmatem vybavený laserovou ablací (LA-ICPMS) a elektronový mikroanalyzátor (EPMA). Elektronový mikroanalyzátor byl použit k identifikaci a studiu vztahů mezi jednotlivými minerálními fázemi ve výbrusech a k určení chemismu hlavních prvků. LA-ICPMS pak byl použit pro přesné určení stopových prvků ve vybraných minerálních fázích, hlavně v apatitu, kalcitu, dolomitu, v menší míře pak v titanitu a v minoritních fázích, jako jsou kosmochlor a Mckelveyite-(Nd). Z práce Ackermana a kol. (2017) byla použita data z analýz horninové chemie, aby bylo možné porovnat chemii jednotlivých minerálních fází s celkovou chemií hornin. Z tohoto článku také byla použita modální zastoupení jednotlivých minerální fází ve výbrusech, díky nimž bylo následně možné vypočítat distribuční koeficienty pro REE v apatitu, kalcitu a dolomit koexistující s karbonatitovou horninou. Distribuční koeficienty pro dolomit v karbonatitu uvedené v této práci jsou vůbec první takovéto hodnoty z karbonatitového systému svého druhu.

Abstract

Carbonatites are unique and enigmatic magmatic rocks of unclear origin, with very specific mineralogy and geochemical properties. They are predominantly composed of magmatic calcite or other carbonate minerals (Le Bas 1987) and have low content of SiO_2 (Le Maitre 2002). Origin of these peculiar magmas is still not clear but they appear to represent an important "window" into processes in Earth's mantle. They are considered either as residual melts from a fractionated carbonated nephelinite or melilitite (Gittins 1989; Gittins and Jago 1998), as immiscible fractions of CO_2-saturated silicate melts (Freestone and Hamilton 1980; Amundsen 1987; Kjarsgaard and Hamilton 1988, 1989; Brooker and Hamilton 1990; Kjarsgaard and Peterson 1991; Church and Jones 1995; Lee and Wyllie 1997; Dawson 1998; Halama et al. 2005; Brooker and Kjarsgaard 2011), or as primary melts which are were generated from CO_2-bearing peridotite through partial melting (Wallace and Green 1988; Sweeney 1994; Harmer and Gittins 1998; Harmer et al. 1998; Ying et al. 2004).

Abundances of rare earth elements (REE) are often high in carbonatites because carbonatitic magmas can dissolve these elements much easily than silicate magmas (Nelson et al. 1988). Carbonatitic magma can also dissolve large quantities of Sr, Ba, P and mainly Zr and Nb, which (together with high solubility of REE) makes some carbonatite bodies an economic source of these elements.

In this study, two carbonatite bodies with associated alkali and silicate rocks – Samalpatti and Sevattur from Tamil Nadu, India, were investigated to gain new knowledge about the distribution of trace elements in carbonatites. These tasks were achieved using the Laser Ablation Inductive Coupled Plasma Mass Spectrometry (LA-ICPMS) and Electron-Probe Micro Analyzer (EPMA). EPMA was used for mineral identification and studying the relationships between the mineral phases in thin section, combined with the determination of major element compositions. LA-ICPMS was used for accurate determination of trace element abundances in selected mineral phases, mainly apatite, calcite and dolomite, into some extent in titanite and minor phases such as kosmochlor and Mckelveyite-(Nd). From the study of Ackerman et al. (2017), whole rock chemical analyses were used in order to link and compare the chemistry of main mineral phases with the whole rock chemistry. Further, modal proportions of minerals were used for calculation of the distribution coefficients off REE for apatite, calcite and dolomite coexisting with a carbonatite host rock. Distribution coefficients for dolomite in carbonatitic host rock presented here are the first such values reported from this system.

České shrnutí

Ve své magisterské práci „Distribuce stopových prvků v karbonatitech pomocí in-situ metod se zvláštním zřetelem k REE" jsem se soustředil na detailní mineralogii a geochemii dvou vybraných karbonatitových těles, Samalpatti a Sevattur, která se nacházejí v oblasti Tamil Nadu v jižní Indii. K jejich studiu prostřednictvím horninových výbrusů bylo použito jednak optické mikroskopie pro petrografii a mineralogii, dále pak elektronové mikroanalýzy (electron probe micro analysis, EPMA) a hmotového spektrometru s indukčně vázaným plazmatem, vybaveného laserovou ablací (LA-ICPMS). Díky EPMA bylo možné změřit zastoupení hlavních prvků v minerálních fázích, nacházejících se v jednotlivých výbrusech, studovat jejich vzájemné vztahy a vyhledávat minerály nesoucí prvky vzácných zemin (REE). Metoda LA-ICPMS pak následně byla použita k přesnému určení koncentrace stopových prvků ve vybraných minerálech. Studované minerály byly převážně apatity, kalcity a dolomity, v menší míře pak titanity, a další minoritní fáze. Cílem práce bylo přispět k pochopení geneze samotných dvou studovaných komplexů a distribuce stopových prvků v hlavních minerálech karbonatitů a spjatých alkalických silikátových hornin (apatit, kalcit dolomit). Celá tato práce byla financována z projektu GAČR 15-08583S řešitele Dr.sc.nat. Tomáše Magny.

Jedním z klíčových výsledků jsou nově spočítané distribuční koeficienty pro prvky vzácných zemin mezi horninou a apatitem, kalcitem a dolomitem, přičemž distribuční koeficienty pro dolomity z karbonatitů jsou první svého druhu.

Tato práce je rozdělená do sedmi částí. První dvě, Úvod a Geologie karbonatitových komplexů Samalpatti a Sevattur, Tamil Nadu, Jižní Indie, mají formu rešerše a představují shrnutí známých poznatků o studovaném tématu. V první části jsou popsány obecné vlastnosti karbonatitů, jejich mineralogie, geochemie a teorie vzniku. Dále jsou popsány prvky vzácných zemin (Rare Earth Elements – REE) a krystalové struktury apatitu a kalcitu, které představují hlavní minerální fáze nacházející se v karbonatitech. Jako posední jsou v úvodu diskutovány možnosti REE jako klíčového geochemického parametru, a také jsou zde diskutovány známé distribuční koeficienty pro REE v minerálních fázích z karbonatitů. V druhé části pak jsou popsány známé poznatky o dvou studovaných komplexech. Ty zahrnují jejich pozici v rámci celkové geologie Indie a publikovaná stáří komplexů – pro Samalpatti 700 ± 30Ma (K–Ar, Moralev et al. 1975) a pro Sevattur –771 ± 18 Ma (Rb–Sr, Kumar and Gopalan, 1991) a 801 ± 11 Ma (Pb–Pb, Schleicher et al., 1997).

Třetí část se zabývá metodologií vlastního výzkumu. Zde je popsána metodika optické mikroskopie, dále pak měření pomocí elektronového mikroanalyzátoru (umístěn na Ústavu petrologie a strukturní geologie Univerzity Karlovy) a hmotového spektrometru s indukčně vázaným plazmatem vybaveným laserovu ablací (v majetku České Geologické Služby). Jelikož v práci jsou použita i geochemická horninová data (hlavní i stopové prvky) publikovaná Ackermanem a kol. (2017), je zde krátce popsána i metodika získání těchto dat.

V části Výsledky jsou uvedeny všechny získané poznatky, dále tato sekce obsahuje množství fotografií jak z optického mikroskopu, tak z EPMA, a také množství tabulek s novými chemickými analýzami. Tato část diplomové práce je rozdělena na tři hlavní sekce, které se pak ještě následně dělí do několika podsekcí. První sekce je nazvána Petrografie a Mineralogie a je rozdělena na dvě podsekce – Samalpatti a Sevattur. Zde jsou prezentovány hlavně výsledky optické mikroskopie, text je doplněn mnoha fotografiemi pro ilustraci toho, jak vypadají studované horniny ve výbrusech. Ze Samalpatti jsou zde popsány karbonatity, silikokarbonatity a pyroxenity. Kromě hlavních horninotvorných minerálů ve studovaných horninách (kalcit, winchit, diopsid, apatit, titanit, albit) je zde také popsán neobvyklý minerál pro silikokarbonatity – chromem bohatý pyroxen kosmochlor ($NaCrSi_2O_6$). Z komplexu Sevattur pak jsou popsány karbonatity a pyroxenity (silikokarbonatity se zde nenacházejí) a zde je popsán neobvyklý minerál Mckelveyite-(Nd) - karbonát bohatý stronciem a REE – [$(Ba,Sr)(Nd,Ce,La)(CO_3)_2 \times 4–10\ H_2O$]. Další sekce se nazývá Horninová geochemie. Zde jsou prezentována geochemická data (pro hlavní i stopové prvky) z obou studovaných komplexů publikovaná Ackermanem a kol. (2017). Tato data publikována ve výše zmíněném článku, na němž se autor této diplomové práce aktivně podílel formou mineralogie a je jedním ze spoluautorů publikace. Poslední sekce v části výsledky se zabývá chemií studovaných minerálních fází, získanou pomocí LA-ICPMS a EPMA. Zde jsou prezentována geochemická data získaná vlastním výzkumem rozdělená do tří podsekcí – Apatity, Kalcity a Dolomity, a Ostatní minerální fáze. V každé sekci se nacházejí data pro hlavní prvky získaná pomocí EPMA a data pro stopové prvky získaná pomocí LA-ICPMS. Ostatní minerální fáze jsou reprezentovány titanitem, amfibolem, kosmochlorem, pyrochlorem a Mckelveyitem-(Nd).

Další část nese název Interpretace a Diskuze, ve které jsou získaná data prezentována formou grafů a normalizovaných hodnot na různé rezervoáry (chondritický a primitivní plášť), interpretována a diskutována v souladu se známým stupněm poznání. Jsou zde dvě sekce, ‘Chování stopových prvků v karbonatitových systémech‘ a ‘Distribuční koeficienty‘. První sekce je dále rozdělena na tři podsekce – HFSE prvky, Systematika poměru Y/Ho a Hydrotermální alterace – byla nějaká? V první podsekci HFSE prvky jsou diskutovány tyto prvky v jednotlivých minerálech v součinnosti s výsledky horninových analýz. Zejména silikokarbonatity se vyznačují velmi netypickými poměry HFSE prvků (Nb/Ta, Zr/Hf, Zr/Nb a Zr/Ta). Ve podsekci Systematika Y/Ho poměru je pak detailně popsán poměr Y/Ho v apatitech, kalcitech a dolomitech, jenž slouží jako jeden z ukazatelů možného postižení hydrotermální alterací a/nebo zvětrávání. Poslední podsekce se věnuje možné hydrotermální alteraci a jejím případném významu pro geochemii a genezi obou komplexů Druhou sekcí jsou ‚Distribuční koeficienty‘, kde se nacházejí vypočtené hodnoty na základě nových horninových analýz, analýz jednotlivých minerálů a také pomocí modálních zastoupení daných minerálních fází ve výbrusech. Získané koeficienty jsou porovnávány s publikovanými hodnotami od různých autorů. Předposlední část

je Závěr, kde jsou shrnuta všechna měření a zjištění, učiněná v předchozích částech, a poslední část představuje seznam literatury, kde jsou uvedeny všechny informační zdroje v požadovaném formátu.

Table of Contents

List of Figures

List of tables

1. INTRODUCTION

1.1 Carbonatites

Carbonatites belong to the most peculiar rocks on Earth even though they represent only a subordinate fraction of Earth's magmatic inventory. They are defined as igneous rocks with at least 50% modal primary carbonate minerals (LeBas 1987) and with less than 20% SiO_2 (Le Maitre 2002). They occur as intrusive, extrusive (lavas), hydrothermal and/or replacement bodies (Streckeisen 1980). As of 2008, 527 known carbonatite occurrences were known (Fig. 1) of which only 49 are extrusive (Woolley and Church 2005; Woolley and Kjarsgaard 2008). From these 49 extrusive carbonatites, 41 are calcio-carbonatites, seven are dolomitic carbonatites, and single natrocarbonatite exists in Oldoinyo Lengai, East African Rift, Tanzania (Woolley and Church 2005), the latter also being known as the sole active carbonatite volcano. They range from Archean to present in age. At present, the oldest known carbonatite is Phalaborwa, South Africa, dated from 2063 to 2013 Ma (Masaki et al. 2005). The Siilinjarvi carbonatite in Finland may be even older, but the reported ages vary significantly. The oldest reported U–Pb zircon age from sövite at 2580±200 Ma (Patchett et al. 1982) is not well constrained and additional K–Ar-based measurements yielded the ages from 1790±30 to 2030±30 Ma on phlogopite, 2530±45 Ma on richterite, 2260±42 Ma on actinolite, and 1850±40 Ma and 2280±40 Ma on phlogopite and richterite from the main carbonatite (Puustinen 1972).

Carbonatites mostly occur in stable intraplate settings, such as shields, cratons and large crystalline blocks. Their occurrence indicates a direct link to orogenic events or plate separation, as can be seen in East Africa (Le Bas 1987; Bell 1989; Veizer et al. 1992). They are also related to mantle plumes and large igneous provinces (LIPs) (Gwalani et al. 2010) which could support their likely mantle origin (Jones et al. 2013) with possible source even in the lower mantle (Kaminsky et al. 2009, 2012; Stoppa et al. 2009). Carbonatites usually do not occur as individual rock units. Instead, they often are associated with a wide variety of alkaline rocks, ultramafic to felsic in chemistry (Jones et al. 2013) and only approximately 20% of carbonatite occurrences are without associated alkaline rocks (Woolley and Kjarsgaard 2008).

Three main theories for the genesis and evolution of carbonatites exist (Jones et al. 2013). (i) They are considered as residual melts from a fractionated carbonated nephelinite or melilitite (Gittins 1989; Gittins and Jago 1998). (ii) They are considered as immiscible fractions of CO_2-saturated silicate melts (Freestone and Hamilton 1980; Amundsen 1987; Kjarsgaard and Hamilton 1988, 1989; Brooker and Hamilton 1990; Kjarsgaard and Peterson 1991; Church and Jones 1995; Lee and Wyllie 1997; Dawson 1998; Halama et al. 2005; Brooker and Kjarsgaard 2011). (iii) They are considered as primary melts which are were generated from CO_2-bearing peridotite through partial melting (Wallace and Green 1988; Sweeney 1994; Harmer and Gittins 1998; Harmer et al. 1998; Ying et al. 2004). The limit of the

depth of formation of carbonatite magmas is unknown but they are believed also exist in the lower mantle (Kaminsky et al. 2009, 2012; Stoppa et al. 2009).

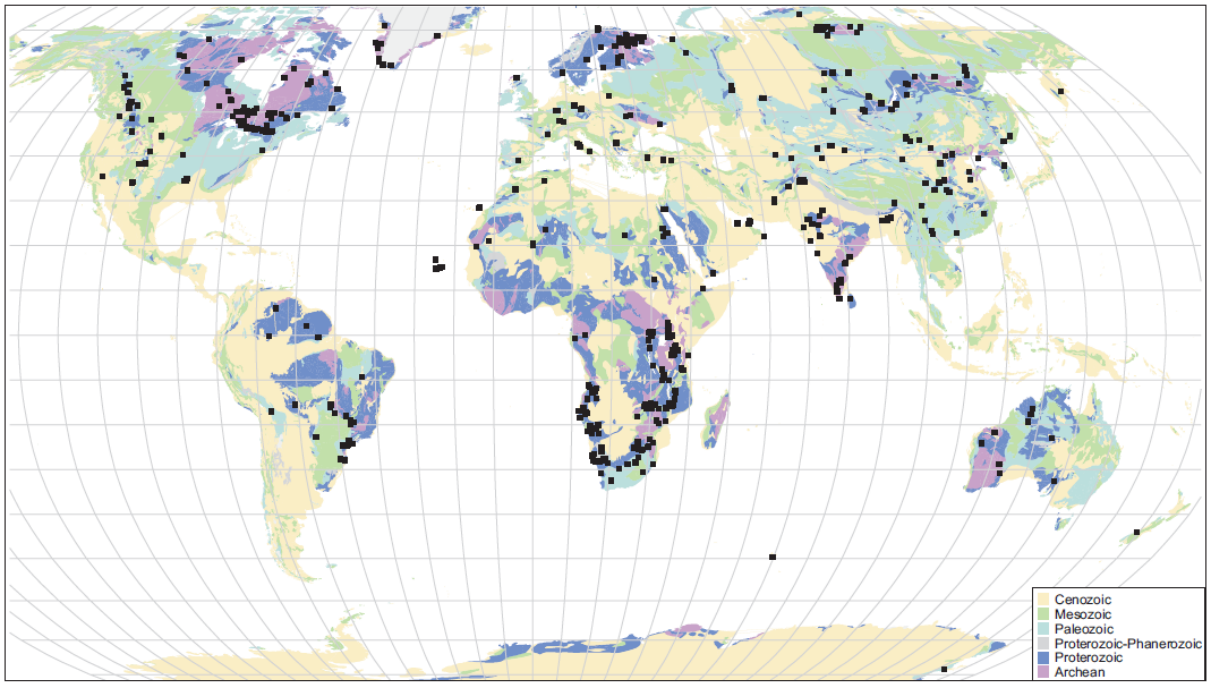

Figure 1. Map of the all known carbonatite occurrences in the world (Woolley and Kjarsgaard 2008).

Carbonatite liquids have some remarkable physical properties which distinguish them from common silicate and alkaline–silicate melts with which they often are spatially associated. The extremely low viscosity (~0.008 to 0.03 Pa.s; Dobson et al. 1996, Wolff 1994) and very low magmatic temperatures of carbonatites at low pressures (~800°C for calcio- and natrocarbonatites, Wolff 1994) make them distinct from silicate magmas (Jones et al. 2013). Only high P–T Fe-rich melts in the Earth's core may reach these extremely low viscosities (Dobson et al. 2000). Carbonate melts as ionic liquids consist of mainly CO_3^{2-} molecular anions and metal cations which do not polymerize as in silicate melts (Mysen 1983). Instead, they interact due to coulombic interactions (Jones et al. 2013). Carbonate melts are considered to have no exact association between metal cations and carbonate molecules, and are generally structure-less (Treiman and Schedl 1983). These features can be studied at the sole active (natro)carbonatite volcano – Oldoinyo Lengai in Tanzania (Treiman and Schedl 1983; Krafft and Keller 1989; Dawson et al. 1990; Oppenheimer 1998).

From the geochemical perspective, carbonatites can be divided into six categories based on major element ratios and/or REE contents (Tab. 1) and their textures may vary significantly. Carbonatite magmas can dissolve many elements which are considered rare in silicate magmas, such as Sr, Ba, P and particularly light rare-earth elements (LREE) (Nelson et al. 1988). This enrichment in REE is a result of the REE transport by molecular CO_3^{2-} complexes in the melt during the separation phase between silicate and carbonate melt, which are immiscible (Jones et al. 2013). This results in elevated

La/Lu ratios in carbonatite melts compared to silicate melts (Cullers and Medaris, 1977). Moreover, carbonatite magmas have the highest melt capacity for dissolving volatile species, such as water and halogens, at crustal pressures (Jones et al. 2013). They also serve as the transport agents of carbon from mantle to crust due to their ability to remain mobile over a range of pressures and temperatures (Jones et al. 2013). Given the high solubility of some critical metals in carbonatite melts (Nb, Zr, REE), carbonatites can be an important economic source of these elements and some deposits are extensively exploited (e.g., Bayan Obo, China; Phalaborwa, South Africa; Kovdor, Russia) which makes them the primary source of REE (Long et al, 2010). Neodymium isotopic data shows that REE are a product of derivation from the parental magma and that their high content indeed is a primary signature (Verplanck et al. 2014).

Table 1. Classification of carbonatites modified from Woolley and Kempe (1989)*, with extension from Jones et al (2013).

Class	**Sub-division**	**Chemical characteristics**
calciocarbonatite*	sövite (coarse-grained); alvikite (medium to fine-grained)	CaO/(CaO+FeO+MgO)>0.80)
dolomite carbonatite	beforsite, rauhaugite	(Ca,Mg)-rich
ferrocarbonatite*	-	$(FeO^T + MnO) > MgO$
magnesiocarbonatite*	-	$MgO > (FeO + MnO)$
Rare earth carbonatite	variable grain sizes modal REE minerals	$RE_2O_3 > 1$ wt.%
natrocarbonatite	lava at Oldoinyo Lengai volcano	$(Na_2O + K_2O) > (CaO+MgO+FeO)$

Major element contents are in weight %.

1.2 Rare earth elements in carbonatites and related alkaline silicate rocks

The rare earth elements (REE) are elements from lanthanum (La; atomic number 57) to lutetium (Lu; atomic number 71) with yttrium (Y; atomic number 39) sometimes added as a consequence of similar chemical properties (Tab. 2). Elements from lanthanum (La) to gadolinium (Gd) are termed the light rare earth elements (LREE) and elements from terbium (Tb) to lutetium (Lu) are termed the heavy rare earth elements (HREE). This division is due to their systematic change in the behavior; for example, with increasing atomic number the ionic radius decreases. Their radius (in six-fold coordination) decreases from 117 pm (La) to 100 pm (Lu); Y has the same radius as Ho (104 pm; Fig. 2) which leads to its similar properties in geochemical process (e.g., Pack et al. 2007).

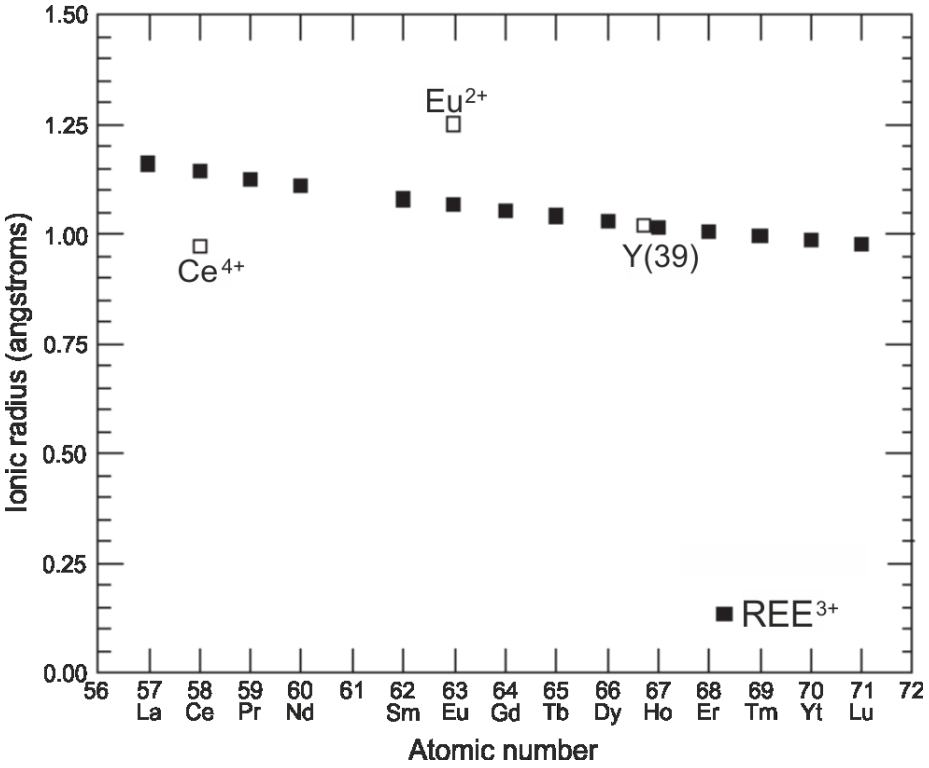

Figure 2. Variations in the ionic radius of the rare-earth elements. From Verplanck et al. (2014).

The nearly identical size of 3+ REE cations lends them very similar geochemical properties. Due to these chemical similarities REE can mutually substitute in a crystal lattice. Consequently, there can be multiple REE present in the mineral structure (e.g., monazite, xenotime) (Castor and Hedrick, 2006). However, because of the slight decrease in the ionic size with increasing atomic number (Fig. 2), there is a small difference in the behavior of LREE and HREE. Furthermore, Ce and Eu also exist in other oxidation states than 3+ (Ce: 4+; Eu: 2+) which may lead to elemental fractionation depending on the process considered.

Table 2. Atomic numbers and abundances of the rare-earths elements and yttrium in the upper crust, chondrite and primitive mantle reservoir from various sources.

Element	Symbol	Atomic number	Upper Crust abundance, *ppm**	Upper Crust abundance, *ppm*¤	Chondrite abundance, *ppm* †	Primitive mantle values, *ppm*‡
Yttrium	Y	39	22	21	1.57 ‡	4.3
Lanthanum	La	57	30	31	0.31	0.648
Cerium	Ce	58	64	63	0.808	1.675
Praseodymium	Pr	59	7.1	7.1	0.122	0.254
Neodymium	Nd	60	26	27	0.6	1.25
Samarium	Sm	62	4.5	4.7	0.195	0.406
Europium	Eu	63	0.88	1	0.074	0.154
Gadolinium	Gd	64	3.8	4	0.259	0.544
Terbium	Tb	65	0.64	0.7	0.047	0.099
Dysprosium	Dy	66	3.5	3.9	0.322	0.674
Holmium	Ho	67	0.8	0.83	0.072	0.149
Erbium	Er	68	2.3	2.3	0.21	0.438
Thulium	Tm	69	0.33	0.3	0.032	0.068
Ytterbium	Yb	70	2.2	2	0.209	0.441
Lutetium	Lu	71	0.32	0.31	0.032	0.068

* Source: Taylor and McLennan 1985

¤ Source: Rudnick and Gao 2003

† Source: Boynton 1984

‡ Source: McDonough. and Sun 1995

Promethium (Pm; Z = 61) is not included in this table because it has no stable or long-lived isotopes in nature. The most stable ^{145}Pm has a half-life of 17.7 years only.

The relative abundance of REE in the nature (Table 2) depends on two main factors. First, the REE with even atomic numbers have a greater abundance in the nature than the REE with odd atomic numbers (the Oddo–Harkins effect, Fig. 3). This is due to their greater stability during nucleosynthesis. Second, the LREE are more incompatible in the magmatic process; they are thus more concentrated in the continental crust compared to HREE.

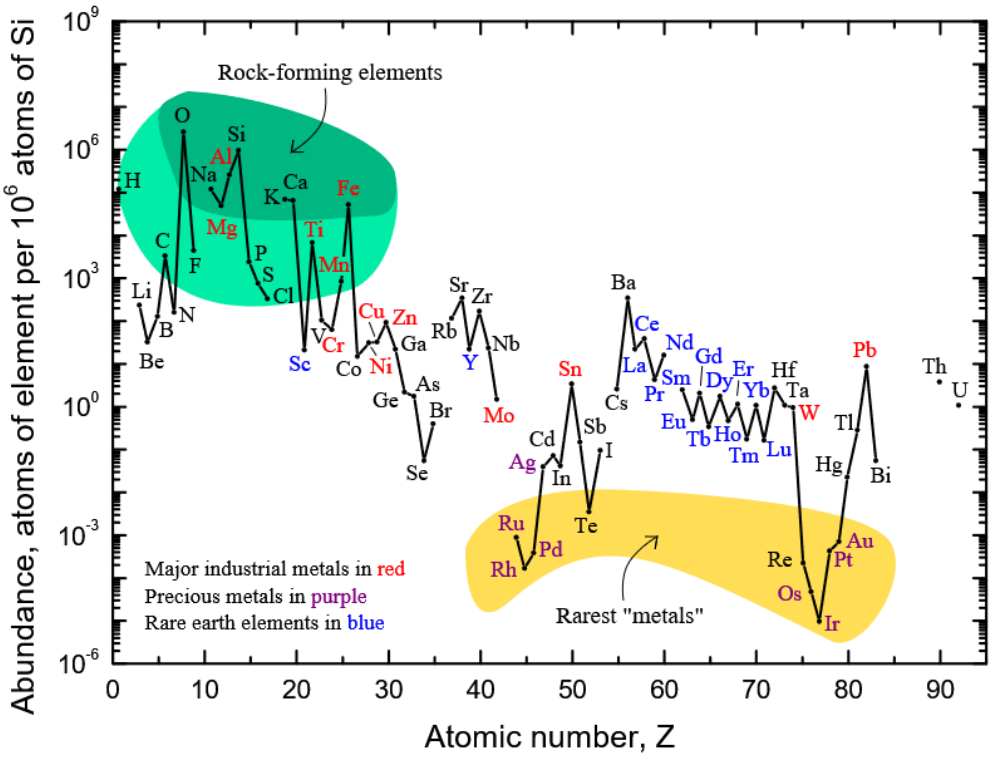

Figure 3. Abundance of the elements in the upper continental crust showing, that the rare earth elements are not so rare as it would appear from the times of their original discovery (Wikipedia, 2017).

The REE only occur in minerals, they do not exist in native form (cf. Au, Cu, Fe etc.). There are more than 200 minerals (Table 3) known to nominally contain one or more REE, but REE also are present in rock-forming minerals due to their ability to substitute for larger ions (e.g., Eu^{2+} substitution for Ca^{2+}in feldspar, REE substitution for Ca in apatite).

Table 3. List of REE-bearing minerals. Minerals in bold have been/are processed to recover the REE. From Verplanck et al. (2014).

Mineral	Formula	Mineral	Formula
Aeschynite (Ce)	$(Ce,Ca,Fe,Th)(Ti,Nb)_2(O,OH)_6$	Hellandite (Y)	$(Y,Ca)_6(Al,Fe^{3+})Si_4B_4O_{20}(OH)_4$
Allanite (Ce)	$(Ce,Ca,Y)_2(Al,Fe^{2+},Fe^{3+})_3(SiO_4)_3(OH)$	Hingganite (Y)	$(Y,Yb,Er)_2Be_2Si_2O_8(OH)_2$
Allanite (Y)	$(Y,Ce,Ca)_2(Al,Fe^{3+})3(SiO_4)_3(OH)$	Huanghoite (Ce)	$Ba(Ce,La,Nd)(CO_3)_2F$
Anatase	$(Ti,REE)O_2$	Iimoriite (Y)	$Y_2(SiO_4)(CO_3)$
Ancylite (Ce)	$SrCe(CO_3)2OH{\cdot}H_20$	Joaquinite (Ce)	$Ba_2NaCe_2Fe^{2+}Ti_2Si_8O_{26}(OH){\cdot}H_2O$
Apatite	**$Ca_5(PO_4)_3F$**	Kainosite (Y)	$Ca_2(Y,Ce)_2Si_4O_{12}(CO_3){\cdot}H_2O$
Baddeleyite	ZrO_2	Kamphaugite (Y)	$Ca(Y,REE)(CO_3)_2(OH){\cdot}H_2O$
Bastnäsite (Ce)	**$(Ce,La)(CO_3)F$**	Karnasurtite (Ce)	$(Ce,La,Th)(Ti,Nb)(Al,Fe^{3+})(Si,P)_2O_7(OH)_4{\cdot}3H_2O$
Brannerite	**$(U,Ca,Y,Ce)(Ti,Fe)_2O_6$**	Keiviite (Y)	$(Y,Yb)_2Si_2O_7$
Britholite (Ce)	$(Ce,Ca)_5(SiO_4,PO_4)_3(OH,F)$	Khanneshite	$(Na,Ca)_3(Ba,Sr,Ce,Ca)_3(CO_3)_5$
Brockite	$(Ca,Th,Ce)(PO_4){\cdot}H_2O$	Kuliokite (Y)	$(Y,Yb)_4Al(SiO_4)_2(OH)_2F_5$
Burbankite	$(Na,Ca)_3(Sr,Ba,Ca,REE)_3(CO_3)_5$	Låvenite	$(Na,Ca)_4(Mn,Fe)_2(Zr,Ti,Nb)_2(Si2O7)_2(O,F)_4$

Calcio-ancylite (Ce)	$(Ca,Sr)Ce_3(CO3)_4(OH)_3 \cdot H_2O$	**Loparite (Ce)**	**$(Ce,Na,Ca)(Ti,Nb)O_3$**
Carbocernaite	$(Ca,Na)(Sr,REE)(CO_3)_2$	Miserite	$K(Ca,Ce)_6Si_8O_{22}(OH,F)_2$
Caysichite (Y)	$Y_4(Ca,REE)_4Si_8O20(CO_3)_6)(OH) \cdot 7H_2O$	**Monazite (Ce)**	**$(Ce,La,Nd,Th)PO_4$**
Cerianite (Ce)	$(Ce^{4+},Th)O_2$	Mosandrite	$(H_3O+,Na,Ca)_3Ca_3REE(Ti,Zr)(Si_2O_7)_2(O,OH,F)_4$
Ceriopyrochlore	$Ce(Nb,Ti)_2O_6$	Nacareniobsite	$Na_3Ca_3(Ce,La)Nb(Si_20_7)OF_3$
Cerite (Ce)	$Ce_9Fe^{3+}(SiO_2)_6[(SiO_3)(OH)](OH)_3$	Parisite (Ce)	$Ca(Ce,La)_2(CO_3)_3F_2$
Cheralite	$(Ca,Ce,Th)(P,Si)O_4$	Perovskite	$(Ca,REE)TiO_3$
Chevkinite	$(Ca,Ce,Th)_4(Fe^{2+},Mg)_2(Ti,Fe^{3+})_3Si_4O_{22}$	Polycrase (Y)	$(Y,Ca,Ce,U,Th)(Ti,Nb,Ta)_2O_6$
Churchite (Y)	$YPO_4 \cdot H_2O$	Pyrochlore	$(Ca,Na,REE)_2Nb_2O_6(OH,F)$
Cordylite (Ce)	$NaBaCe_2(CO_3)_4F$	Rhabdophane (Ce)	$(Ce,La)PO_4 \cdot H_2O$
Crandallite	$CaAl_3(PO_4)_2(OH)_5 \cdot H_2O$	Rhabdophane (La)	$(La,Ce)PO_4 \cdot H_2O$
Daqingshanite (Ce)	$(Sr,Ca,Ba)_3(Ce,La)(PO_4)(CO_3)_{3-X}(OH,F)_x$	Rinkite (rinkolite)	$(Ca,Ce)_4Na(Na,Ca)_2Ti(Si_2O7)_2F_2(O,F)_2$
Davidite (Ce)	$(Ce,La)(Y,U,Fe^{2+})(Ti,Fe^{3+})_{20}(O,OH)_{38}$	Rosenbuschite	$(Ca,Na,Ce)_3(Zr,Ti)(Si_2O_7)(F,O)_2$
Doverite	$YCaF(CO_3)_2$	Sahamalite	$(Mg,Fe)(Ce,La,Nd,Pr)_2(CO3)_4$
Eudialyte	$Na_4(Ca,Ce)_2(Fe^{2+},Mn^{2+},Y)ZrSi_8O_{22}(OH,Cl)_2$	Samarskite	$(REE,Fe^{2+},Fe^{3+},U,Th,Ca)(Nb,Ta,Ti)O_4$
Euxenite (Y)	$(Y,Ca,Ce,U,Th)(Nb,Ta,Ti)_2O_6$	Sphene (titanite)	$(Ca,REE)TiSiO_5$
Fergusonite (Ce)	$(Ce,La,Y)NbO_4$	Steenstrupine (Ce)	$Na_{14}Ce_6Mn_2Fe_2(Zr,Th)(Si_6O_{18})_2(PO_4)_7 \cdot 3H_2O$
Fergusonite (Y)	$YNbO_4$	Stillwellite (Ce)	$(Ce,La,Ca)BSiO_5$
Fersmite	$(Ca,Ce,Na)(Nb,Ta,Ti)_2(O,OH,F)_6$	Synchysite (Ce)	$Ca(Ce,La)(CO_3)_2F$
Florencite (Ce)	$CeAl_3(PO_4)_2(OH)_6$	Synchysite (Y) (doverite)	$Ca(Y,Ce)(CO_3)_2F$
Florencite (La)	$(La,Ce)Al_3(PO_4)_2(OH)_6$	Tengerite (Y)	$Y_2(CO_3)_32–3H_2O$
Fluocerite (Ce)	$(Ce,La)F_3$	Thalenite (Y)	$Y_3Si_3O_{10}(F,OH)$
Fluocerite (La)	$(La,Ce)F_3$	Thorite	$(Th,U,REE)SiO_4$
Fluorapatite	$(Ca,Ce)_5(PO_4)_3F$	Titanite (Y)	$(Ca,Y)TiOSiO_4$
Fluorite	$(Ca,REE)F$	Uraninite	$(U,Th,Ce)O_2$
Formanite (Y)	$YTaO_4$	Vitusite (Ce)	$Na_3(Ce,La,Nd)(PO_4)_2$
Gadolinite (Y)	$Y_2Fe^{2+}Be_2Si_2O_{10}$	Wöhlerite	$Na(Ca,Ce,La)_2(Zr,Nb)(Si_2O_7)(O,OH,F)_2$
Gagarinite (Y)	$NaCaY(F,Cl)_6$	Xenotime (Y)	YPO_4
Gerenite (Y)	$(Ca,Na)_2(Y,REE)_3Si_6O_{18} \cdot 2H2O$	Yttrialite (Y)	$Y_2Si_2O_7$
Gorceixite	$(Ba,REE)Al_3[(PO_4)_2(OH)_5] \cdot H_2O$	Yttrofluorite	$(Ca,Y)F_2$
Gittinsite	$CaZrSi_2O_7$	Yttrotantalite (Y)	$(Y,Ca,Fe^{2+})(Ta,Nb)O_4$
Goyazite	$SrAl_3(PO_4)_2(OH)_5 \cdot H_2O$	Zircon	$(Zr,REE)SiO_4$

1.3 Crystal structure of apatite

Apatite [nominally $Ca_5(PO_4)_3(F,Cl,OH)$] is a common accessory phosphate mineral phase in magmatic, metamorphic and sedimentary rocks which crystallizes in the hexagonal space group *P*63/*m* (Bragg et al. 1965). General apatite formula is $A_5[TO_4]_6X$, where A stands for Ca^{2+}, Sr^{2+}, Mg^{2+}, Mn^{2+}, Fe^{2+}, REE^{3+}, Y^{3+} and Na^{+}, the tetrahedral T-site is occupied by P^{5+}, Si^{4+}, S^{6+}, and probably C^{4+}, and X is occupied by OH^{-}, Cl^{-} and F^{-} ions. Apatite has a large capacity to incorporate in its mineral lattice significant concentrations of trace elements. This feature makes it one of the most important minerals controlling the amount and variations of the REE in magmatic lithologies (Watson and Green 1981; Harrison and Watson 1984; Hoskin et al. 2000). In carbonatites, the most common phosphate mineral phase is fluorapatite [$Ca_5(PO_4)_3F$)] (Hogarth 1989).

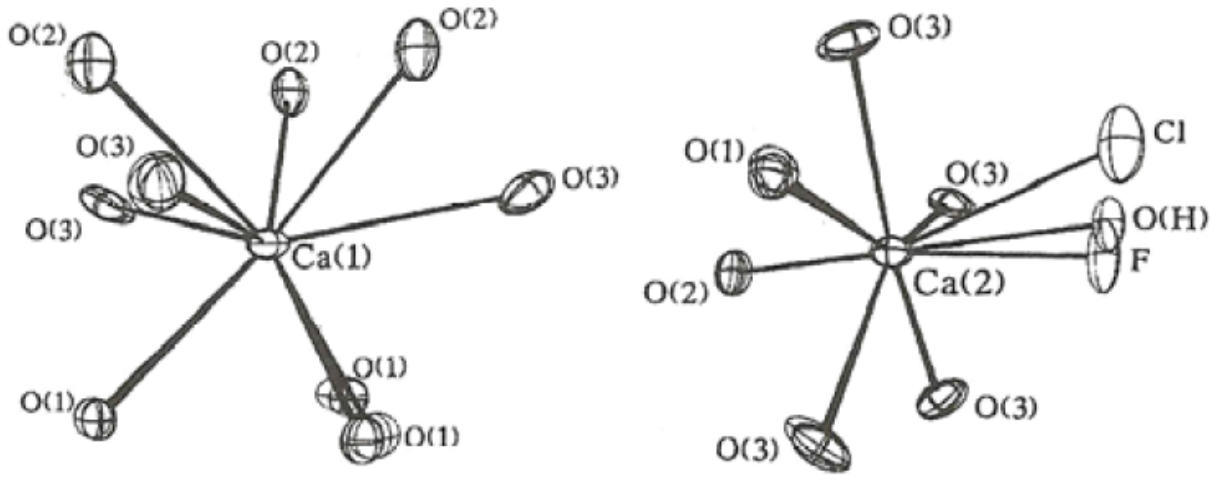

Figure 4. Ca1 (on the left) and Ca2 (on the right) polyhedra in fluorapatite. In the Ca1 situation, Ca ion is surrounded by nine oxygen atoms – six closer and three more distant. In the Ca2 situation, the central Ca ion is half-surrounded by six oxygen atoms. From Hughes et al. (1989).

The internal structure of apatite is represented by phosphate "tubes" which are lined internally by Ca ions (Klemme and Dalpé 2003). Two Ca-sites exist in the apatite structure (Mackie and Young 1973, Fleet and Pan 1995; Hughes et al. 1989, 1991) which plays an important role in the substitution of REE for Ca^{2+} in the apatite structure. The first site is referred as to A1 or Ca1 whereas the second site is referred to as A2 or Ca2 (Fig. 4). The subject of REE site occupancy and its crystal-chemical controls are still under discussion. Hughes et al. (1991) showed that La^{3+}–Pr^{3+} have the preference for the A2/Ca2 site while the Sm^{3+}–Lu^{3+} have preference for the A1/Ca1 position. However, Fleet and co-workers (Fleet and Pan 1995, 1997; Fleet et al. 2000) found a general preference of REE for the A2/Ca2 position.

1.4 Crystal structure of calcite and dolomite

Calcite ($CaCO_3$) is one the most abundant minerals on the Earth's surface. It is mainly present in sediments and sedimentary rocks in form of biogenic and inorganic precipitates. It is a dominant mineral phase in metamorphic marbles but is also quite frequent in volcanic rocks, mainly in carbonatites and kimberlites, where it is believed to be derived from a mantle source. Most common varieties

of calcite include dolomite ($CaMg(CO_3)_2$) and siderite ($Fe(CO)_3$). Calcite (rhombohedral calcium carbonate – $CaCO_3$; Fig. 5) is a hexagonal mineral with point group *3 2/m* and space group *R3c*. Dolomite is rather similar to calcite in that it has the space group R-3, but it appears to incorporate much less trace elements in comparison with calcite (Chakhmouradian et al. 2015).

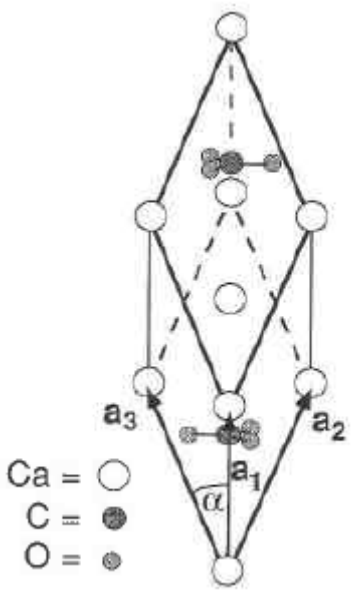

Figure 5. Rhomboehedral unit cell od calcite (from Skinner et al. 1994).

The REE can be incorporated into calcite structure in several ways such as via substitution for Ca^{2+} in calcite and Mg^{2+} in dolomite, by filling positions in lattice formed by defects, or adsorption due to remnant ionic charges (Qing and Mountjoy, 1994).

1.5 REE as a petrogenetic tracer in carbonatites

The REE are widely used as tracers of geological processes. Many experimental data (e.g., Wood, 1990; Haas et al., 1995; Migdisov et al., 2008) and empirical data (e.g., Morogan, 1989; Williams-Jones et al., 2000; Wall and Zaitsev, 2004; Bühn, 2008) exist on hydrothermal REE transport and partitioning, which improved our understanding of behavior of REE during water–rock interactions. Comparatively less data exists on the behavior of REE in carbonatites during crystal fractionation and separation during multi-stage magma evolution.

Because apatite is interpreted as a liquid phase in carbonatite melts (Eby, 1975; Le Bas and Handley, 1979; Eriksson et al., 1985; Le Bas, 1989; Gittins, 1989), trace element partition coefficients ($D^{apatite/carbonatite\ melt}$) can shed light on the genesis and origin of carbonatite intrusions. However, only a few $D^{apatite/carbonatite\ melt}$ data with contrasting results have been reported in the literature. A single measurement of $D^{mineral/carbonatite\ melt}$ also exists for calcite (Bühn et al. 2001), dolomite (Dawson and Hinton, 2003) and clinopyroxene (Klemme et al., 1995; Blundy and Dalton, 2000), the other important carriers of incompatible trace elements in carbonatites. The partition coefficients for REE

between a carbonatitic liquid and these mineral phases have been determined both experimentally and empirically, and the published results are listed in Table 4.

Bühn et al. (2001) calculated $D^{apatite/carbonatite\ melt}$ for a fractionated assemblage of calcite–fluorapatite–clinopyroxene in order to reproduce the natural relationship in selected carbonatites from Africa and concluded that (i) REE are compatible in apatite with $D^{apatite/carbonatite\ melt} > 1$, and (ii) the compatibility increases in a regular manner from La to Lu. Klemme and Dalpé (2003) in their experimental study, performed at 1 GPa and 1250 C along the join $CaCO_3$–$Ca_5(PO_4)_3(OH,F,Cl)$, analyzed apatite compositions crystallized from a carbonatite melt. Their $D^{apatite/carbonatite\ melt}$ values showed that REE are incompatible in apatite (contrary to the results of Bühn et al. 2001 and all others) and that D values form a convex upward pattern. Thus, the intermediate REE (Sm–Gd) have the highest D values in apatite. This convex upward pattern of D values of REE in apatite corresponds with the observation of Watson and Green (1981) who measured D values for apatite in various silicate systems. The very low $D^{apatite/carbonatite\ melt}$ values (<1) could be related to a very low silica activity in the carbonatite melt (Klemme and Dalpé, 2003). In silicate systems, REE are compatible in apatite but the D values are decreasing with the decreasing silica content in the system granite → basanite (Watson and Green, 1981). Another possibility for the changes in compatibility/incompatibility is the behavior of D values under different P–T conditions which have a profound effect on mineral/melt partitioning (Blundy and Wood, 2003).

Dawson and Hinton (2003) calculated inter-mineral partitioning coefficients for calcite, dolomite and apatite in Phalaborwa carbonatite, South Africa. Their derived D values for apatite show a steady decrease from La to Lu (contrary to the findings of Bühn et al. 2001), whilst D values for calcite show an increase from La to Lu; dolomite D values remain essentially constant for all REE. Fleet and Pan (1997) studied the partitioning of REE between fluorapatite and H_2O-bearing phosphate–fluoride melts at 700–800 C and 0.10–1.15 GPa. The D values also produced a convex upward pattern with the peak close to D value for Nd. REE in apatite are also compatible by Brassinnes et al. (2005) and also form convex-upward pattern. They used the same approach as it is used in this thesis (see section 5.2). Chakhmouradian et al. (2017) calculated distribution coefficients in apatite using a modified Rayleigh fractionation equation. In their study REE are compatible in apatite, distribution coefficients form convex-upward pattern, but there is not that apparent decrease of D values for HREE as in the other studies.

Table 4. Estimated distribution coefficients for REE from literature.

		La	Ce	Pr	Nd	Sm	Eu	Gd
Brassinnes et al. (2005)	ap	4.1, 18.1	4.7, 15.9	5.4, 20.1	6.1, 23.6	6.1, 34.2	6.1, 23.9	5.9, 19.0
Bühn et al. (2001)	ap	0.9-1.5	1.8-2.5	2.4-3.4	2.8-4.5	3.6-6.5	4.1-7.1	4.5-7.5
Chakhmouradian et al. (2017)	ap	2.10-9.4	3.53-9.76	3.83-10.10	3.88-11.40	3.91-11.2	4.21-9.86	4.92-13.7
Dawson and Hinton (2003)	ap	4.16	4.6	4.49	4.8	-	3.93	2.96
Fleet and Pan (1997)	ap	5.3	7.3	8.2	8.4	7.8	6.7	5.7
Hammouda et al. (2010)	ap	1.43	1.87	2.23	2.4	2.82	2.88	3.05
Klemme and Dalpé (2003)	ap	0.23-0.33	0.19-0.40	0.31-0.45	-	0.43-0.55	-	0.49-0.58
Klemme et al. (1995)	cpx	0.07	0.09	0.11	0.11	0.13	0.22	0.26
Bühn et al. (2001)	cc	0.05	0.045	0.04	0.035	0.029	0.026	0.02
Dawson and Hinton (2003)	dol	0.22	0.23	0.22	0.21		0.18	0.18
		Tb	Dy	Ho	Er	Tm	Yb	Lu
Brassinnes et al. (2005)	ap	-	4.4, 17.0	3.8, 17.2	2.1, 9.2	-	1.0, 8.4	-, 8.4
Bühn et al. (2001)	ap	4.8-7.8	5.1-8.1	5.4-8.4	5.6-8.7	5.8-9.1	6.0-9.5	6.2-10.0
Chakhmouradian et al. (2017)	ap	3.83-11.4	3.87-11.0	3.64-10.17	2.97-8.56	2.35-8.33	2.26-6.11	2.13-6.61
Dawson and Hinton (2003)	ap	3.49	2.57	2.84	2.92	3.08	2.88	1.87
Fleet and Pan (1997)	ap	-	3.9	-	2.5	-	1.4	1
Hammouda et al. (2010)	ap	3.15	3.16	3.17	3.17	3.13	2.96	2.9
Klemme and Dalpé (2003)	ap	-	-	-	-	-	-	0.23-0.34
Klemme et al. (1995)	cpx	-	0.29	-	0.41	-	-	-
Bühn et al. (2001)	cc	0.023	0.018	0.016	0.014	0.013	0.011	0.01
Dawson and Hinton (2003)	dol	0.16	0.21	0.18	0.16	0.17	0.23	0.22

2. GEOLOGICAL SETTING OF CARBONATITE COMPLEXES IN TAMIL NADU - SOUTH INDIA

Precambrian magmatism in the Eastern Ghats Mobile Belt (Schleicher et al., 1998) produced many carbonatite complexes (Samalpatti, Sevattur, Hogenakal, Mulakkadu–Pakkanadu) together with associated alkaline–peralkaline rocks, such as syenites, pyroxenites, and dunites. Host rocks for this magmatic activity were the 2.55 Ga granitic gneisses (Peucat et al et al. 1993), and carbonatitic and silicate alkaline magmas were emplaced into the series of deep NNE–SSW to NE–SW trending fracture zones (Grady 1971). These fracture zones represent the SW margin of the Eastern Ghats Mobile Belt – a zone of intense faulting and thrusting. Due to later tectonic processes and accretion the entire arc is now a part of the Nilgiri–Madras granulite belt (Fig. 6) which represents a transition zone between the cratonic terrain in the north (Dharwar craton, non-charnockitic, amphibolite facies) and the mobile granulite facies in the south (charnockitic, granulite facies) (Condie et al. 1982; Condie and Allen 1984). A range of geochronological data for the silicate alkaline–carbonatite complexes shows Neoproterozoic ages which correspond to the breakup of the Rodinia supercontinent and related rifting events (Pandit et al. 2002).

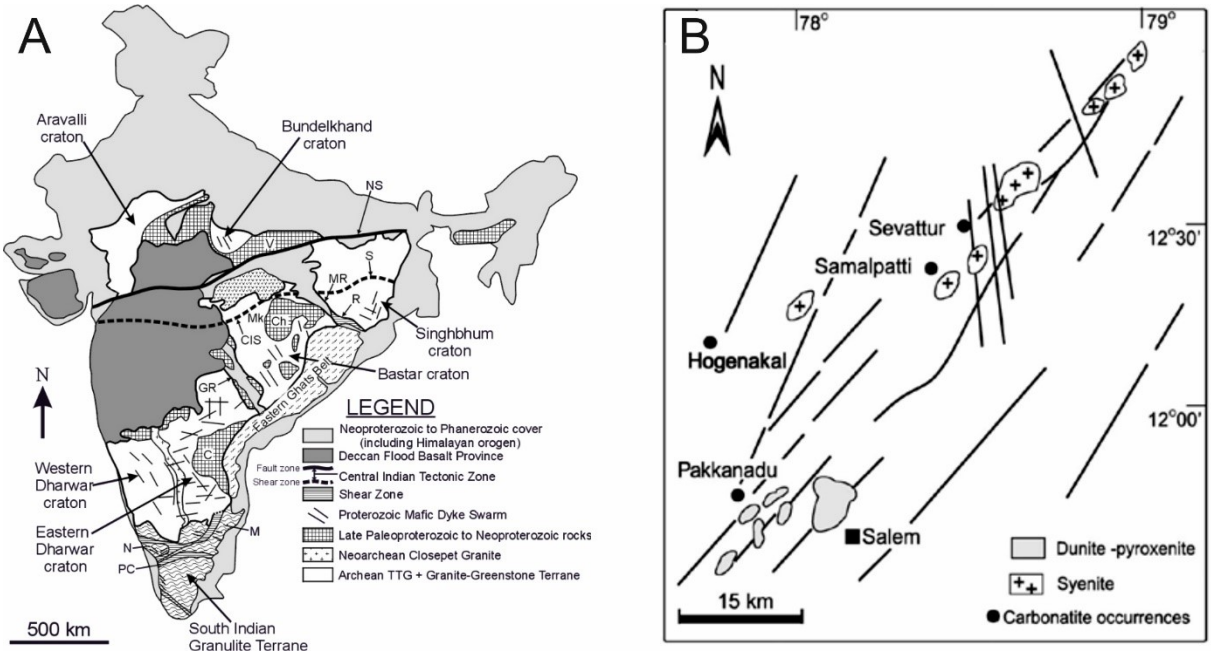

Figure 6. (A) – A simplified geological map of the Indian shield from Ernst and Srivastava, 2008 (modified after French et al., 2008). Ch - Chattisgarth Basin; CIS - Central Indian Shear Zone; GR - Godavari Rift; M - Madras Block; Mk - Malanjkhand; MR - MahanadiRift; N - Nilgiri Block; NS - Narmada-Son Fault Zone; PC - Palghat-Cauvery Shear Zone; R - Rengali Province and Kerajang Shear Zone; S - Singhbhum Shear Zone; V - Vindhyan Basin. (B) - Carbonatite-related occurrences in India with focus on the southern part (from Pandit et al., 2002).

The Samalpatti complex covers >125 km^2 and consists of carbonatites, Cr-rich silicocarbonatites, calc-silicate marbles, syenites, pyroxenites and minor bodies of albite–epidote metasomatic rocks and serpentinized dunites (Fig. 7). The entire suite intruded the hornblende gneisses (Moralev et al. 1975;

Subramanian et al. 1978). The central syenite body/plutonic mass is surrounded by the rings of pyroxenite together with dunite (Fig. 7). The carbonatites are exposed only as boulders, mounds or dikes in both syenite and pyroxenite. The K–Ar phlogopite age of the Samalpatti complex at 700±30Ma (Moralev et al. 1975) appears to be somewhat younger than that reported for Sevattur despite a close spatial relationship (see below).

The Sevattur carbonatite complex also consists of a central syenite body, but pyroxenites, albite–epidote metasomatic rocks and dunites are only present in the northern part together with the inward-dipping carbonatite body (Fig. 7) sandwiched between pyroxenites and syenites. Sevattur carbonatites predominantly are calcite-rich (sövite) with minor dolomite-rich members (IC11A, IC16A, IC16B). Pyroxenite is usually fenitized to phlogopite. The age of the Savattur complex is still unclear although several attempts have been made to date the carbonatite intrusion. Whole rock–mineral Rb–Sr age of 771 ± 18 Ma (Kumar and Gopalan, 1991) is very similar to the whole-rock Pb–Pb age of 801 ± 11 Ma (Schleicher et al., 1997) which is interpreted to represent the age of the carbonatite emplacement. Recent preliminary K–Ar data of Rapprich et al. (2017) display significantly younger ages for the Samalpatti syenites at ~560–576 Ma and ~510–540 Ma for the Sevattur syenites (biotite and feldspar were used for the analyses) compared to the coexisting carbonatites.

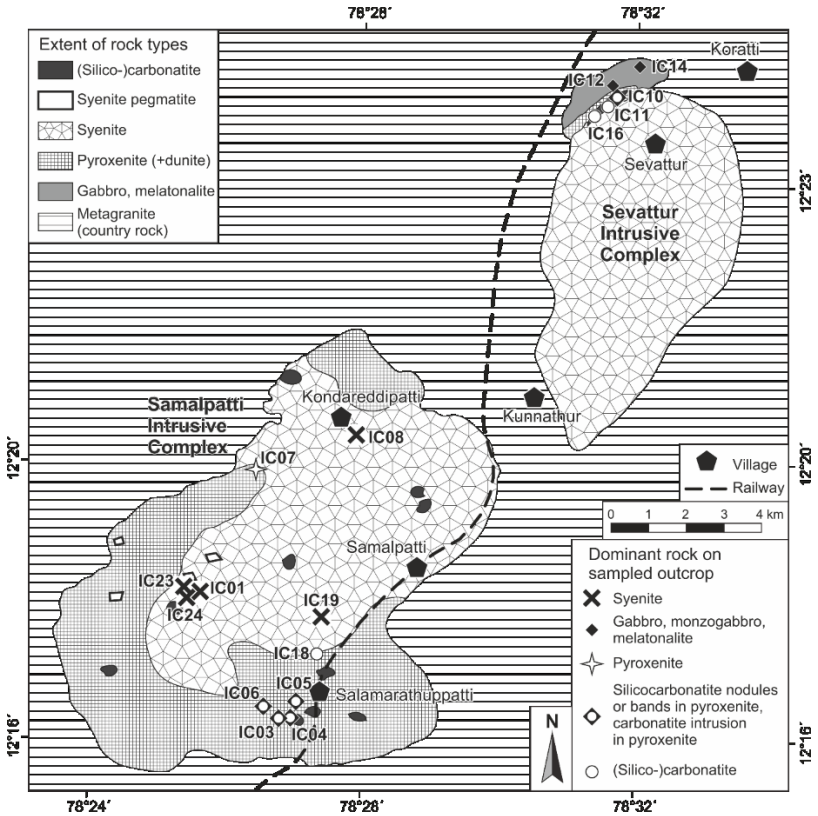

Figure 7. Simplified geological map of the Samalpatti and Sevattur complexes (adapted from Ackerman et al. 2017) with marked sampling points.

3. METHODOLOGY

Analytical methods for bulk rock geochemistry, electron probe micro analyses (EPMA) and inductively coupled plasma mass spectrometry (ICPMS) are described in detail by Ackerman et al. (2017) and are only briefly summarized here. Major element compositions of the entire suite were determined by classical wet techniques (AAS, flame 160 photometry, titration) at the Czech Geological Survey following the methods of Dempírová et al. (2010). Total sulfur and CO_2 contents were determined with an Eltra CS 500 C–S analyser, and F contents were determined after sample decomposition via pyrohydrolysis. The precision of major element determinations ranged between 5 and 10% (RSD). Analyses of JG-3 granodiorite (GSJ) and COQ-1 carbonatite (USGS) international standards were used to monitor the accuracy of the analytical protocol. The whole-rock trace element concentrations were determined using an Agilent 7900x ICPMS, housed at the Czech Geological Survey. Sample powders were decomposed in closed Savillex beakers using a mixture of concentrated HF and HNO_3 (6:1 v/v) at 130°C for 72 hours. The solutions were evaporated to dryness and refluxed repeatedly with small amounts of concentrated HNO_3 to break fluoride bonds. The dried residues were thereafter re-dissolved in 6M HCl and equilibrated at 70°C for 24 hours. This procedure produced solutions optically free of precipitates which could fractionate significant amounts of some trace elements, such as REE and HFSE. Chromium and Ni in carbonatites, and V in all samples were determined using XRF because of severe spectral interferences during the ICPMS measurements. The results are listed in Ackerman et al. (2017).

3.1 Optical microscopy

Optical microscope Nikon ECLIPSE 80i with the attached Nikon DS-Fi1 camera, housed at the Czech Geological Survey, was used to acquire pictures in both plane-polarized and cross-polarized light. The NIS-Elements AR 2.30 software was used for processing the pictures.

3.2 Electron Probe Micro Analyzer

Electron Probe Micro Analysis (EPMA) was used for studying the thin sections as well as for the chemical analyses of selected mineral phases. The microanalyses of the rock-forming minerals were performed at the Laboratory of electron microscopy and microanalysis at the Institute of Petrology and Structural Geology (Faculty of Science, Charles University, Prague, Czech Republic). The data were acquired using the FEG-EPMA JXA-8530F (Jeol) under the following analytical conditions: accelerating voltage 15 kV, beam current 20 nA for silicates and 15 nA for phosphates and carbonates. Pyroxenes, amphiboles, and spinels were analyzed with a focused beam, whereas other mineral phases were analyzed with the beam defocused to a diameter of 5 μm. The following standards (synthetic and/or natural phases) were used for the quantitative analysis: apatite (F, P), albite (Na), MgO (Mg), corundum (Al), quartz (Si), tugtupite (Cl), calcite (Ca), barite (Ba, S), sanidine (K), rutile (Ti),

Cr_2O_3 (Cr), rhodonite (Mn), magnetite (Fe), ZnO (Zn), celestite (Sr), YAG (Y), REE pentaphosphates (La, Ce, Nd).

3.3 Laser Ablation Inductive Coupled Plasma Mass Spectrometry

To study the distribution of incompatible trace elements in selected samples from Sevattur and Samalpatti, we employed laser ablation (LA) in tandem with ICPMS instrument. This has allowed us to investigate the co-existing mineral phases in (silico)carbonatites and associated alkaline rocks in situ at a high resolution. These latter analyses and their interpretations represent the integral part of this MSc. study. For the evaluation of raw LA-ICPMS data, backscattered electron (BSE) images were taken to determinate the crystal structure and possible chemical zoning of the unknown samples, and major element concentrations were acquired by EPMA. ^{43}Ca was used as an internal standard for LA-ICPMS calibration and correction of inter-element fractionation, and differences in the absolute amount of material that was ablated and transported during individual analysis. The GCDkit software (Janoušek et al. 2006) was used for data handling and plotting.

Laser ablation ICPMS (LA-ICPMS) was employed for in-situ determination of trace element concentrations in apatite, carbonate (both calcite and dolomite), and selected silicate phases in thick sections (thicker than those for conventional optical microscopy). The LA-ICPMS tandem at Czech Geological Survey consists of an Analyte Excite 193 nm excimer laser system (Proton Machines) equipped with a two-volume HelEx ablation cell securing ultra-fast washout times, which is connected to an Agilent 7900x quadrupole ICPMS instrument. Samples were ablated in He atmosphere (0.8 $l.min^{-1}$), and the laser was fired at 5 Hz using a spot size of 40 μm and laser fluence of 7.59 $J.cm^{-2}$. Other important instrumental parameters are listed in Table 5. Each measurement consisted of 20 s of blank acquisition followed by ablation of the sample for 60 s and washout for 40 s. NIST 610, NIST 612, and NIST 614 silicate glass wafers (Norman 1996; Jochum et al. 2011) were used as external standards to monitor the accuracy and precision of analytical procedures. In addition, the USGS reference basalt glass BHVO_2G, two in-house apatite standards (Apatite 1, Apatite 2) and a pelletized sample of carbonatite IC05F1 (prepared by pressing the powdered sample at 20 MPa for 10 minutes without any agglutinant) were also periodically measured during the analytical sessions. The analytical data for NIST glasses, BHVO standard, IC05F1 carbonatite as well as for two natural reference materials are listed in Table 6a and 6b, in parallel to the recommended (NIST 610, NIST 612, NIST 614, BHVO_2G; Jochum et al. 2005) and published (bulk sample analysis – IC05F1; Ackerman et al. 2017) values.

A typical LA-ICPMS analytical run consisted of spot analysis of NIST 614, 612 and 610 glasses (using NIST 612 as the primary standard), followed by the analyses of two in-house reference apatites (Apatite 1, Apatite 2), BHVO_2G and IC05F1. 15 to 20 unknown samples were then measured and the run was finished with a second block of reference materials. The following masses were collected: ^{7}Li, ^{9}Be, ^{28}Si,

^{43}Ca, ^{44}Ca, ^{45}Sc, ^{47}Ti, ^{51}V, ^{52}Cr, ^{59}Co, ^{60}Ni, ^{63}Cu, ^{66}Zn, ^{71}Ga, ^{85}Rb, ^{86}Sr, ^{88}Sr, ^{89}Y, ^{90}Zr, ^{93}Nb, ^{94}Zr, ^{133}Cs, ^{137}Ba, ^{139}La, ^{140}Ce, ^{141}Pr, ^{146}Nd, ^{147}Sm, ^{153}Eu, ^{157}Gd, ^{158}Gd, ^{159}Tb, ^{163}Dy, ^{165}Ho, ^{166}Er, ^{169}Tm, ^{172}Yb, ^{175}Lu, ^{178}Hf, ^{180}Hf, ^{181}Ta, ^{182}W, ^{208}Pb, ^{232}Th and ^{238}U using the SEM detector, with one point per mass peak and the total sweep time of 2.134 s for one mass scan. Data reduction was performed using the Glitter software (developed by the ARC National Key Centre for Geochemical Evolution and Metallogeny of Continents (GEMOC) and CSIRO Exploration and Mining).

Table 5. Analytical conditions of LA-ICPMS measurements.

ICPMS Agilent 7900x		Analyte Excite 193 nm excimer LA	
Forward power	1300 W	Repetition rate	5 Hz
Carrier gass	0.7 l.min^{-1} Ar	Fluence	7.59 J.cm^{-2}
ThO^+/Th^+	<0.2%	Carrier gass	0.8 l.min^{-1} He
$^{232}Th/^{238}U$	>0.95 for NIST 612	Beam diameter	40 μm

Table 6a, b. Analytical data for used standards.

	NIST612					NIST610					NIST614					IC05F1				
Element	mean	2 SD	RSD (%)	st	unc	mean	2 SD	RSD (%)	st	unc	mean	2 SD	RSD (%)	st	unc	mean	2 SD	RSD (%)	st	unc
Li (ppm)	41.9	3.35	7.99	40.2	1.3	497	35.2	7.07	468	24	4.38	1.51	34.42	1.69	0.09	3.73	1.02	27.4	3.8	
Be	38.1	2.89	7.58	37.5	1.5	466	30.4	6.54	476	31	0.83	0.30	35.78	0.75	0.05	0.34	0.26	76.7	-	
Sc	41.4	2.63	6.36	39.9	2.5	488	33.9	6.95	455	10	2.02	0.60	29.99	0.74	-	0.91	0.48	53.3	1.8	
Ti	48.6	3.42	7.04	44	2.3	556	42.3	7.60	452	10	4.03	0.92	22.90	3.61	0.25	276	236	85.5	-	
V	39.6	2.63	6.64	38.8	1.2	472	29.7	6.29	450	9	0.98	0.10	10.46	1.01	0.04	5.88	4.08	69.4	<2	
Cr	40.3	2.64	6.56	36.4	1.5	488	41.9	8.58	408	10	1.91	0.47	24.67	1.19	0.12	7.7	3.79	48.9	4	
Co	35.6	2.31	6.49	35.5	1	425	28.1	6.61	410	10	0.73	0.05	6.69	0.79	0.09	0.75	1.03	137	<2	
Ni	38.8	2.55	6.56	38.8	0.2	466.0	31.7	6.79	458.7	4	0.92	0.07	7.37	1.10	0.10	2.01	1.74	86.9	6.3	
Cu	37.1	2.42	6.52	37.8	1.5	384	37.0	9.63	441	15	2.61	0.27	10.30	1.37	0.07	1.08	0.72	66.1	4.4	
Zn	38.3	2.50	6.53	39.1	1.7	476	30.2	6.35	460	18	2.51	0.20	7.80	2.79	0.38	10.9	7.53	68.8	14	
Ga	36.6	2.41	6.58	36.9	1.5	446	29.2	6.56	433	13	1.14	0.08	6.81	1.31	0.09	1.23	0.88	71.2	2.6	
Rb	32.0	2.07	6.48	31.4	0.4	437.0	28.0	6.40	425.7	1	0.85	0.06	6.53	0.86	0.01	12.4	15.2	122	19	
Sr	77.1	5.70	7.39	78.4	0.2	521.6	36.7	7.04	515.5	1	43.76	2.73	6.23	45.80	0.10	295	37.4	12.7	339	
Y	38.7	2.55	6.60	38.3	1.4	482	28.8	5.98	462	11	0.82	0.11	12.99	0.79	0.03	4.94	0.85	17.1	5.5	
Zr	36.3	2.33	6.40	37.9	1.2	437	28.4	6.49	448	9	0.81	0.07	8.67	0.85	0.03	6.57	6.43	97.9	20	
Nb	38.5	2.49	6.47	38.9	2.1	480	31.0	6.45	465	34	0.78	0.05	6.17	0.82	0.03	0.66	0.79	121	1.6	
Cs	42.1	2.76	6.56	42.7	1.8	376	24.3	6.47	366	9	0.66	0.04	6.34	0.66	0.03	0.64	0.84	131	1	
Ba	38.1	2.49	6.53	39.3	0.9	446	28.3	6.34	452	9	3.08	0.27	8.71	3.20	0.09	154	59.4	38.5	268	
La	36.1	2.31	6.39	36	0.7	448	30.0	6.70	440	10	0.70	0.06	8.35	0.72	0.01	6.11	0.70	11.4	6.5	
Ce	38.8	2.61	6.74	38.4	0.7	464	30.7	6.62	453	8	0.76	0.06	7.78	0.81	0.03	12.5	1.49	11.9	14	
Pr	37.6	2.58	6.86	37.9	1	449	28.9	6.45	448	7	0.73	0.05	7.00	0.77	0.02	1.43	0.17	11.9	1.6	
Nd	35.6	2.55	7.15	35.5	0.7	442	30.3	6.86	430	8	0.74	0.09	12.26	0.75	0.01	5.44	0.63	11.6	6.2	
Sm	37.1	2.48	6.68	37.7	0.8	456	30.0	6.59	453	11	0.77	0.09	11.90	0.75	0.01	1.07	0.15	14.1	1.3	
Eu	34.8	2.32	6.66	35.6	0.8	449	29.6	6.58	447	12	0.74	0.06	7.77	0.77	0.02	0.22	0.03	15.0	0.28	
Gd	37.3	2.44	6.53	37.3	0.9	452	31.3	6.92	449	12	0.72	0.09	13.16	0.76	0.02	0.91	0.15	16.2	1.2	
Tb	36.3	2.32	6.40	37.6	1.1	425	31.3	7.38	437	9	0.71	0.05	7.06	0.74	0.02	0.13	0.02	14.4	0.17	

Dy	36.3	2.33	6.41	35.5	0.7	458	32.0	6.99	437	11	0.74	0.06	8.11	0.75	0.02	0.82	0.14	16.9	0.87
Ho	38.3	2.44	6.36	38.3	0.8	444	31.8	7.16	449	12	0.74	0.05	6.52	0.75	0.02	0.16	0.02	14.7	0.2
Er	37.8	2.49	6.60	38	0.9	461	31.4	6.80	455	14	0.73	0.06	7.78	0.74	0.02	0.46	0.08	18.3	0.52
Tm	38.0	2.45	6.45	36.8	0.6	432	30.3	7.02	435	10	0.73	0.05	6.58	0.73	0.02	0.07	0.01	16.8	0.07
Yb	40.3	2.62	6.49	39.2	0.9	488	34.1	6.99	450	9	0.80	0.06	7.88	0.78	0.02	0.45	0.08	16.8	0.49
Lu	38.1	2.48	6.51	37	0.9	436	30.0	6.88	439	8	0.73	0.04	6.10	0.73	0.02	0.07	0.01	17.4	0.08
Hf	35.1	2.24	6.39	36.7	1.2	423	27.7	6.54	435	12	0.68	0.04	6.53	0.71	0.02	0.18	0.18	98.4	0.83
Ta	40.2	2.59	6.44	37.6	1.9	469	31.1	6.65	446	33	0.80	0.06	7.29	0.81	0.03	0.06	0.06	97.4	0.21
W	40.0	2.75	6.89	38	1.1	487	31.3	6.43	444	29	0.82	0.07	8.77	0.81	0.07	0.13	0.26	194	-
Pb	39.4	2.80	7.11	38.57	0.2	474	35.1	7.40	426	1	2.48	0.20	7.90	2.32	0.04	5.54	1.63	29.5	5.1
Th	37.6	2.47	6.57	37.79	0.08	443.8	29.2	6.58	457.2	1	0.74	0.05	7.00	0.75	0.01	1.43	0.29	20.3	1.4
U	37.6	2.61	6.95	37.38	0.08	441.9	32.2	7.29	461.5	1	0.82	0.06	7.09	0.82	0.00	0.25	0.09	35.6	0.63

Table 6b.

	BHVO-2G					Apatite 1					Apatite 2				
Element	mean	2 SD	RSD (%)	st	unc	mean	2 SD	RSD (%)	st	unc	mean	2 SD	RSD (%)	st	unc
Li (ppm)	6.8	2.2	32.0	4.4	0.8	3.64	0.98	26.87	2.05	0.5	3.77	1.27	33.7	2.82	1
Be	1.1	0.3	30.4	1.3	0.2	0.13	0.08	65.77	0.18	0.1	0.12	0.06	48.4	0.17	0.1
Sc	32.0	2.8	8.9	33	2	0.53	0.42	78.86	0.23	0.1	0.27	0.05	17.7	0.17	0.1
Ti	19969	2091	10.5	16300	900	7.06	1.89	26.83	5.52	2.3	6.00	1.84	30.6	4.72	1.8
V	339	29.5	8.7	308	19	26.5	4.61	17.4	25.8	2.2	41.8	4.71	11.3	39	3.6
Cr	332	30.3	9.1	293	12	0.83	0.28	33.28	0.6	0.2	0.88	0.29	33.3	0.67	0.2
Co	48.7	4.3	8.7	44	2	0.09	0.04	40.6	0.06	0	0.10	0.02	24.8	0.08	0
Ni	131	12.0	9.2	116	7	0.29	0.11	36.4	0.21	0.1	0.23	0.00	0.00	0.2	0.1
Cu	124	11.1	9.0	127	11	0.22	0.12	54.3	0.16	0.1	0.14	0.02	10.8	0.16	0.1
Zn	126	11.3	9.0	102	6	0.84	0.62	73.8	0.64	0.8	0.70	0.64	92.7	0.6	0.3
Ga	22.7	1.9	8.6	22	3	0.94	0.10	10.9	0.89	0.1	21.5	1.00	4.6	21	0.9
Rb	10.0	0.8	8.3	9.2	0.04	0.05	0.01	20.8	0.03	0	0.06	0.01	17.1	0.07	0
Sr	378	31.8	8.4	396	1	1257	106	8.44	1176	71.0	498	31.7	6.36	488	28.9

Y	22.7	2.0	8.8	26	2	47.9	5.25	11.0	47.4	3.6	832	46.4	5.58	824	65.6
Zr	145	11.4	7.9	170	7	6.76	1.44	21.3	7.55	1.3	0.93	0.38	41.5	0.87	0.2
Nb	17.2	1.5	9.0	18.3	0.8	0.39	0.05	12.5	0.42	0.1	0.02	0.02	64.9	0.02	0
Cs	0.1	0.0	9.1	0.1	0.02	0.03	0.02	73.9	0.01	0	0.02	0.01	26.5	0.01	0
Ba	128	11.3	8.9	131	2	3.46	1.47	42.5	3.93	1.2	1.84	0.20	10.9	1.76	0.2
La	14.9	1.4	9.1	15.2	0.2	104	13.1	12.6	99.1	6.9	3833	198	5.16	3784	177
Ce	38.0	3.1	8.1	37.6	0.2	177	21.3	12.0	172	10	5104	267	5.22	5057	233
Pr	5.1	0.4	8.5	5.35	0.22	17.7	1.99	11.2	17.3	1.4	430	21.7	5.03	425	22.5
Nd	24	2.1	8.9	24.5	0.2	61.4	6.83	11.1	59.9	4.5	1435	70.6	4.92	1421	73.0
Sm	5.7	0.5	9.6	6.1	0.03	10.4	1.12	10.8	10.3	0.7	195	9.79	5.03	193	11.6
Eu	2.0	0.2	11.2	2.07	0.01	2.38	0.25	10.6	2.31	0.2	16.9	0.82	4.85	16.7	0.8
Gd	5.8	0.5	8.4	6.16	0.05	9.78	1.07	11.0	9.47	0.6	173	7.79	4.51	170.8	8.9
Tb	0.8	0.1	8.7	0.92	0.04	1.39	0.14	10.2	1.36	0.1	21.5	1.04	4.82	21.1	1.4
Dy	4.9	0.4	8.9	5.28	0.05	8.76	0.90	10.2	8.57	0.6	127	6.08	4.80	125.0	8.8
Ho	0.9	0.1	9.9	0.98	0.04	1.72	0.17	10.1	1.69	0.1	24.8	1.24	5.02	24.6	1.8
Er	2.3	0.2	7.8	2.56	0.02	4.67	0.48	10.2	4.58	0.3	66.5	3.33	5.01	65.8	4.7
Tm	0.3	0.0	8.3	0.34	0.02	0.63	0.07	10.4	0.62	0	8.48	0.44	5.20	8.35	0.6
Yb	1.9	0.2	9.4	2.01	0.02	3.77	0.41	11.0	3.73	0.3	46.9	2.40	5.12	46.3	3.1
Lu	0.3	0.0	9.1	0.279	0.003	0.49	0.06	11.6	0.49	0	5.47	0.28	5.15	5.37	0.4
Hf	3.9	0.3	8.0	4.32	0.18	0.04	0.03	89.5	0.04	0	0.02	0.03	102	0.02	0
Ta	1.1	0.1	8.7	1.15	0.1	0.01	0.00	55.5	0.01	0	0.01	0.00	40.1	0.01	0.00
W	0.3	0.0	18.5	0.23	0.04	0.16	0.06	40.5	0.12	0.1	0.04	0.04	102	0.02	0
Pb	2.1	0.3	12.5	1.7	0.2	10.11	1.31	13.0	10.3	0.7	0.94	0.31	33.5	0.84	0.1
Th	1.2	0.1	10.2	1.22	0.05	130	16.5	12.8	139	8.4	277	15.6	5.64	270	17.7
U	0.5	0.0	10.8	0.403	0.003	61.5	8.22	13.4	65.7	4.7	13.4	1.01	7.51	12.8	1

4. RESULTS

4.1 Petrography and mineralogy

4.1.1 Samalpatti

Carbonatites from Samalpatti occur in form of thin dykes or bands. In both thin-section and hand-specimen scale, carbonates (major calcite/minor dolomite) are the main rock forming minerals with a grain size of ~0.8 mm. They also contain pyroxene and accessory apatite (Fig. 8).

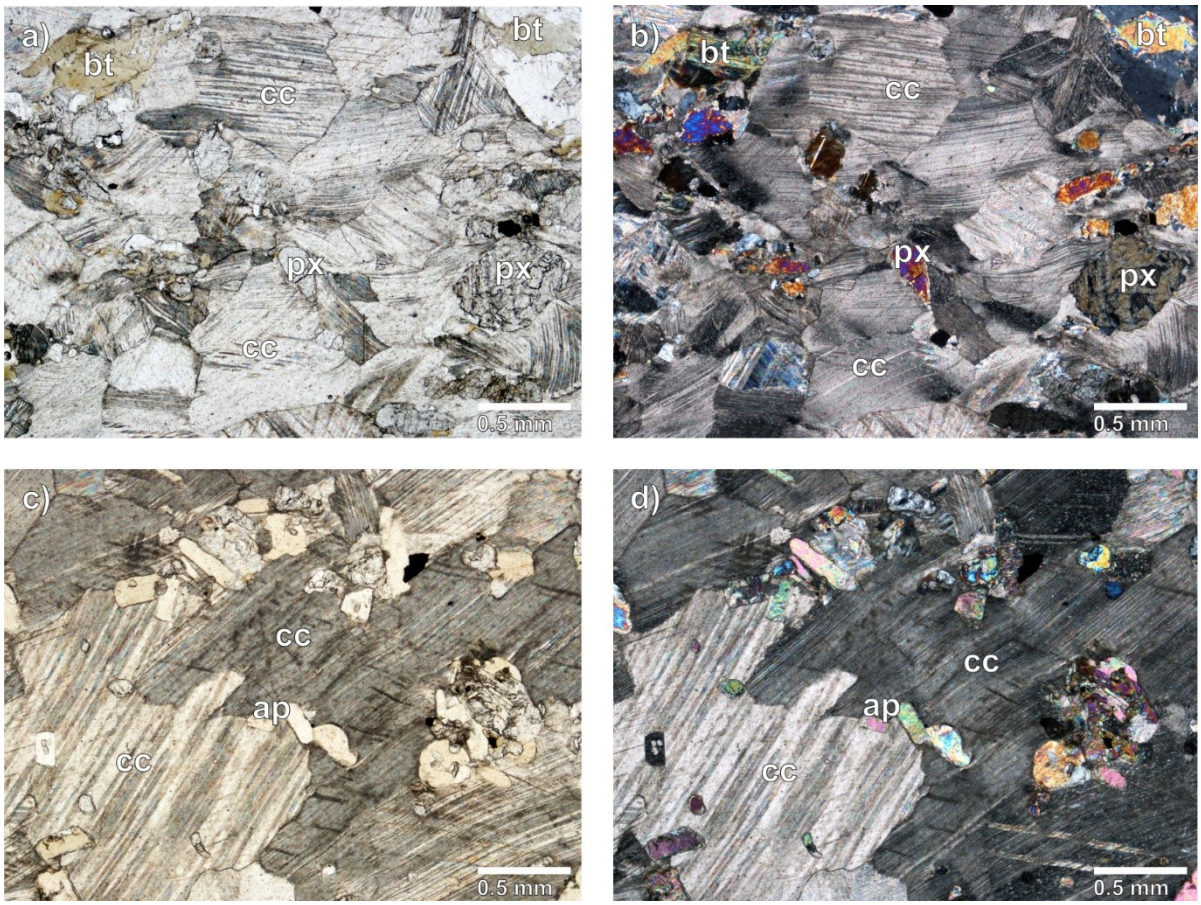

Figure 8. Microphotographs of the carbonatites from the Samalpatti. Pictures on the left side are in plane-polarized light and on the right are same pictures in the cross-polarized light. a,b) sample IC05A small light brown biotite and larger pyroxene in calcite matrix. c,d) sample IC05F large calcite crystals enclosing smaller grains of apatite. Mineral abbreviations: ap – apatite, cc – calcite,px - pyroxene.

Silicocarbonaties are present as centimeter- to decimeter-sized xenolith enclaves enclosed in pyroxenites; they rarely form dykes. Silicocarbonatites mainly are composed of randomly oriented needles of sodic amphibole winchite, calcite, minor plagioclase (pure albite), K-feldspar, and accessory apatite and titanite (Fig. 9).

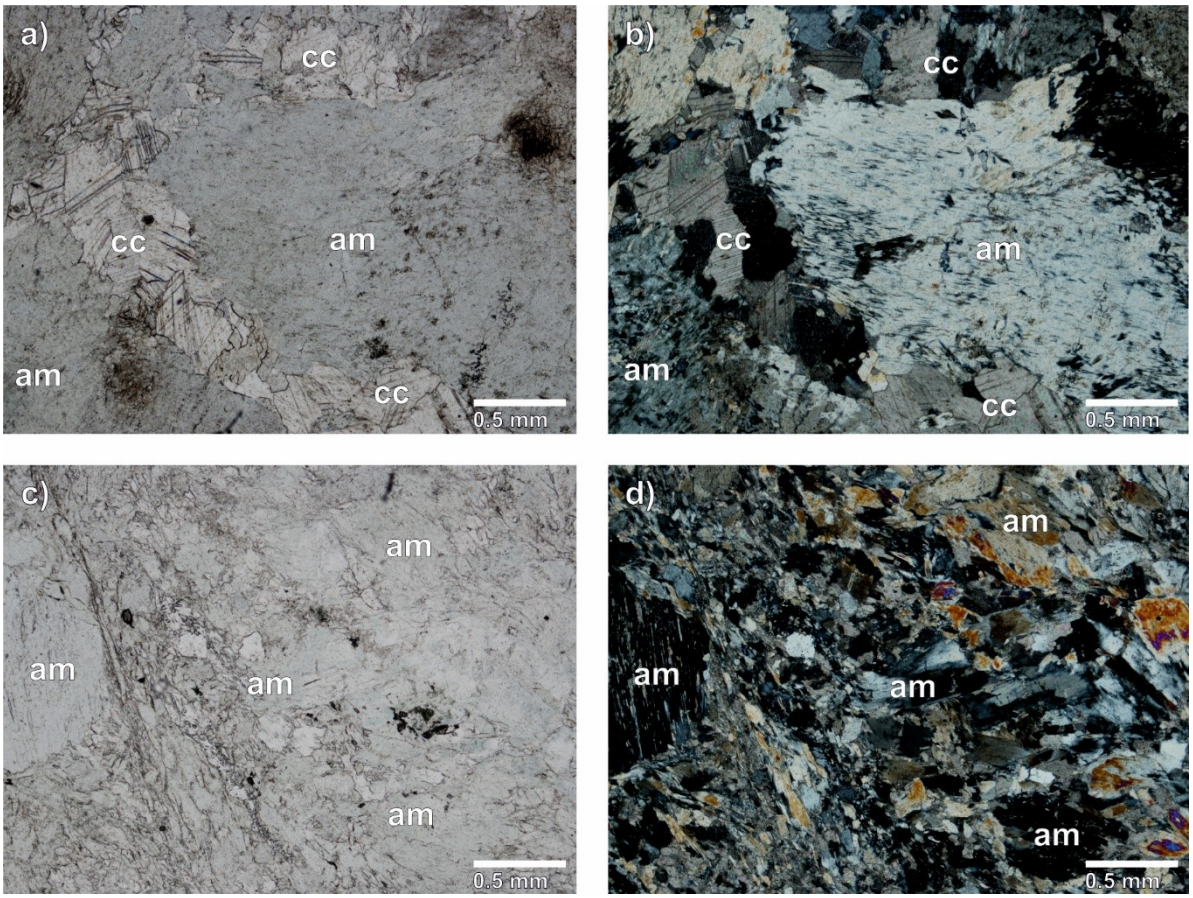

Figure 9. Microphotographs of the silicocarboantites from Samalpatti. Pictures on the left side are in plane-polarized light and on the right, are same pictures in the cross-polarized light. a,b) sample IC03A with large crystal of amphibole and vein-like distributed calcites. c,d) sample IC03B with both large and small crystals of amphibole a no calcite. Mineral abbreviations: am – amphibole, cc – calcite.

In silicocarbonatites IC03B and IC04A, exotic Na–Cr-rich clinopyroxene kosmochlor (nominally $NaCrSi_2O_6$) was found. It is suggested to represent a Cr analogue of jadeite (Frondel at al., 1965). So far, it has been reported only from a limited range of lithologies –iron meteorites Coahuila, Toluca, and Hex River Mountains (Frondel at al., 1965), high-pressure low-temperature jadeitites (Yi-Nok Ng et al., 2016), and kimberlites (Gor'kovets et al. 2013). Kosmochlor in samples IC03B and IC04A is associated with chromite and titanite, and is present in form of micron-size grains with a maximum grain size reaching roughly 25 microns. Although we cannot deconvolve a more detailed genetic association of kosmochlor, it appears to represent the primary phase that underwent decomposition to chromite. Overall habitus of kosmochlor grains and aggregates resembles remnants of larger, partly dissolved

grains of kosmochlor with exsolved chromite (Fig. 10a). Chromite forms either skeletal aggregates (Fig. 10a) or exsolutions in kosmochlor (Fig. 10b, c) which both seem to be secondary.

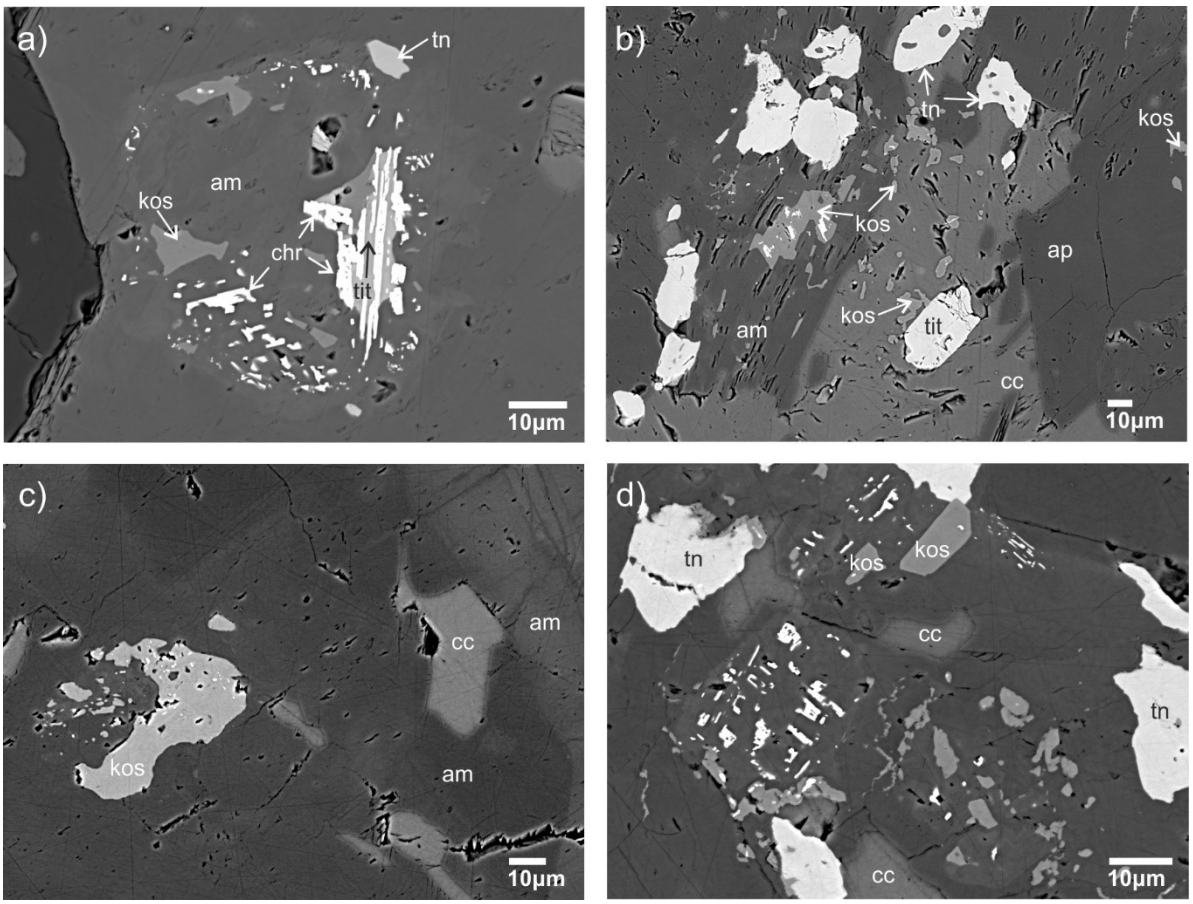

Figure 10. Different kosmochlor grains found in silicocarbonatite samples IC04 (a) and IC03B (b, c, d) - from Samalpatti. Mineral abbreviations: am – amphibole, cc – calcite, chr – chromite, kos – kosmochlor, tn - titanite.

Pyroxenites are present both as enclosed enclaves within carbonatites as well as separate bodies, and occur together with monzogabbros. They are composed of randomly oriented pyroxenes (diopside) with the grain size reaching up to 3 cm, and amphibole (rarely biotite) which partly replaced pyroxenes. Other common mineral phases include apatite and Fe–Ti oxides (mainly titanite). Sample IC05C (Fig. 11a, b) represents an unaltered pyroxenite with pristine grains of diopside and apatite. Sample IC07D (Fig. 11c, d) represents a pyroxenite, where primary pyroxene assemblage is overprinted by later amphibole (winchite), penetrating the pyroxene grains (Fig. 11c). Titanite is resistant to this replacement.

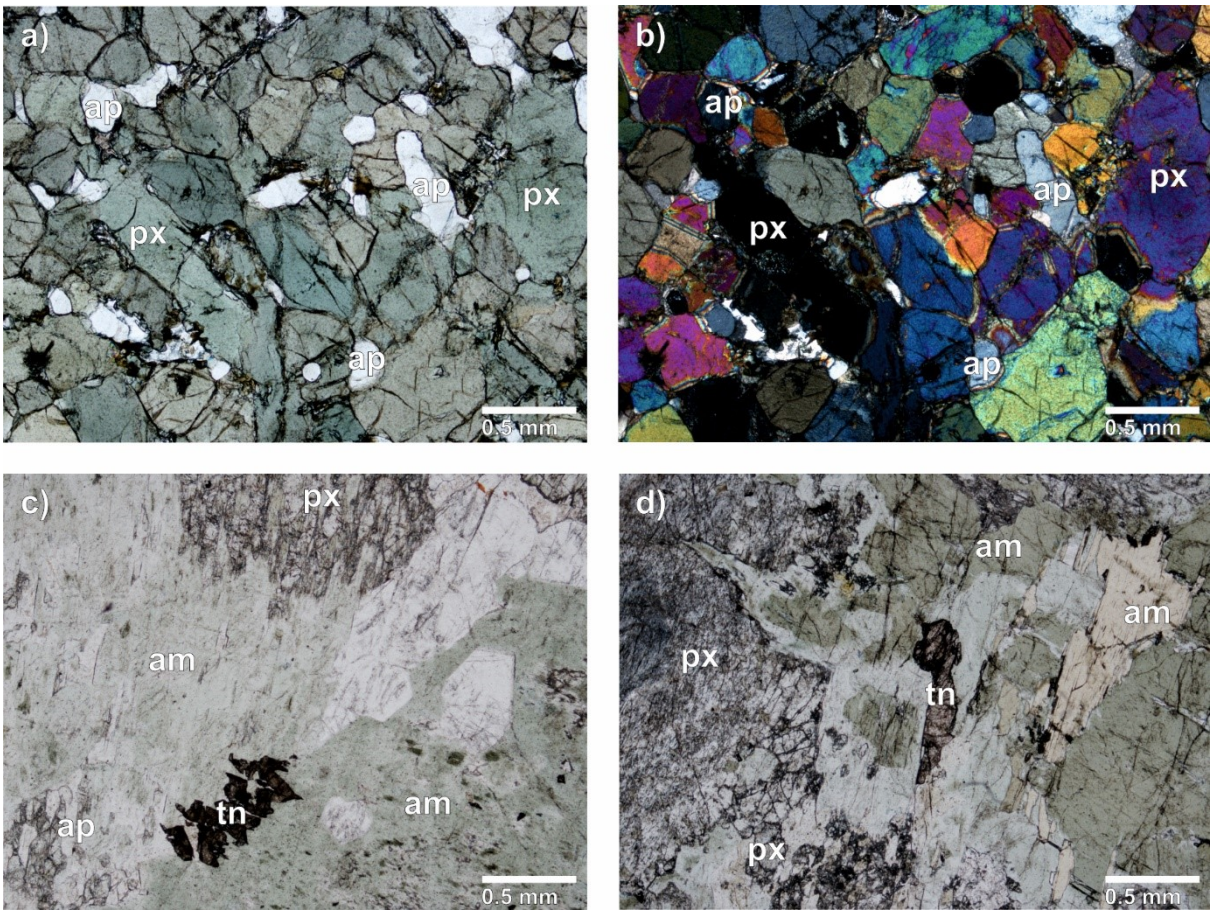

Figure 11. Microphotographs of the pyroxenites from Samalpatti. Only picture b) is in crossed-polarized light, a,c,d) are in plane-polarized light. a,b) sample IC05C with ubiquitous green pyroxenes and colorless randomly scattered apatites. c,d) sample IC07D with large greenish tabular amphiboles enclosing titanite and apatite and overbearing primary pyroxene. Mineral abbreviations: ap – apatite, am – amphibole, px – pyroxene, tn - titanite.

4.1.2 Sevattur

Carbonatites from Sevattur form either intrusions into pyroxenite or NE–SW trending dykes. They consist almost exclusively of coarse-grained calcite (~1 cm, Fig. 12), whereas other mineral phases are rare (mainly aegirine and biotite). Several samples (e.g., IC10J) contain significant amounts of apatite (up to 6 wt.%). Magnetite is also common while pyrochlore is rare. When dolomite is present, it is scattered in calcite in form of unoriented exsolutions, visible only using EPMA (see section 4.3.1). This was also reported from the Phalaborwa carbonatite complex, South Africa (Dawson and Hinton, 2003), where it was interpreted to be texturally similar to high-temperature metamorphic marbles described already by Goldschmidt (1960) form various locations.

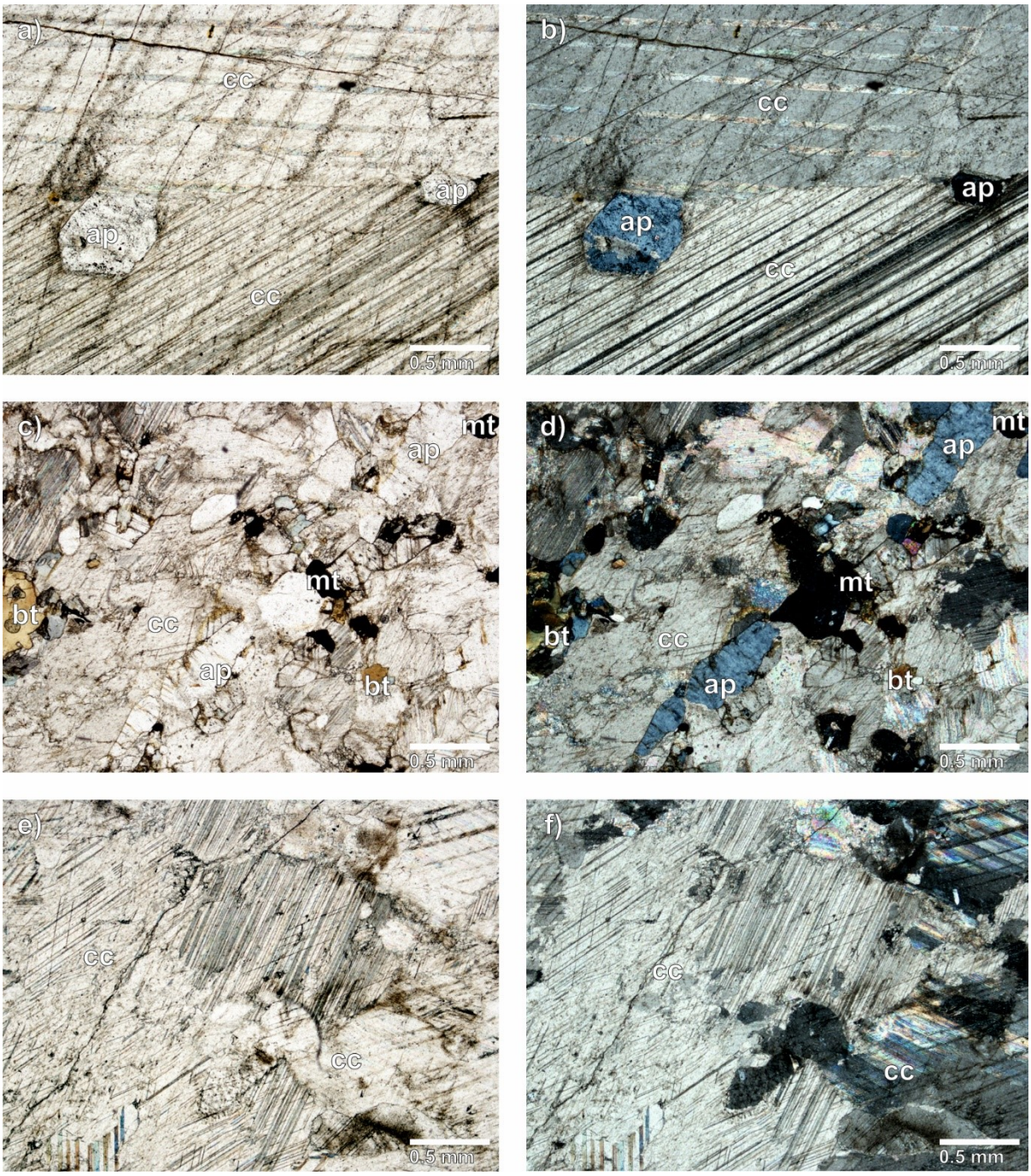

Figure 12. Microphotographs of the carbonatites from Sevattur. Pictures on the left side are in plane-polarized light and on the right, are the same pictures in the cross-polarized light. a,b) sample IC10A dominated by large crystals of calcite with grains of apatite. c,d) sample IC11A composed mainly of calcite with minor biotite and magnetite with elongated crystals of apatite. e,f) . Mineral abbreviations: ap – apatite, bt – biotite, cc – calcite, mt – magnetite.

Pyroxenites (Fig. 13) are composed of preferentially oriented grains of aegirine (up to 8 mm long), biotite and Na–Mg amphibole (winchite), both replacing aegirine. Main accessory minerals are apatite, titanite, Fe–Ti oxides, and calcite.

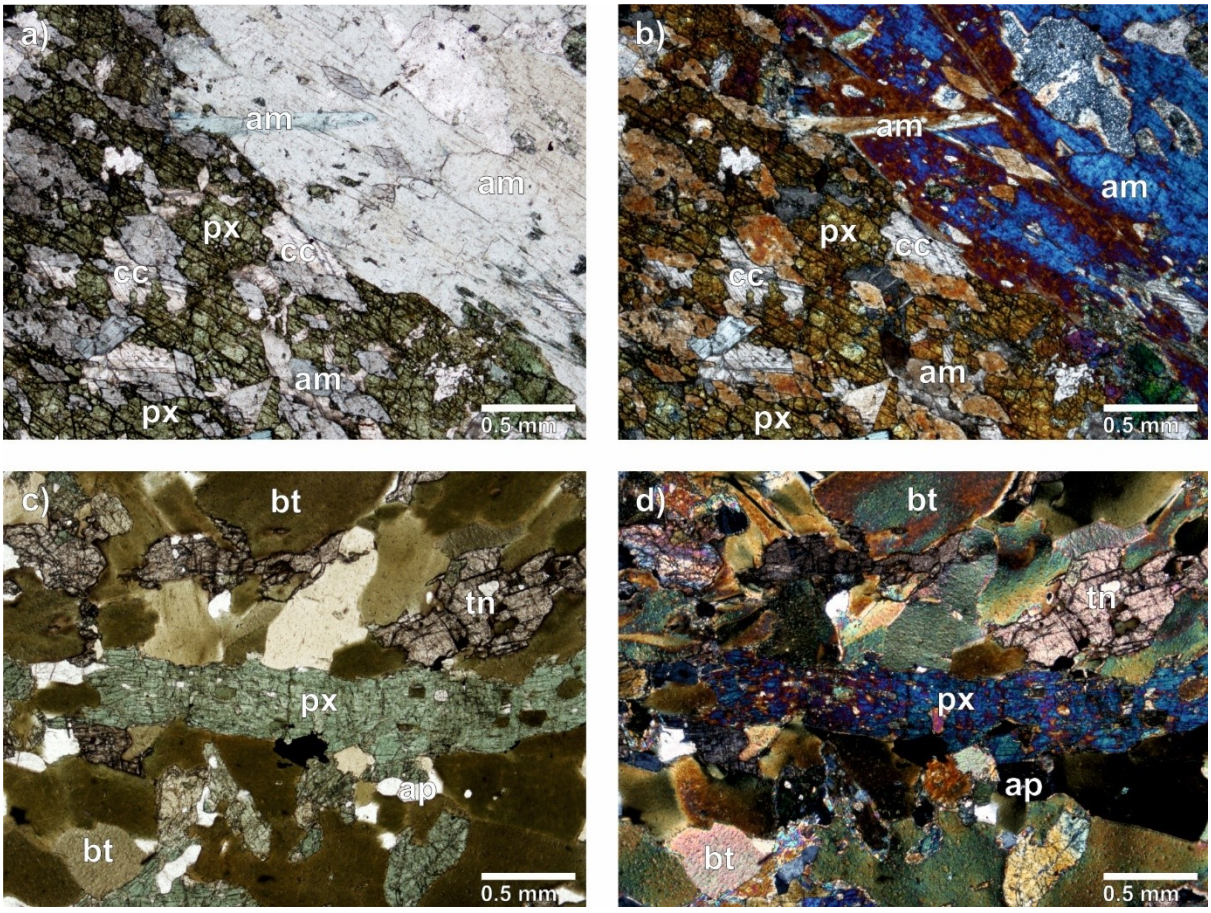

Figure 13. Microphotographs of the pyroxenites from Sevattur. Pictures on the left side are in plane-polarized light and on the right in the cross-polarized light. a,b) sample IC10G is represented by both pyroxene (with interstitial calcite and amphibole) and amphibole, which is debunking pyroxene. c,d) sample IC15 (biotitized pyroxenite) is composed mainly of biotite, pyroxene, large titanite grains and apatite. Mineral abbreviations: am – amphibole, ap - apatite, bt – biotite, cc – calcite, px – pyroxene, tn - titanite.

In carbonatites IC10A and IC10F, Mckelveyite-(Nd) [nominally (Ba,Sr)(Nd,Ce,La)$(CO_3)_2 \times 4–10\ H_2O$] was identified. It is present either as subtle nano-scale oriented phases in calcite (Fig. 14a) or scattered submicron- to micron-scale grains (Fig. 14b).

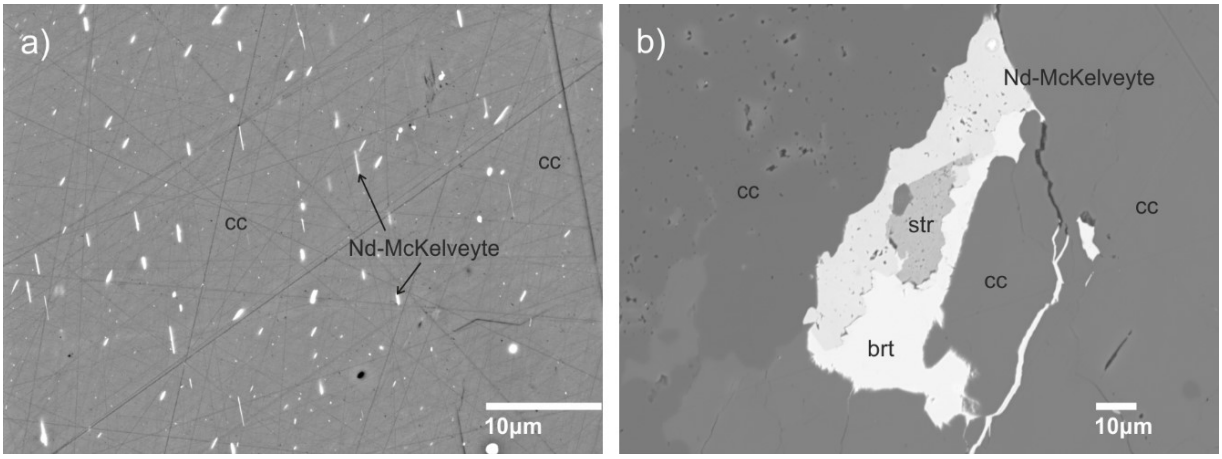

Figure 14. Small LREE-bearing mineral phase in the Sevattur carbonatite – Mckelveyite-(Nd). Mineral abbreviations: brt – barite, cc – calcite, str – strontianite.

In some carbonatite samples from Samalpatti and Sevattur, enclaves of silicate minerals enclosed in carbonatite matrix were also found. In pyroxenite IC05C from Samalpatti (Fig. 15b, d), these enclaves mostly consist of phlogopite, clinopyroxene, K-feldspar (sometimes Ba-rich with up to 3.3 wt.% Ba) and plagioclase. Aggregates in carbonatite IC16B from Sevattur (Fig. 15a, c) consist mainly of pyroxene (diopside), amphibole (winchite), andradite-rich garnet, epidote, and large grains of apatite. Other mineral phases include small grains of barite and monazite. One particular enclave from sample IC16B shows several peculiar features (Fig. 15c) compared to other enclaves from the same sample. The central part of this enclave consists of amphibole and K-feldspar, with minor amounts of monazite and unidentified Nb–Ta phase, and is devoid of apatite. The entire central part is enclosed by large rutile crystals.

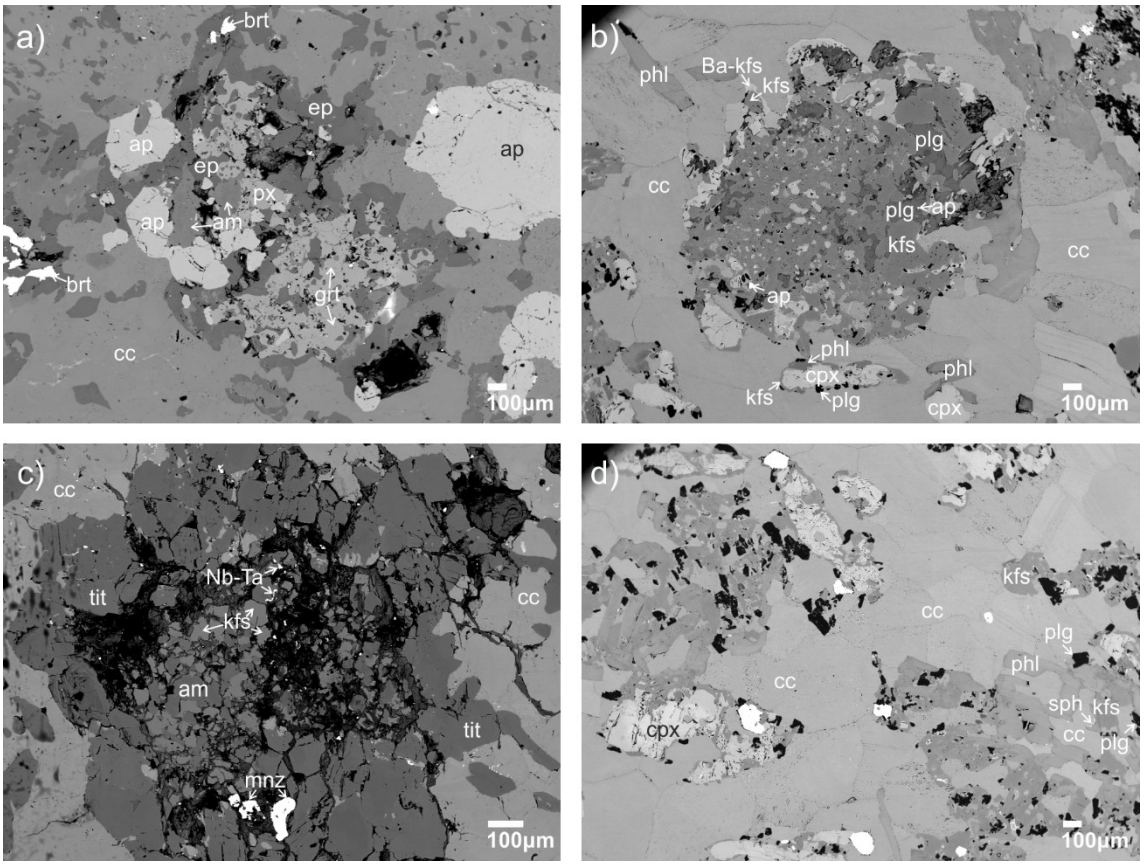

Figure 15. Different silicate mineral enclaves in the sample IC16B from Sevattur (a, c) and IC05C from Samalpatti (b, d) carbonatites. Mineral abbreviations: am – amphibole, ank – ankerite, ap – apatite, brt – baryte, cc – calcite, cpx – clinopyroxene, ep – epidote, grt – garnet, kfs – K-feldspar, mnz – monazite, phl – phlogopite.

4.2 Whole-Rock Geochemistry

Major and trace element data for bulk samples were published in Ackerman et al. (2017) and are only briefly discussed here. Carbonatites from Samalpatti can be divided into two groups based on their SiO_2 contents – the SiO_2-rich CaO-poor silicocarbonatites (41.0–44.8 wt. % SiO_2, 18.2–19.9 wt. % CaO) and the SiO_2-poor CaO-rich carbonatites (0.72–14.4 wt. % SiO_2, 37.8–53.9 wt. % CaO) (Table 7). In comparison with SiO_2-poor carbonatites, the silicocarbonatites (IC03A, IC03B, IC03D, IC03E, IC4A) have also elevated contents of MgO (13.7–16.7 vs. 2.0–12.6 wt.%), Fe_2O_3 (1.9–3.5 vs. 0.02–0.7 wt.%), FeO (0.94–1.7 vs. 0.27–0.82 wt.%), K_2O (0.76–1.8 vs. 0.09–1.1 wt.%) and Na_2O (2.6–4.6 vs. 0.01–0.36 wt.%). Phosphorus and F contents do not vary greatly between carbonatites and silicocarbonatites. Trace element concentrations vary greatly in both carbonatites and silicocarbonatites (Table 7; Ackerman et al. 2017).

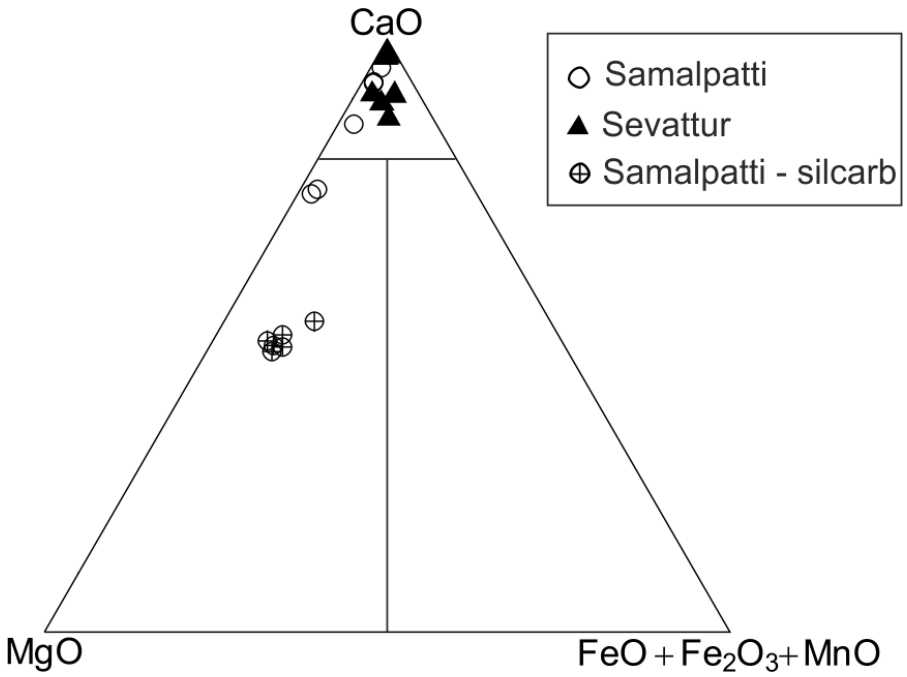

Figure 16. Classification diagram of the Samalpatti and Sevattur carbonatites and silicocarbonatites. Sevattur carbonatites are exclusively calcium-rich. Samples from Samalpatti are more chemically diverse with magnesium-rich silicocarbonatites. No iron-rich carbonatites are present among the samples.

The silicocarbonatites are more enriched in lithophile elements such as Sc (35–48 vs. 0.93–5.6 ppm), V (38–74 vs. 2–28 ppm), Co (30–36 vs. 2–5.1 ppm), Ni (165–207 vs. 4.0–8.4 ppm) and most significantly in Cr (924–1,803 vs. 4–14 ppm), likely as a consequence of the presence of Cr-rich minerals. The ranges in REE concentrations are comparable in both rock types, recognized at Samalpatti: 16.0–120 ppm ΣREE in carbonatites and 13.7–216 ppm ΣREE in silicocarbonatites. Both rock types are depleted in Ta (0.07–0.36 ppm) and display a large range in Nb contents (0.78–33.0 and 6.4–92 ppm, respectively).

Table 7. Major and trace element concentration of carbonatites from the Samalpatti area (Ackerman et al. 2017). Values for normalization are from Boyton, 1984. Abbreviations: carb – carbonatite; silico-carb – silicocarbonatite.

Sample	IC05A	IC05D	IC05F1	IC05F2	IC03A	IC03B	IC03D	IC03E	IC04A	IC06E	IC18B	IC18C
Locality	Samalpatti	Samalpatti	Samalpatti	Samalpatti	Samalpatti	Samalpatti	Samalpatti	Samalpatti	Samalpatti	Samalpatti	Samalpatti	Samalpatti
Rock	carb	carb	carb	carb	silico-carb	silico-carb	silico-carb	silico-carb	silico-carb	silico-carb	carb	carb
SiO_2 (wt. %)	9.48	10.32	5.13	0.72	41.92	42.61	41.25	41.03	44.81	41.03	14.44	11.84
TiO_2	0.12	0.07	0.11	0.04	0.21	0.23	0.21	0.22	0.14	0.24	0.25	0.17
Al_2O_3	2.01	1.33	2.03	0.88	1.33	0.78	1.01	1.53	0.76	0.85	3.66	1.94
Fe_2O_3	0.15	0.7	0.18	0.02	2.57	1.85	2.68	2	2.32	3.47	0.35	0.68
FeO	0.78	0.24	0.46	0.27	1.35	1.18	0.94	1.7	1.18	1.35	0.82	0.4
MgO	2.86	12.61	3.03	1.96	15.57	16.79	16.78	15.69	16.21	13.09	11.53	5.7
MnO	0.03	0.02	0.02	0.01	0.1	0.06	0.09	0.1	0.08	0.18	0.04	0.04
CaO	48.37	38.88	50.02	53.88	18.23	19.35	18.51	19.63	18.51	19.92	37.83	41.18
Na_2O	0.36	< 0.01	0.22	0.13	4.15	3.22	3.94	3.51	2.62	4.62	0.14	0.15
K_2O	1.11	0.09	0.39	0.25	1.41	0.98	1.77	0.95	0.76	1.56	1.07	0.1
P_2O_5	0.06	0.01	0.04	0.04	0.06	0.14	0.1	0.04	0.03	0.35	0.05	0.04
F	0.08	0.16	0.06	0.04	0.14	0.12	0.16	0.09	0.03	0.06	0.15	0.1
CO_2	35.01	31.44	36.67	39.99	10.43	10.69	10.04	10.5	9.39	10.65	26.53	29.55
S	0.02	0.12	0.12	0.03	< 0.010	< 0.010	< 0.010	< 0.010	0.02	0.03	0.27	0.01
H_2O+	< 0.05	3	0.51	0.94	2.24	1.76	2.27	2.13	2.26	1.83	< 0.05	4.85
H_2O-	0.09	0.14	< 0.05	0.08	< 0.05	0.11	0.05	0.05	0.08	< 0.05	3.19	2.71
Total	99.75	99.43	99	99.29	99.76	99.86	99.8	99.18	99.18	99.23	99.32	99.36
Li (ppm)	2.8	0.97	3.8	2.2	5.2	3.1	7.4	1.6	2.1	9.5	2	2.2
Sc	2.7	2.3	1.8	0.93	42	37	38	36	35	48	5.6	3
V	18	13	<2	5	71	48	63	64	38	74	28	13
Cr	7	12	4	5	1071	1285	1670	924	1803	1025	14	13
Co	3.9	2.6	<2	<2	34	30	31	34	33	36	5.1	3.5
Ni	4	7.4	6.3	4.4	176	172	173	175	207	165	8.4	8.1
Cu	6.2	47	4.4	1.2	3.2	4.4	4.7	2.8	5.9	2	15	15
Zn	18	77	14	8.9	73	24	65	28	14	150	12	32
Ga	4.3	3.2	2.6	1.2	3.6	2.4	3.2	2.7	1.7	3.9	4.9	4.4

Rb	64	3.8	19	8.9	1.5	0.93	2.2	1.4	3	2	40	1.6
Sr	390	314	339	248	468	238	298	401	115	990	224	102
Y	7.8	6.5	5.5	3	20	5.5	13	5	2	45	7.7	14
Zr	27	22	20	5.5	7.4	4.6	12	3.4	2.2	59	41	19
Nb	1.6	1.4	1.6	0.78	72	6.9	37	29	6.4	22	3.5	33
Cs	3.2	0.2	1	0.58	0.08	0.08	0.1	0.07	0.13	0.04	1.9	0.79
Ba	563	299	268	150	1027	496	539	496	360	673	777	197
La	11	7.9	6.5	3.1	6.7	5.8	7.2	7.3	2.3	18	10	24
Ce	22	17	14	6.7	27	17	27	17	4.8	72	21	53
Pr	2.4	1.9	1.6	0.73	4.4	2.3	4.2	2.1	0.64	11	2.4	5.6
Nd	9.4	7.5	6.2	2.9	22	10	21	9.1	3.1	60	9.2	22
Sm	1.9	1.5	1.3	0.58	6.5	2.4	5.6	2.1	0.83	16	1.9	4.4
Eu	0.46	0.3	0.28	0.13	1.9	0.66	1.5	0.61	0.25	4.7	0.43	1.1
Gd	1.8	1.4	1.2	0.59	5.3	2	4.2	1.8	0.77	14	1.8	3.9
Tb	0.25	0.21	0.17	0.09	0.74	0.25	0.56	0.23	0.1	1.9	0.25	0.52
Dy	1.3	1.1	0.87	0.46	3.4	1.1	2.5	1	0.43	8.4	1.3	2.4
Ho	0.28	0.24	0.2	0.1	0.68	0.21	0.47	0.2	0.08	1.6	0.28	0.49
Er	0.75	0.63	0.52	0.28	1.7	0.5	1.2	0.46	0.19	4	0.74	1.2
Tm	0.1	0.09	0.07	0.04	0.22	0.06	0.14	0.06	0.02	0.52	0.1	0.15
Yb	0.71	0.6	0.49	0.26	1.5	0.36	0.87	0.35	0.14	3.6	0.7	1
Lu	0.12	0.1	0.08	0.04	0.23	0.06	0.12	0.06	0.02	0.62	0.11	0.15
Hf	1.1	0.92	0.83	0.3	0.37	0.27	0.39	0.19	0.16	1.4	1.6	0.92
Ta	0.24	0.21	0.21	0.13	0.36	0.1	0.09	0.07	0.07	0.07	0.36	0.33
Pb	6.8	67	5.1	4.6	10	10	15	8.7	23	27	5.9	11
Th	3.9	2.9	1.4	0.27	1.6	1.5	41	2.7	2.6	0.65	3.6	6.4
U	0.57	0.52	0.63	0.7	0.12	0.14	0.26	0.11	0.29	0.41	0.62	0.22
ΣREE	52.47	40.47	33.48	16	82.27	42.7	76.56	42.37	13.67	216.34	50.21	119.91
LaN/YbN	10.45	8.88	8.94	8.04	3.01	10.86	5.58	14.06	11.08	3.37	9.63	16.18

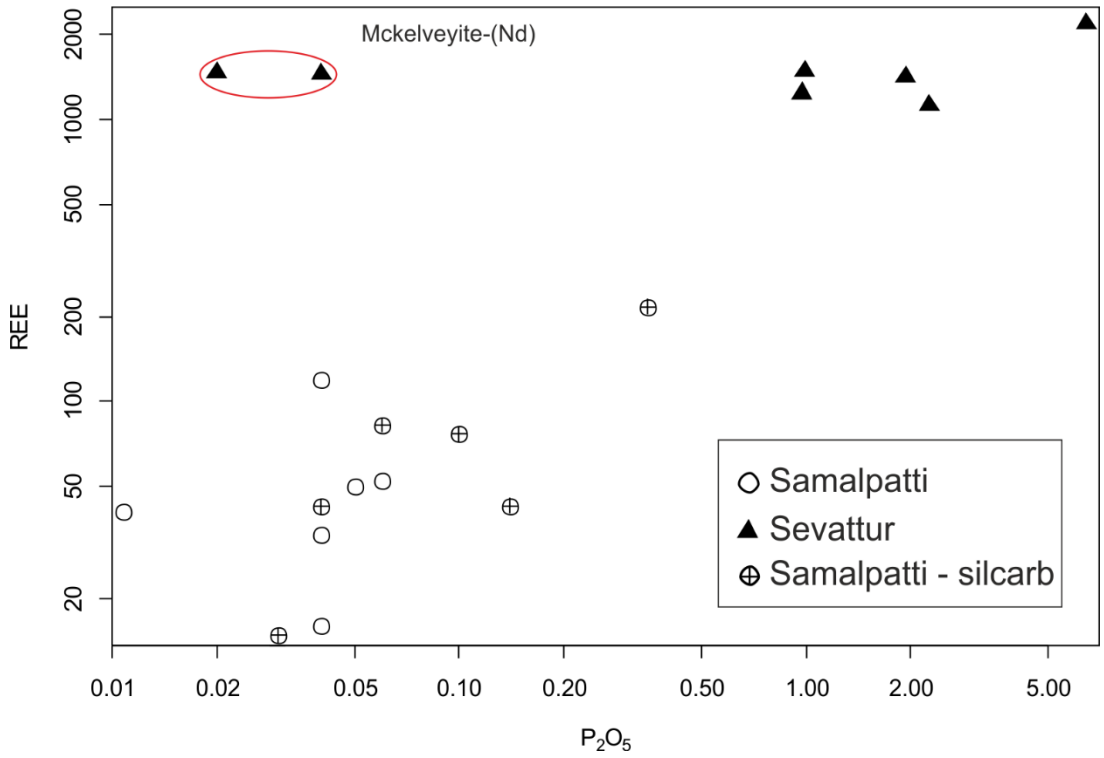

Figure 17. Phosphorus versus REE contents in Samalpatti and Sevattur bulk-rock samples. It illustrates the relationship between REE and P2O5 contents. Most REE appear to be hosted in apatite while high REE contents in two samples from Sevattur are not paralleled by elevated P_2O_5 contents. Combined with EPMA analyses this indicates presence of Mckelveyite-(Nd).

Samples from the Sevattur complex are more homogeneous in terms of major elements (Table 8) than carbonatites from Samalpatti. The CaO contents vary between 46.0 and 54.5 wt.%. Silica contents are also uniformly low and vary between <0.10 and 0.40 wt. % SiO_2, with the exception of IC10J (apatite-rich carbonatite; 3.3 wt. % SiO_2) and IC11A (magnetite-rich carbonatite; 6.2 wt. % SiO_2). These two samples are also enriched in Fe_2O_3 (1.5 and 2.0 wt.%). Variations in P_2O_5 (0.02–6.8 wt. %) and F (0.01–0.52 wt. %) contents directly reflect the modal content of apatite in the rock. Trace element concentrations in Sevattur samples are less variable than those from Samalpatti. Sevattur carbonatites are distinctly enriched in REE (ΣREE = 1,125–2,200 ppm, Fig. 17). Samples IC10J and IC11A are enriched in particular elements relative to other Sevattur carbonatites, such as V (90 and 78 ppm vs. <2–14 ppm), Co (16 and 17 ppm vs. 0.87–3 ppm), Zr (15 and 8.1 ppm vs. 0.14–1.8 ppm) and especially Nb (55 and 135 ppm vs. 0.45–48 ppm). Sample IC16B has high concentrations of these elements, including U (23 ppm) while it does not show any particular enrichment in modal proportion of any incompatible element-bearing phase, such as zircon or magnetite (like samples IC10J and IC11A, which contain not only magnetite, but pyrochlore as well).

Table 8. Major and trace element concentration of carbonatites from the Sevattur complex (Ackerman et al. 2017). Values for normalization are from Boyton, 1984. Abbreviations: Ap – apatite-rich, carb – carbonatite, Mt – magnetite-rich.

Sample	IC10A	IC10F	IC10I	IC10J	IC11A	IC16A	IC16B
Locality	Sevattur	Sevattur	Sevattur	Sevattur	Sevattur	Sevattur	Sevattur
Rock	carb	carb	carb	Ap-carb	Mt-carb	carb	carb
SiO_2 (wt. %)	0.39	0.2	0.4	3.3	6.18	0.1	< 0.10
TiO_2	0.01	0.11	< 0.01	0.45	0.13	0.01	0.04
Al_2O_3	0.27	0.05	0.04	0.27	0.08	0.03	0.1
Fe_2O_3	0.16	0.06	0.02	1.53	2.03	0.03	0.48
FeO	0.61	0.44	0.29	1.42	1.36	1.1	1.72
MgO	0.71	0.5	0.87	2.01	3.39	3.7	3.39
MnO	0.13	0.12	0.08	0.3	0.26	0.29	0.35
CaO	54.4	54.49	54.1	50.9	46.0	50.5	49.6
Na_2O	0.2	0.05	0.07	0.34	0.3	0.04	0.13
K_2O	0.19	0.02	0.03	0.06	0.07	0.02	0.05
P_2O_5	0.04	0.02	0.99	6.78	1.93	0.97	2.26
F	0.01	0.04	0.07	0.52	0.17	0.07	0.17
CO_2	42.1	44.5	42.2	30.6	37.6	43.6	40.0
S	0.02	bdl	0.01	0.02	0.02	bdl	0.04
H_2O+	0.65	bdl	0.08	0.66	bdl	bdl	0.73
H_2O-	bdl	0.05	0.06	0.41	0.15	0.06	bdl
Total	99.9	99.22	99.27	99.49	99.35	99.47	99.13
Li (ppm)	0.63	0.17	0.11	0.73	1.2	0.05	0.69
Sc	1.7	0.66	2.4	17	23	14	17
V	bdl	2	bdl	90	78	bdl	14
Cr	bdl	bdl	bdl	9	3	bdl	bdl
Co	1.3	0.91	0.87	16	17	1.4	3
Ni	19	21	19	26	14	22	19
Cu	8.5	5.1	0.58	77	18	0.87	2.8
Zn	3.1	24	1.3	27	17	0.23	12
Ga	12	11	12	19	12	9.8	9.1
Rb	3.9	0.8	0.19	0.52	2.5	0.11	1.3
Sr	6268	5845	5805	4958	8007	9008	8847
Y	84	81	81	110	108	89	102
Zr	0.41	0.14	0.74	15	8.1	0.18	1.8
Nb	0.97	0.45	0.17	55	135	1.1	48
Cs	0.14	0.04	0.03	0.04	0.1	0.02	0.1
Ba	2039	2004	1591	4282	1961	2455	2341
La	327	331	329	482	263	239	195
Ce	658	664	682	1004	626	547	486
Pr	69	70	71	106	71	62	57
Nd	262	266	272	408	288	248	237
Sm	44	44	44	70	55	46	49
Eu	12	12	11	18	14	12	13
Gd	40	39	39	59	48	41	42

Tb	4.5	4.4	4.2	6.4	5.5	4.8	5
Dy	19	18	17	25	23	20	21
Ho	3.4	3.3	3	4.2	4	3.6	3.7
Er	8.1	7.7	7	9.4	9.2	8.4	8.9
Tm	0.88	0.82	0.73	1	1	0.95	1
Yb	5.1	5	4.3	5.5	6.2	5.7	6.1
Lu	0.8	0.74	0.65	0.82	0.94	0.88	0.93
Hf	0.14	0.12	0.14	0.87	0.4	0.13	0.22
Ta	0.12	0.08	0.06	3.1	53	0.36	5.5
Pb	48	29	7.3	23	69	19	25
Th	0.18	0.12	1.6	15	0.81	0.16	1.9
U	0.33	0.05	0.18	1.1	77	0.56	23
ΣREE	1453	1465	1484	2199	1414	1238	1125
LaN/YbN	43.2	44.6	51.6	59.1	28.6	28.3	21.6

4.3 Trace element chemistry of mineral phases from LA-ICPMS and EPMA analyses

In order to more closely investigate the distribution of REE in samples from Sevattur and Samalpatti, thin-sections of selected carbonatites, pyroxenites and one albite–epidote metasomatic rock with a high proportion of apatite were analyzed using LA-ICPMS to obtain *in-situ* trace element concentrations in individual grains of apatite, calcite, dolomite, pyroxene, amphibole, titanite and kosmochlor. Major element concentrations were analyzed using EPMA thereafter next to LA spots to obtain bulk chemical composition of the studied grains and F contents in apatites. The final data are reported as mean concentrations for clarity and the individual chemical analyses are listed in Supplementary Tables 1-4.

4.3.1 Apatites

Apatites from five carbonatite samples were analyzed, one from Samalpatti (IC05F) and four from Sevattur (IC10A1, IC10E, IC11A, IC16A). The EPMA analyses have revealed that carbonatites from Sevattur are more apatite-rich than those from Samalpatti. Further, apatites from two pyroxenites (IC05C, IC07D) and one albite–epidote metasomatic rock (IC07A) from Samalpatti were analyzed because, unlike carbonatites, silicate rocks from Sevattur are apatite-poor. Their average compositions obtained by EPMA are used for further investigation and are listed in Table 9. Major element concentrations in the analyzed apatites do not display a large variability and all analyzed grains from both localities can be classified as fluorapatites with F contents varying from 2.1 to 3.9 wt.% (Table 9). In further discussion, we use the term 'apatite' for better text clarity. Contents of P_2O_5 vary between 40.4 and 43.1 wt.% with higher P_2O_5 contents found for samples from Sevattur. In contrast, Samalpatti apatites show higher CaO contents (54.1–56.0 wt.%).

Trace element concentrations in apatites from carbonatites vary significantly between both complexes and even between individual samples. Apatites from Sevattur are more enriched in almost all trace elements compared to apatites from Samalpatti, mainly in Sr (4,007–6,706 vs. 248 ppm) and ΣREE

(5,665–19,487 vs. 98.1 ppm) where the differences in trace element concentrations are most striking (Fig. 19). In contrast, apatites from Samalpatti are generally more enriched in high-field strength elements (HFSE) than apatites from Sevattur. Apatites from sample IC05F have the highest concentrations of U (176 vs. 3.0–30.2 ppm), Zr (21.8 vs. 0.17–1.8 ppm) and Ti (25.0 vs. 4.4–8.6 ppm) of all apatites from carbonatites with no apparent presence of inclusions containing these specific elements.

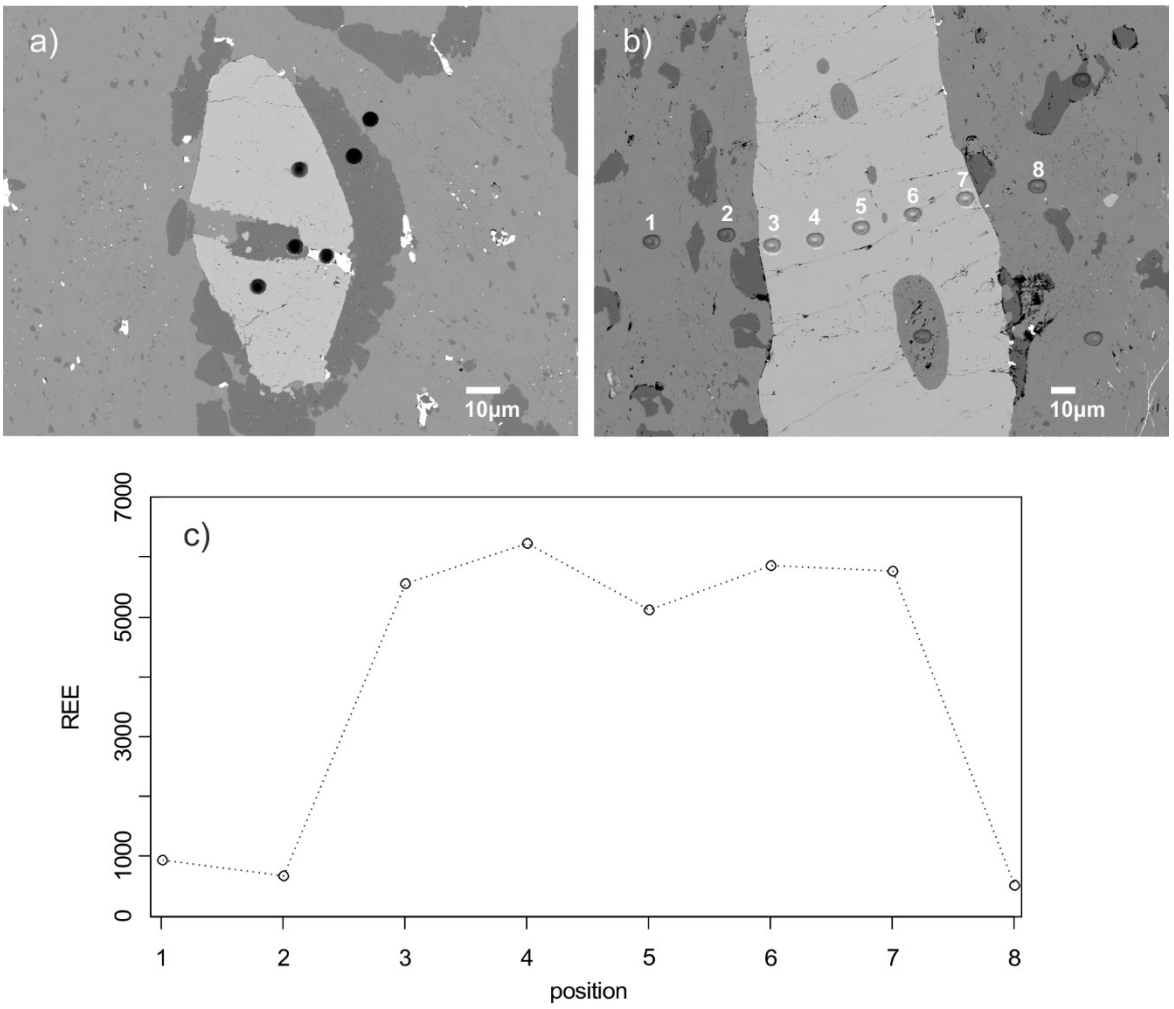

Figure 18. EPMA microphotographs of thin-sections following in-situ LA analyses. (a) Large grain of apatite from sample IC16A with dolomite rim in calcite matrix. (b) A profile across large apatite grain in sample IC11A (Table X) with the changes in the REE concentration shown in parallel (c). Calcite (spots 1,2,8) is significantly depleted in REE compared with the coexisting apatite (spots 3–7), which displays the highest concentration between the core (5) and rims (3, 4, 6, 7).

Apatites from silicate rocks from Samalpatti (pyroxenites IC05C and IC07D, and albite–epidote metasomatic rock IC07A) have variable trace elements concentrations. Trace element concentrations in apatites from IC05C and IC07D differ significantly, which could perhaps reflect differences in the bulk chemistry of these samples (see Ackerman et al. 2017). Apatite from IC05C has low contents, relative to apatite IC07A and IC07D, of Sr (191 vs. 1,350 and 1,644 ppm) and ΣREE (371 vs. 646 and 1,530 ppm). It also has higher content of V (55.7 vs. 15.1 and 16.4 ppm), Co (8.6 vs. 1.68

and 0.10 ppm), Zn (9.8 vs. 1.9 and 0.66 ppm), Zr (14.5 vs. 2.1 and 1.2 ppm), and mainly Th (289 vs. 42.5 and 37.4 ppm) and U (73.9 vs. 8.7 and 7.9 ppm). Apatite from IC07A has trace element concentrations similar to IC07D, only with depletion in LREE. Apatites from pyroxenite IC05C are similar to apatites from carbonatite IC05F1 in that they both are rich in U, Zr and both have low ΣREE, Y and Sr (Table 9). Combined with petrographic observations, there is no obvious link between the contents of REE and other trace elements in apatite and position of the individual apatite grains in the thin section, i.e., the surrounding minerals (calcite, pyroxene, titanite, dolomite) do not seem to affect trace element concentrations in apatite.

Table 9. Average major and trace element concentrations in apatites. Abbreviations: alb–ep – albite–epidote metasomatic rock, carb – carbonatite, Mt – magnetite-rich.

Sample	IC05C	IC05F	IC07A	IC07D	IC10A1	IC10E	IC11A	IC16A
Locality	Samalpatti	Samalpatti	Samalpatti	Samalpatti	Sevattur	Sevattur	Sevattur	Sevattur
Rocktype	pyroxenite	carb	alb–ep	pyroxenite	carb	contact	carb	carb
	n=18	n=8	n=9	n=11	n=3	n=9	n=27	n=16
SiO_2 (wt. %)	0.50	0.49	0.17	0.11	0.18	0.44	0.05	0.04
CaO	55.92	55.98	56.00	55.81	54.85	54.65	54.13	54.81
P_2O_5	40.41	41.76	41.82	43.07	42.15	42.00	42.39	42.55
Na_2O	0.12	0.18	0.01	0.01	0.16	0.09	0.24	0.25
MgO	0.06	0.07	0.00	0.00	0.00	0.01	0.05	0.07
FeO	0.24	0.06	0.05	0.01	0.09	0.05	0.05	0.09
MnO	0.03	0.01	0.02	0.02	0.03	0.04	0.73	0.04
F	2.06	2.63	2.12	2.30	2.35	3.94	2.41	2.49
Li (ppm)	2.50	1.32	1.96	0.54	0.00	2.13	0.14	0.61
Be	0.09	0.11	0.04	0.05	0.04	0.09	0.06	0.05
Sc	0.41	0.09	0.20	0.06	1.27	0.17	0.94	1.21
Ti	49.0	25.0	6.39	8.38	4.42	6.80	8.60	5.10
V	55.7	13.3	15.1	16.4	4.11	12.3	9.59	4.60
Cr	0.51	1.49	2.60	0.76	1.04	0.91	0.71	0.49
Co	8.64	0.11	1.68	0.10	0.30	0.10	3.51	0.24
Ni	0.63	1.20	1.21	0.00	0.39	0.24	0.15	0.04
Cu	0.70	2.35	0.60	0.08	4.45	2.41	1.04	0.15
Zn	9.80	4.39	1.91	0.66	2.90	1.69	2.17	2.12
Ga	1.07	0.49	1.71	3.37	44.1	15.0	13.2	12.9
Rb	0.67	1.13	0.34	0.04	0.17	0.30	0.12	0.06
Sr	191	248	1350	1644	5762	4007	6580	6706
Y	43.3	7.72	101	102	492	300	256	226
Zr	14.5	21.8	2.05	1.16	0.17	1.23	1.82	1.67
Nb	1.22	0.14	0.03	0.02	0.51	0.17	5.62	0.33
Cs	0.09	0.07	0.01	bdl	0.02	bdl	0.01	0.02
Ba	0.49	70.3	16.0	56.2	689	82	107	105
La	46.3	19.7	102	284	4805	1730	1087	1010
Ce	134	43.5	246	634	8974	3074	2713	2448
Pr	20.3	5.14	32.2	80.2	979	306	348	316

Nd	99.5	19.2	148	357	3480	1119	1470	1323
Sm	22.7	3.36	32.9	63.5	543	144	258	227
Eu	4.50	0.75	9.82	13.0	120	31.3	60.4	52.8
Gd	18.7	2.65	31.0	51.1	337	110	186	162
Tb	2.16	0.34	3.53	4.87	32.0	11.2	18.5	16.2
Dy	11.4	1.81	19.2	23.3	137	59.2	81.5	70.7
Ho	1.91	0.30	3.52	3.84	18.6	10.7	11.2	9.6
Er	4.61	0.72	9.11	8.64	36.7	27.5	21.4	18.4
Tm	0.58	0.08	1.16	0.95	3.88	3.55	2.15	1.82
Yb	3.41	0.44	6.78	5.06	19.7	22.6	10.2	8.63
Lu	0.47	0.05	0.89	0.66	2.18	3.18	1.13	0.97
Hf	0.07	0.12	0.01	0.02	0.02	0.04	0.03	0.01
Ta	0.02	0.01	0.00	0.00	0.01	0.00	0.17	0.00
W	1.62	1.32	1.49	2.91	0.17	3.08	0.12	0.01
Pb	24.4	9.86	6.95	6.57	73.9	24.9	10.7	9.44
Th	289	90.0	42.5	37.4	116	129	48.0	32.2
U	73.9	176	8.73	7.89	30.2	11.0	5.20	3.02
ΣREE	371	98.1	646	1530	19487	6652	6267	5665
$(La/Yb)_N$	9.15	30.2	10.2	37.9	164	51.7	72.1	78.9
$(La/Sm)_N$	1.28	3.70	1.96	2.82	5.57	7.57	2.66	2.80

Chondrite-normalized mean values of apatite grains show enrichments in LREE compared to HREE from both localities, apparent in La_N/Yb_N values (from 9.15 to 164). Apatites from Sevattur are more enriched in REE than apatites from Samalpatti (Fig. 19), most likely reflecting a LREE-rich character of the entire Sevattur suite (Ackerman et al. 2017; this study). However, REE patterns in individual samples display several distinctive trends (Fig. 19). Samples IC10A1 and IC05F show smooth REE profiles and a steady decrease in REE concentrations. Samples IC05C, IC07D, IC11A and IC16A display less steep patterns from La to Nd while the slopes of HREE are more or less identical to those of IC10A1 and IC05F. Sample IC10E displays a similar LREE pattern as IC10A1 and IC05F but it also shows a flat HREE pattern. A mildly negative Eu anomaly has been found for nearly all apatites and only the apatite in IC07A shows absent Eu anomaly.

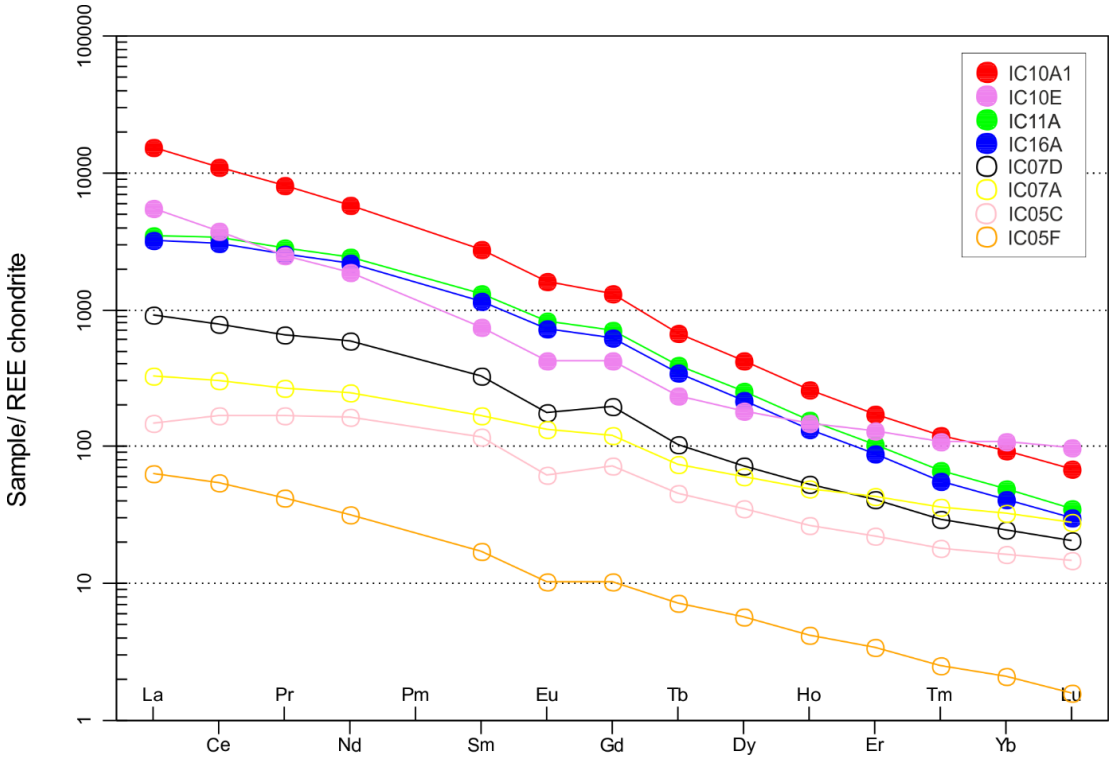

Figure 19. Chondrite normalized REE patterns of the average apatite. Closed symbols represent samples from Sevattur and open symbols represent those from Samalpatti. Chondrite values are taken from Boyton (1984).

Core-to-rim profiles of REE in apatites from Sevattur and Samalpatti are listed in Tables 10a and 10b and plotted in Fig. 18c. The results indicate that most grains display a homogeneous distribution of REE with no preferential enrichment in either core or rim. Subtle differences between core and rim concentration data have been found for several apatite grains. The most apparent difference is found for IC07A grain #2, where the rim has almost twice as much REE as the core. On the other hand, the core in IC16A grain #2 is significantly enriched in ΣREE relative to the rim (8,193 vs. 4,805 ppm) while the grain #3 from the same sample has almost identical ΣREE concentrations in both core and rim (4,401 vs. 4,471 ppm).

Table 10a, b. Core-to-rim profiles of REE, Y and Sr across apatite grains. Abbreviations: alb–ep - alkali albite–epidote metasomatic rock.

Sample	IC07A				IC07D				IC10E					IC011A			
Locality	Samalpatti				Samalpatti				Sevattur					Sevattur			
Rocktype	alb–ep				pyroxenite				contact					carbonatite			
Grain n.	1	1	2	2	1	1	2	2	1	1	1	2	2	1	1	2	2
Position	core	rim	core	rim	core	rim	core	rim	core	rim	rim	core	rim	core	rim	core	rim
La (ppm)	98.73	64.42	82.22	202	176	185	361	266	1574	2073	1837	2062	1334	1202	1245	1141	939
Ce	264.18	182.94	229.36	493	449	459	808	603	2842	3531	3290	3897	2658	2898	3058	2831	2295
Pr	35.85	25.53	33.5	63.3	59.1	58.2	101	78.4	286	343	329	395	286	374	390	361	296
Nd	167.41	124.79	160.94	284	278	261	435	345	1059	1222	1186	1484	1098	1523	1652	1540	1231
Sm	36.8	32.8	37.58	55	51.2	47.5	74.6	60.8	137	153	152	198	151	265	283	259	211
Eu	9.71	10.3	11.13	14.2	10.9	10.1	15.5	13.7	30	32.3	33.2	44.4	35.1	61.5	65	60.4	49.6
Gd	32.88	32.26	35.64	48.8	43.9	37.6	58.2	49	105	113	117	153	118	186	205	191	154
Tb	3.84	3.74	3.96	5.33	4.17	3.59	5.53	4.69	10.8	11.7	11.9	15.6	12.3	18.9	20.3	18.6	15.2
Dy	20.5	21.25	21.68	27.8	20.1	17.7	25.9	22	56.9	60.4	62.9	83.9	65.6	82.1	88.5	81.6	68
Ho	3.75	3.87	3.9	5.15	3.32	2.96	4.27	3.66	10.3	10.8	11.3	15.1	12.1	11.4	12	11	9.38
Er	9.54	9.94	10.4	13.17	7.47	6.82	9.6	8.53	25.9	27.8	28.9	39.1	31.3	22.4	23.2	21.3	18
Tm	1.24	1.27	1.32	1.7	0.84	0.75	1.05	0.91	3.36	3.58	3.75	5.13	4.08	2.21	2.35	2.09	1.83
Yb	7.34	7.44	7.57	10.2	4.54	4.17	5.47	5.08	21.26	22.73	23.68	32.93	26.2	10.82	11.07	10.21	8.87
Lu	0.97	0.97	1.01	1.33	0.59	0.56	0.74	0.66	3.04	3.12	3.35	4.66	3.77	1.19	1.2	1.13	1.03
Sr	1514	1280	1260	1491	1358	1309	1818	1483	3938	4215	4010	4106	4242	6532	6474	6893	6696
Y	111	110	112	151	92.2	79	106	100	285	300	312	440	332	261	281	264	213
ΣREE	400	693	640	1225	1109	1095	1905	1462	6165	7609	7090	8431	5834	6657	7057	6529	5299

Table 10b.

Sample	IC16A										IC11A - profile				
Locality	Sevattur										Sevattur				
Rocktype	carbonatite										carbonatite				
Grain n.	1	1	1	2	2	3	3	4	4	4	5	5	5	5	5
Position	core	rim	rim	core	rim	core	rim	core	rim	rim	rim		core		rim
La (ppm)	1045	1172	916	1477	800	724	807	1099	876	1008	1001	1136	933	1083	1029
Ce	2498	2712	2188	3536	2025	1767	1944	2682	2089	2399	2425	2745	2236	2581	2518
Pr	317	338	284	451	268	228	248	353	267	308	305	338	283	317	315
Nd	1314	1391	1172	1928	1160	948	1024	1440	1104	1301	1280	1409	1173	1327	1340
Sm	218	228	202	325	216	166	176	247	188	223	226	240	198	227	230
Eu	52.5	53.2	46.6	75.4	51.9	39.1	41.2	57.1	44.2	50.8	51.7	55.4	46.7	52.5	54.3
Gd	156	168	147	230	159	120	126	175	137	159	158	172	146	164	171
Tb	15.6	16.6	15.1	22.5	16.0	12.3	12.9	17.2	13.9	16.0	15.8	17.0	14.4	15.9	16.3
Dy	67.8	73.0	66.4	96.0	69.9	54.6	57.7	75.6	63.4	69.7	69.8	75.2	62.9	70.6	72.4
Ho	9.36	10.0	9.13	13.0	9.48	7.46	7.89	10.3	8.53	9.51	9.71	10.5	8.71	9.77	9.89
Er	17.9	19.0	17.8	24.5	18.5	14.7	15.8	19.3	17.1	18.0	18.7	20.0	16.6	18.8	19.4
Tm	1.78	1.93	1.79	2.37	1.81	1.48	1.59	1.93	1.72	1.86	1.86	2.01	1.68	1.87	1.91
Yb	8.29	9.24	8.90	10.8	8.71	7.09	7.68	8.71	8.55	8.71	8.76	9.56	8.07	8.88	8.99
Lu	1.02	0.95	1.00	1.15	1.02	0.82	0.89	1.01	0.97	1.00	0.97	1.08	0.91	0.96	1.01
Sr	6037	6511	7196	7945	7151	6515	7047	6570	7194	6862	6780	6735	5795	6215	6185
Y	220	236	219	306	217	182	189	233	205	233	224	235	198	221	225
ΣREE	5722	6194	5076	8193	4805	4091	4471	6189	4819	5573	5573	6232	5130	5877	5787

4.3.2 Calcites and dolomites

Major element concentrations in calcites do not vary greatly (CaO between 49.6 and 52.8 wt.%, MgO between 0.66 and 2.7 wt.%; Table 11). However, trace element abundances show a significant variability between the individual samples, with samples from Sevattur generally displaying higher concentrations of trace elements. This is in accord with bulk sample data (Ackerman et al. 2017). In particular, Sr, Ba and REE vary on the order of several magnitudes between Sevattur and Samalpatti. Strontium contents range between 22 and 9,646 ppm, Ba contents between 2.9 and 1,672 ppm, and ∑REE is between 22.5 and 1,683 ppm. Trace element concentrations in calcites from Samalpatti almost do not vary, even though lithologically diverse pyroxenite IC05C and carbonatite IC05F were analyzed. Calcites from pyroxenite IC05C and carbonatite IC05F have completely different chondrite-normalized REE patterns compared to other calcite analyses (Fig. 20). The pattern of IC05C is generally flat with a slight increase in HREE.

Dolomites were only present in samples IC11A and IC16A from Sevattur and display a mutually almost identical chemical composition and trace element abundances. Compared to calcite, they are enriched in Zn (>28 vs. <8 ppm) and Co (4.9–5.4 vs. 0.08–2.6 ppm). Their ∑REE contents are slightly lower than those found in co-existing calcite (283 and 247 ppm vs. 779–1,683 ppm) but higher than those measured for calcite from Samalpatti (52.9 and 22.5 ppm). REE profiles of dolomite from IC16A and IC11A are flatter compared with the coexisting calcites. Dolomites from sample IC11A display the highest Nb content from all carbonate and non-carbonate minerals (17.6 ppm), indicating that Nb enrichment is intrinsic to carbonate and not merely to any accompanying silicate phase.

Table 11. Mean major and trace element concentrations of calcites and dolomites. Abbreviations: bdl – bellow detection limit, carb – carbonatite, Mt – magnetite-rich.

Sample	IC05C	IC05F	IC10A1	IC11A	IC11A	IC16A	IC16A
Locality	Samalpatti	Samalpatti	Sevattur	Sevattur	Sevattur	Sevattur	Sevattur
Rocktype	pyroxenite	carb	carb	carb	Mt-carb	carb	carb
Mineral	calcite	calcite	calcite	calcite	dolomite	calcite	dolomite
	n=10	n=12	n=4	n=20	n=5	n=7	n=4
SiO_2 (wt. %)	0.03	0.02	0.02	0.01	0.02	0.03	0.02
CaO	52.76	53.64	51.81	51.81	28.66	51.89	29
P_2O_5	0.16	0.14	0.14	0.04	0.01	0.15	0.1
Na_2O	0	0.01	0.02	0.02	0.01	0.02	0.01
MgO	1.12	1.02	0.66	1.02	18.1	0.88	17.48
FeO	0.76	0.12	0.88	0.69	3.94	0.66	4.09
MnO	0.1	0.01	0.2	0.15	0.36	0.25	0.45
Li (ppm)	bdl	bdl	bdl	bdl	bdl	bdl	bdl
Be	0.11	0.04	0.02	0.04	0.1	0.03	0.03
Sc	1.8	0.3	2.3	14.5	13.9	20	15.2
Ti	4.02	2.52	0	0.87	0.62	0.29	0
V	1.71	0.58	0.19	0.76	3.4	1.18	6.18

Cr	1.77	1.46	9.45	1.94	2.37	1.85	2.86
Co	2.1	0.08	0.35	2.42	4.89	0.53	5.39
Ni	3.83	0.11	4.18	0.37	0.22	0.09	0.7
Cu	3.03	0.03	0.73	1.11	1.15	0.45	0.08
Zn	5.19	2.15	3.92	5.11	30.8	2.88	28.4
Ga	0.11	0.05	3.66	1.3	0.61	1.64	0.57
Rb	0.01	0.07	0.05	0.06	0.02	0.11	0.29
Sr	229	254	7325	9140	3975	9646	4281
Y	13	3.64	126	105	14.9	115	12
Zr	0.33	0.78	0.1	0.11	0.32	0.02	0.04
Nb	0.02	0.01	0.02	2.2	17.6	0.15	0.07
Cs	0	0	0.01	0.01	bdl	bdl	0.02
Ba	2.92	37.5	1277	1834	151	1145	163
La	6.42	4.83	384	99.4	59	92	53.5
Ce	17.2	9.46	735	252	125	277	112
Pr	2.54	1.08	82.9	34.5	14.5	42.4	12.8
Nd	12.9	4.03	315	158	57.5	205	47.4
Sm	3.09	0.76	54	37.8	9.8	51.1	7.88
Eu	0.71	0.15	14.1	10.4	2.42	13.5	1.89
Gd	3.21	0.63	41.7	34.8	7.21	43.3	5.73
Tb	0.4	0.09	4.94	4.31	0.79	5.17	0.62
Dy	2.46	0.61	26.6	23.1	3.74	26.2	2.94
Ho	0.5	0.12	4.39	3.88	0.58	4.12	0.45
Er	1.41	0.32	10.7	9.35	1.3	9.45	0.99
Tm	0.21	0.05	1.37	1.19	0.16	1.18	0.12
Yb	1.57	0.32	8.22	7.42	0.94	7.28	0.76
Lu	0.26	0.05	1.1	1.05	0.13	0.99	0.1
Hf	bdl	bdl	bdl	0.01	0.01	0.02	bdl
Ta	bdl	bdl	bdl	0.02	0.02	bdl	bdl
W	0.04	0.02	0.01	0.08	0.01	0.01	0.01
Pb	5.37	4.28	95.9	24	4.88	15.9	5.03
Th	5.55	3.25	1.33	0.11	0.11	1.32	bdl
U	1.38	5.19	0.24	1.12	1	0.24	0.04
ΣREE	52.9	22.5	1684	677	283	779	247
La_N/Yb_N	2.76	10.2	31.5	9.03	42.32	8.52	47.4
La_N/Sm_N	1.31	4	4.47	1.65	3.79	1.13	4.27

The chondrite-normalized REE patterns for calcite and dolomite from carbonatites from Sevattur are generally parallel to patterns for Sevattur apatites, best observed for IC10A1, where the patterns are almost identical (Fig. 20). The HREE profile of pyroxenite IC05C is similar to that of carbonatite IC05F, while LREE appear to be somewhat more depleted in IC05C (Fig. 20). Sample IC05F displays a decrease in LREE, similar to some calcites and dolomites from Sevattur whilst the HREE pattern is flatter. Both samples show a greater extent of Eu depletion relative to other calcite/dolomite samples.

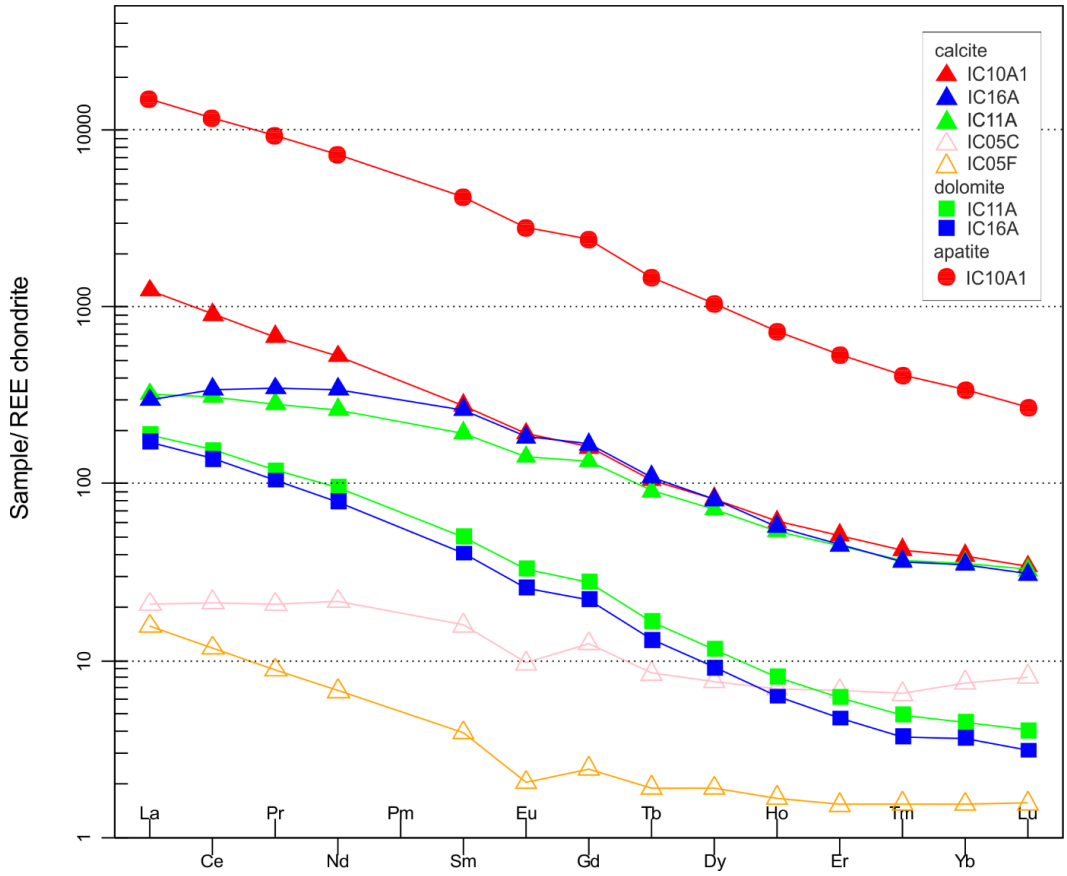

Figure 20. Chondrite-normalized REE patterns of the mean REE concentrations in calcite and dolomite, with the apatite IC10A1 values added for comparison. Closed and open symbols represent samples from Sevattur and Samalpatti, respectively. Chondrite values are taken from Boyton, 1984.

4.3.3 Kosmochlor

Major element concentrations in kosmochlor were analyzed using EPMA in order to characterize this rare Na–Cr-rich pyroxene. It was found in two silicocarbonatite samples IC03B and IC04A, but it is expected to be present also in other silicocarbonatites (samples IC03A, IC03D, IC03E and IC06E) because all of these samples have high Cr contents. Kosmochlor is determined by its Cr_2O_3 content, which is 33.46% Cr_2O_3 for the pure end member composition. It forms a solid solution with other pyroxene end members, diopside ($MgCaSi_2O_6$) and aegirine ($NaFeSi_2O_6$) (Fig. 21).

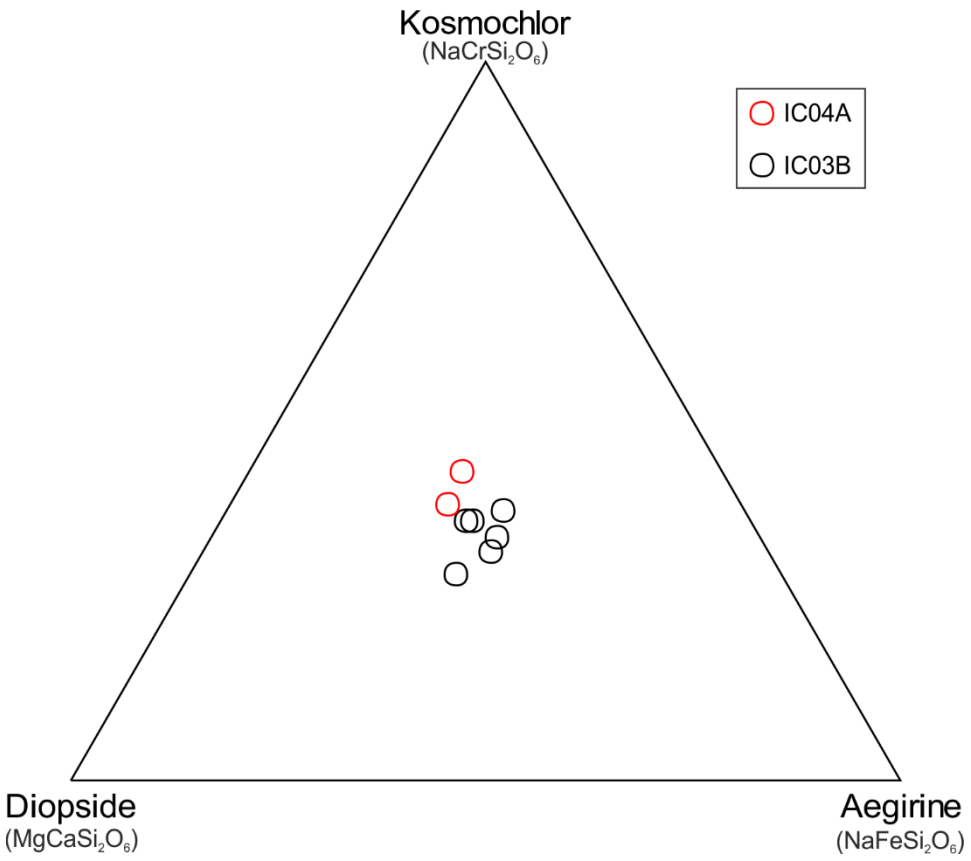

Figure 21. Ternary diagram of kosmochlor composition with the pyroxene end member compositions.

The presence of kosmochlor is somewhat enigmatic. Rosenthal et al (2014) proposed in their experimental study that kosmochlor could be formed in the reaction zone layer (RZL) between eclogitic melt and peridotitic mantle according to the following reaction:

$(Ca,Mg)_3(Cr,Fe^{3+})_2Si_3O_{12} + 2NaAlSi_2O_6 = 2Na(Cr,Fe^{3+})Si_2O_6 + (Ca,Mg)_3Al_2Si_3O_{12}$

[Cr–Fe^{3+}garnet (peridotite) + jadeite (eclogitic melt) = kosmochlor/acmite (RZL) + grossular (RZL)].

Kosmochlor grains analyzed in this study fall into the middle composition of the proposed ternary diagram (Fig. 21), supporting the existence of solid solutions over a range of natural compositions. The analyzed kosmochlor grains from IC03B and IC04A have Cr_2O_3 contents from 9.8 to 12.8 wt. %, and between 13.2 and 14.6 wt. %, respectively (Table 12). Elevated Cr contents in kosmochlor from IC04A reflects a higher Cr content in the bulk sample IC04A (1,803 ppm Cr) relative to IC03B (1,285 ppm Cr; Ackerman et al. 2017). Most kosmochlor grains investigated in this study were small (usually micron-size) and only one grain from IC03B was suitable for trace element measurements by means of laser ablation analysis. The single analysis showed that kosmochlor does not show

any particular enrichments in trace elements (∑REE = 9.2 ppm; La_N/Yb_N = 11.5), with the exception of Ti (6,134 ppm) and Zn (2,193 ppm).

Table 12. Major elements of kosmochlor analyzed by EPMA.

Sample	IC03B						IC04A	
Locality	Samalpatti						Samalpatti	
Rocktype	silico-carbonatite						silico-carbonatite	
Mineral	K	K	K	K	K	K	K	K
Na_2O (wt. %)	8.77	9.02	9.40	9.10	8.08	8.91	9.13	8.63
K_2O	0.00	0.01	0.00	0.01	0.00	0.00	0.00	0.00
CaO	9.38	8.74	8.09	8.66	10.68	8.98	8.57	9.38
MgO	6.16	6.03	5.22	5.73	7.08	6.04	5.62	6.37
MnO	0.02	0.04	0.05	0.02	0.04	0.02	0.04	0.03
FeO	7.38	8.73	8.10	8.44	8.24	7.60	6.02	6.82
Al_2O_3	0.80	0.93	1.39	1.45	0.77	0.84	0.82	0.81
SiO_2	53.69	53.63	53.65	53.74	53.92	53.95	53.75	53.77
TiO_2	0.41	0.85	0.11	0.12	0.29	0.40	0.26	0.22
Cr_2O_3	12.38	10.90	12.79	11.55	9.82	12.40	14.61	13.15
F	bdl	0.01	bdl	bdl	bdl	bdl	bdl	bdl
Total	99.01	98.89	98.80	98.80	98.92	99.14	98.81	99.19

4.3.4 Titanite, amphibole and Nb–Ta phase

Several titanite grains were identified in samples IC03B and IC10E, which were suitable for LA-ICPMS analysis of trace element inventory. The individual chemical analyses are listed in the Supplementary Table 4. Two grains from IC10E show elevated REE contents (∑REE = 6,922 and 19,809 ppm) while those from IC03B have ∑REE between 607 and 1,450 ppm. The REE patterns show convex-upward profiles for titanites from both samples, but they are more distinct for titanites from sample IC03B with a slightly more pronounced La–Ce loss in titanites from IC03B (Fig. 22). All analyzed grains are uniformly enriched in Nb (1,137–18,288 ppm) while only titanite from IC10E shows a parallel enrichment in Ta (>425 ppm). These analyses indicate that titanite may be the main carrier of Nb in the sample IC03B, and possibly in all silicocarbonatites. Trace element patterns of titanites from IC03B (Fig. 23) display a strong enrichment in Nb, but a general depletion in other HFSE elements – Zr, Hf and even Ta, which generally is a strong geochemical twin with Nb. In contrast, titanites from IC10E are not that significantly depleted in HFSE and Ta is even more enriched than Nb. They also have higher concentrations of all trace elements than titanite from IC03B, with the exception of Ba.

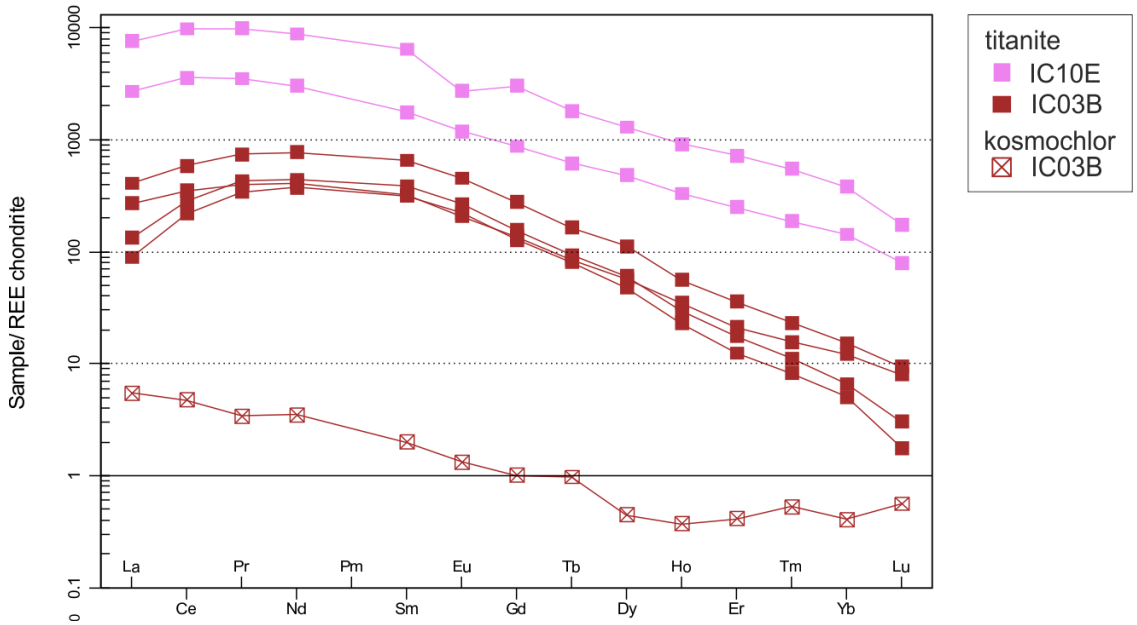

Figure 22. Chondrite-normalized REE patterns of titanites and one kosmochlor. Chondrite values are taken from Boyton, 1984.

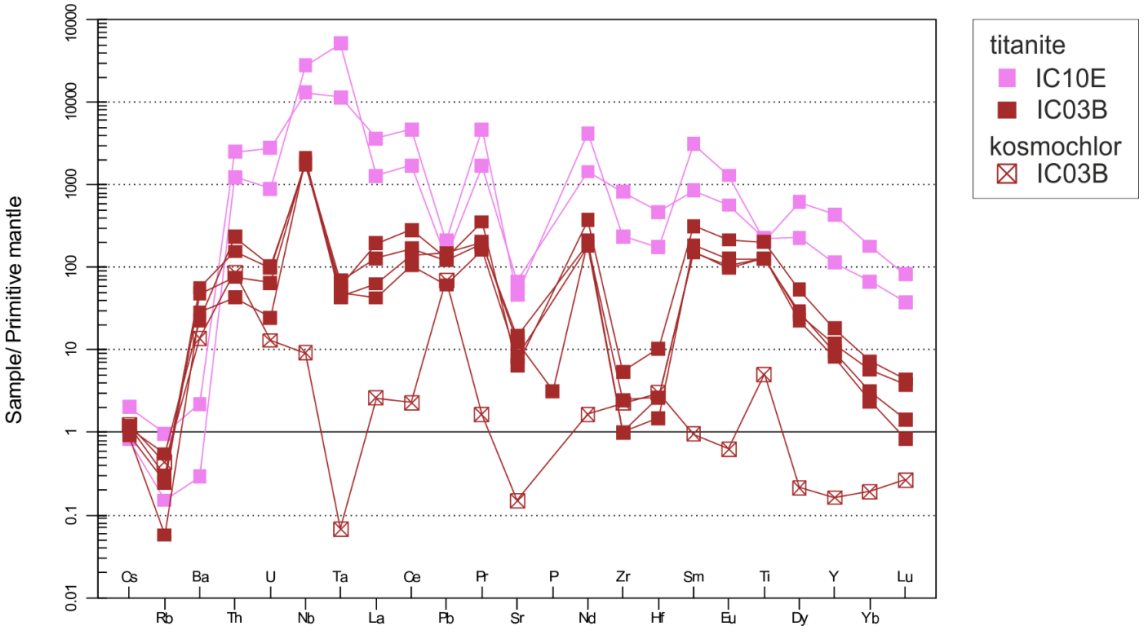

Figure 23. Extended spider plot of trace element concentrations in titanites and one kosmochlor. Primitive mantle values are taken from McDonough and Sun, 1995.

Amphibole was analyzed in samples IC10A1, IC10G and IC03B. In all investigated cases, it has rather low contents of trace elements with the exception of elevated concentrations of HFSE. The ∑REE is <105 ppm for all analyzed grains and two analyses of amphibole from IC03B have ∑REE <4 ppm. The individual chemical analyses are also listed in the Supplementary Table 4. The REE patterns are variable. Sinusoidal patterns with higher concentrations of LREE compared to HREE prevail in amphiboles from IC10G. The REE patterns for amphiboles from other samples are less regular because these amphiboles contain very little REE (Fig. 24). Amphiboles from both IC10A1 and IC10G are enriched in HFSE, but in amphiboles from IC03G, the HFSE are depleted while they are strongly enriched in Pb (Fig. 25).

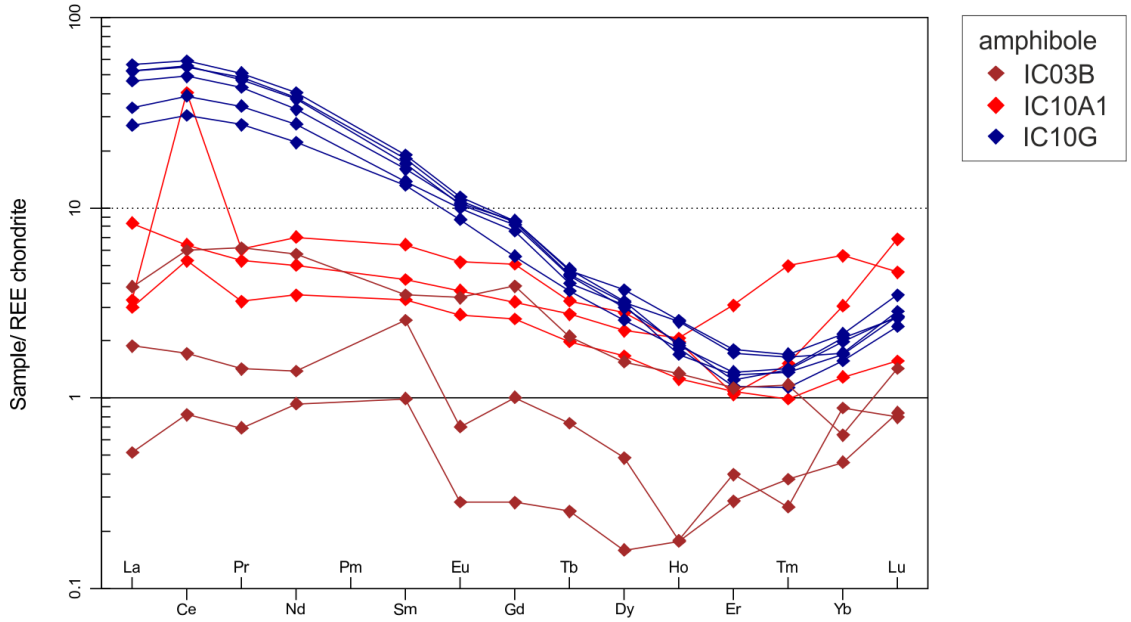

Figure 24. Chondrite-normalized REE patterns of amphiboles. Chondrite values are taken from Boyton, 1984.

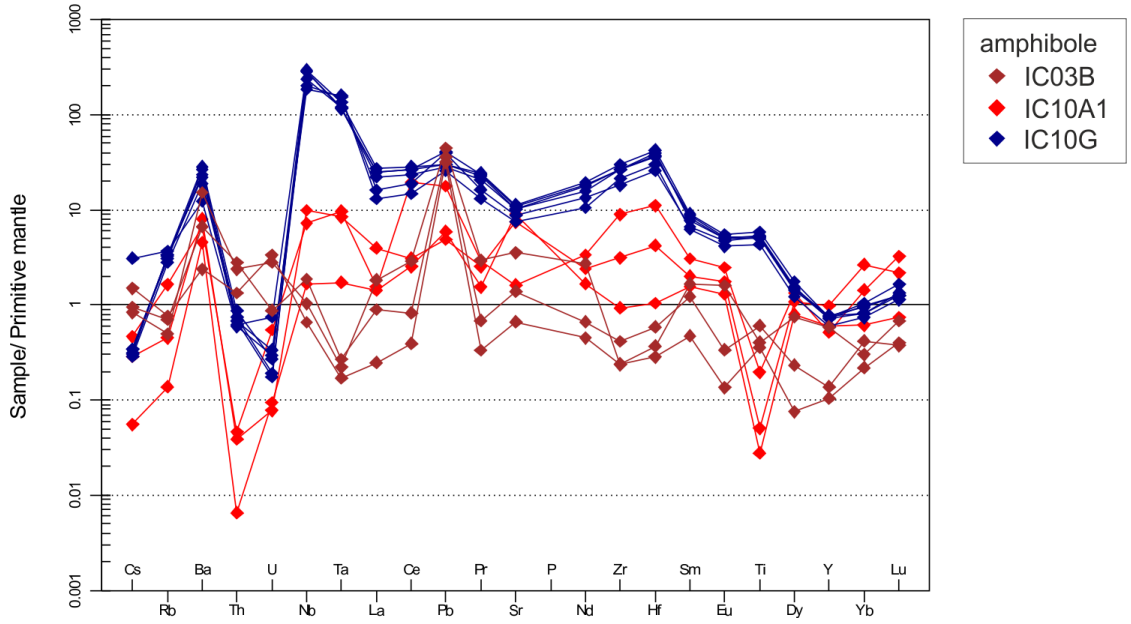

Figure 25. Extended spider plot of trace element concentrations in amphiboles. Primitive mantle values are taken from McDonough and Sun, 1995.

In sample IC11A two grains of U-rich minerals belonging to the pyrochlore group were found. An ideal formula of pyrochlore is $NaCaNb_2O_6F$. Based on the LA-ICPMS analysis, these pyrochlores have up to 6 wt.% U and 1.9 wt.% REE (from which 1.1 wt.% is Ce) (Supplementary Table 4). Unfortunately, a precise determination of specific mineral chemistry using EPMA was impossible due to unsuitable surface. However, it is probably the same type of pyrochlore already described from Sevattur carbonatites by Viladkar and Bismayser (2014), which is similar to uranopyrochlore [nominally $(U,Ca,Ce)_2(Nb,Ta)_2O_6(OH,F)$] described by Hogarth (1977). The high Ta and Nb abundances have been confirmed with the new LA-ICPMS measurements showing up to ~120,000 ppm Ta and ~194,000 ppm Nb (Table 13).

Three EPMA analyses of Mckelveyite-(Nd) were performed because no grain large enough for the LA-ICPMS analysis was revealed. (Table 14). They are listed in Table X and show high concentrations of SrO (up to 16.0 wt. %), La_2O_3 (up to 10.0 wt. %) and Ce_2O_3 (up to 24.2 wt. %).

Table 13. Major elements of Mckelveyite-(Nd) analyzed by EPMA. Rest to the 100% sum are volatile components like CO3 and H2O.

Sample	IC10F		
Locality	Sevattur		
Rocktype	carbonatite		
Mineral	Mc	Mc	Mc
SrO (wt. %)	14.825	14.545	16.024
La_2O_3	8.879	9.348	9.959
Ce_2O_3	24.067	23.792	24.202
CaO	0.777	0.931	1.387
BaO	0.114	bdl	bdl
FeO	0.706	1.524	0.725
MgO	bdl	0.115	bdl
Total	49.368	50.255	52.297

5. INTERPRETATION AND DISCUSSION

The whole-rock geochemical data mainly reflects the mineralogical variety of these two studied complexes (Ackerman et al. 2017). The new study confirms these earlier findings and identifies mineral phases responsible for the enrichments in incompatible elements as well as their major carrier phases using in-situ LA-ICPMS analyses combined with EPMA data.

5.1 Constraints on the behavior of trace elements in carbonatite systems

It is apparent that, given the modal abundance of individual crystal phases, apatite carries the highest proportion of REE, followed by calcite and dolomite (Tables 9 and 11; Figs. 19 and 20). However, calcite is significantly more abundant than apatite and REE in some calcite samples are rather high (e.g., IC10A1). Therefore, apatite in some cases will not be the sole REE carrier and other major phases must also be taken into account. This is apparent from the results for titanite and Nb–Ta-rich phase, which could under some circumstances carry a non-negligible portion of REE and other trace elements. From analyses of REE-rich P_2O_5-poor samples IC10A and IC10F it also follows that beside apatite, other phases may carry large amounts of REE.

We note that despite the large range in REE concentrations of apatites, the chondrite-normalized patterns are rather similar (Fig. 19) irrespective whether the apatites are from calciocarbonatites or silicocarbonatites. Accordingly, no difference in REE profiles is found for Sevattur versus Samalpatti. Subtle LREE depletion is observed for a subset of apatites from both carbonatite complexes (Fig. 19) and is therefore independent of possible post-emplacement low-temperature histories, as disclosed by recent studies (Ackerman et al. 2017; Magna et al. in preparation). This appears to be in contrast with distinctive REE patterns reported from, for example, terrestrially surface-weathered meteorites (Crozaz et al. 2003) where remobilization due to extensive exchange with low-temperature fluids has led to modification of the original REE profiles. Chondrite-normalized REE patterns for calcites and dolomites are more variable than those for apatites. In particular, calcites from Samalpatti show less regular profiles (Fig. 20). LREE profiles of calcites and dolomites from Sevattur mutually differ but HREE profiles are rather similar. This illustrates a relatively constant partitioning of HREE between calcite and dolomite while different LREE patterns could reflect either different partitioning of LREE between calcite and dolomite, or different susceptibility/resistance of mineral phases to alteration processes. Patterns of calcite from Samalpatti are generally flat, so they may have underwent remobilization of REE by hydrothermal processes (see section 5.1.3).

5.1.1 High-field strength elements

The high-field strength elements (HFSE) generally have high charge/ionic radius ratios (Z/r >2) and form a peculiar group of elements (Hf, Zr, Ti, Nb and Ta), typically incompatible in magmatic process (Rowlinson, 1983). However, they have significantly different thermodynamical properties, so that even the geochemically similar pairs Nb–Ta and Zr–Hf behave in different ways in magmas and hydrothermal fluids (Chakhmouradian, 2006).

Apatites analyzed in this study are depleted in HFSE (Fig. 26). The in-situ LA-ICPMS data largely reflect bulk-rock data of Ackerman et al. (2017) in that the most REE-rich samples show the greatest depletion in HFSE.

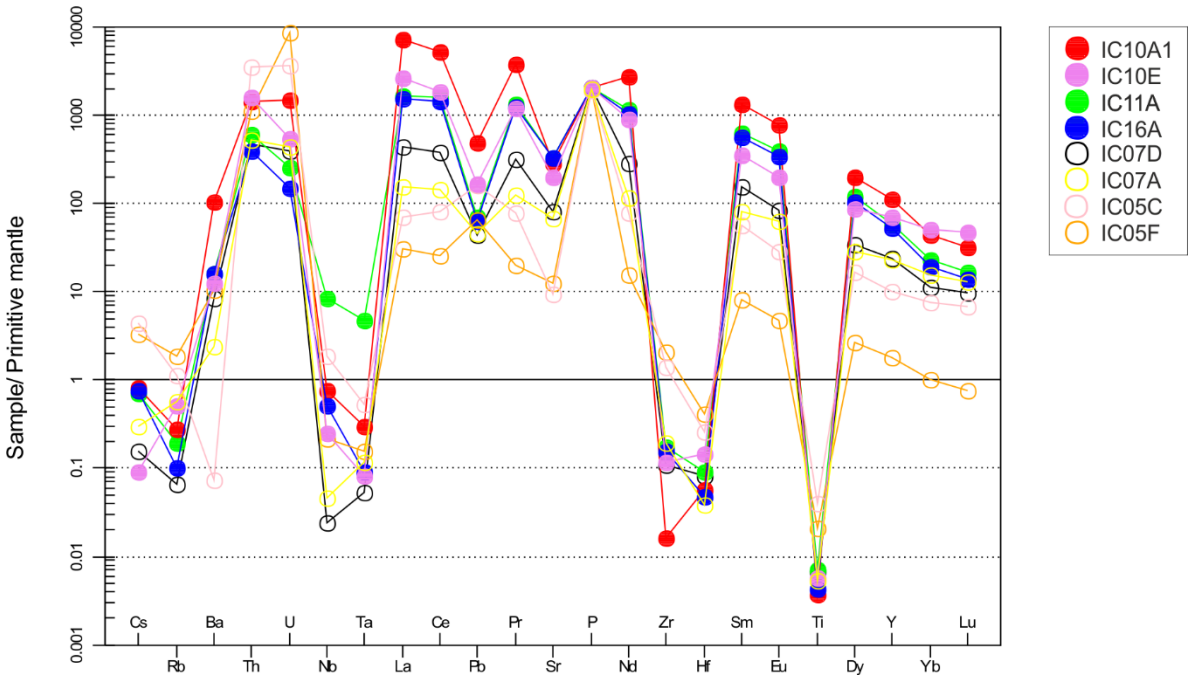

Figure 26. Extended spider plot of trace element concentrations in apatites from Samalpatti (open circles) and Sevattur (closed circles), acquired using LA-ICPMS. Primitive mantle values are from McDonough and Sun, 1995.

Calcite and dolomite also show a similar extent of depletion in HFSE (Fig. 27). It is thus clear that apatite, calcite and dolomite do not represent the major carrier for HFSE.

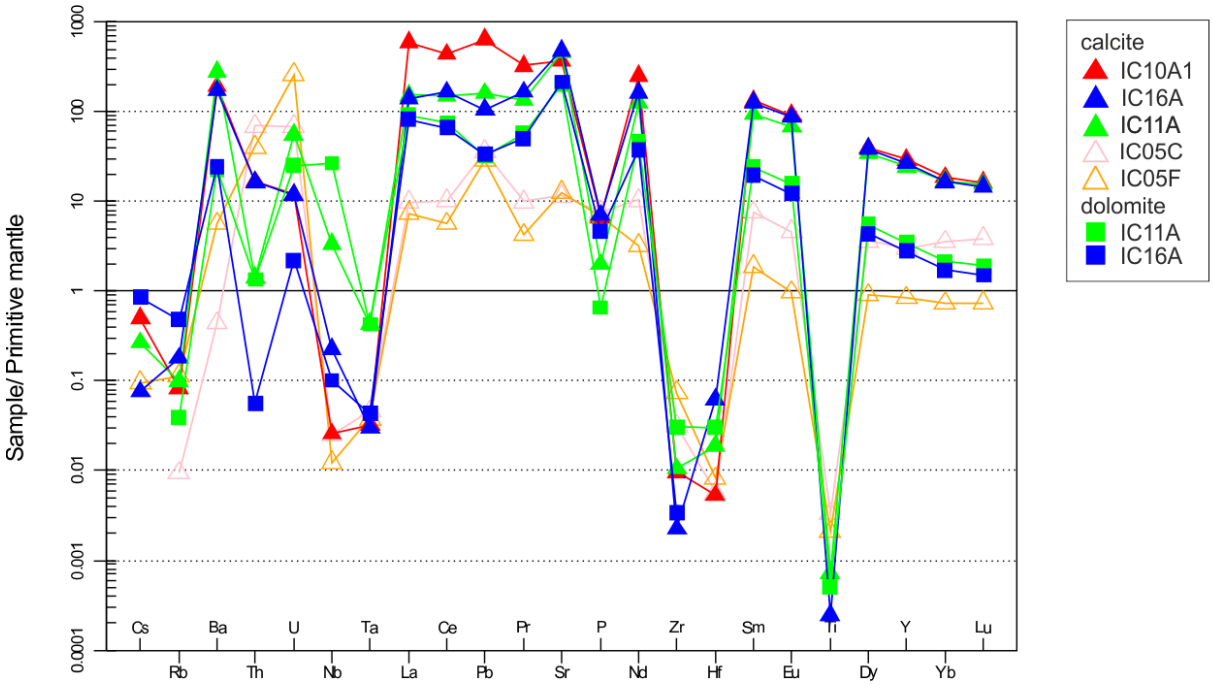

Figure 27. Extended spider plot of trace element concentrations in calcites and dolomites from Samalpatti (open symbols) and Sevattur (closed symbols), yielded using LA-ICPMS. Primitive mantle values are from McDonough and Sun, 1995.

Contrary to this, titanite shows significant enrichments in HFSE for both Samalpatti and Sevattur carbonatites. The same applies to amphibole showing significant HFSE enrichments relative to neighboring elements (Fig. 25) although the absolute level of concentrations of these elements is far below that found for titanite (Fig. 23). Compared with a compilation of HFSE data from other carbonatites (Table 15; Chakhmouradian 2006), the Tamil Nadu carbonatites do not display uniform behavior of HFSE. Combined with bulk rock data (Ackerman et al. 2017), carbonatites from Tamil Nadu are depleted in HFSE in comparison with data for carbonatites published by Chakhmouradian (2006).

Table 14. Variation in the HSFE ratios from the literature (from Chakhmouradian, 2006) in comparison with this work (whole-rock geochemical data). a,b,c,d,e stands for remote values, which differ significantly from the rest of the values in a certain rock type.

	Element ratios				Data source
	Nb/Ta	Zr/Hf	Zr/Nb	Zr/Ta	
Primitive mantle	18	37	16	284	McDonough and Sun (1995)
Alkali complexes (Kola)	17	46	3.6	63	Arzamastsev et al. (2001)
Olivine-melilite melanephelinite	18	47	2.1	39	Ivanikov et al. (1998)
Carbonatite	35	60	0.8	29	Chakhmouradian (2006)
	Nb/Ta	Zr/Hf	Zr/Nb	Zr/Ta	This work
Carbonatites Samalpatti	6-10 (100)[a]	18-26	(0.58)[b]7-17	42-114	
S-carbonatites Samalpatti	69-414	14-42	0.1-2.7	21-132(843)[c]	
Pyroxenites Samalpatti	5.6-30	18-28	4.1-37	125-208	
Carbonatites Sevattur	2.6-8.7(18)[d]	1.2-20	0.04-0.4(4.4)[e]	0.2-12	
Pyroxenites Sevattur	13-27	18-30	1-2.3	12-43	

The diverse element ratios of HFSE display a large variability among carbonatites and associated silicate rocks. The most significant variations are found for Nb/Ta where silicocarbonatites display two orders of magnitude variations and where normal carbonatites show low Nb/Ta compared with data compiled by Chakhmouradian (2006) (Table 15). It also appears that Nb/Ta correlates with Cr content (based on bulk rock geochemistry; Fig. 28), whereby in silicocarbonatites the main carrier of Cr and Nb is kosmochlor and titanite, respectively. Zirconium/Hf ratios in calciocarbonatites from Tamil Nadu are also low compared to the global average (1.2–26 versus 60), which may have consequences for their origin. This also applies to accompanying silicate rocks from Tamil Nadu (syenites, pyroxenites) which show marginally lower Zr/Hf ratios compared to alkaline rocks from elsewhere (Table 15). Nevertheless, the exact relations between individual HFSE in carbonatites and associated alkaline silicate rocks are yet unclear and will require further targeted studies. Chakhmouradian (2006) also suggested that carbonatites depleted in HFSE and enriched in Sr, Ba and LREE in comparison with the associated sillicate rocks attest to their derivation by liquid immiscibility or crystal fractionation from a common parent source. This is well displayed in Fig. 28 where carbonatites from Sevattur have the highest Sr and LREE contents of all carbonatites and pyroxenites. They are also interpreted to be the oldest rock type from the Sevattur–Samalpatti complexes (see Section 2).

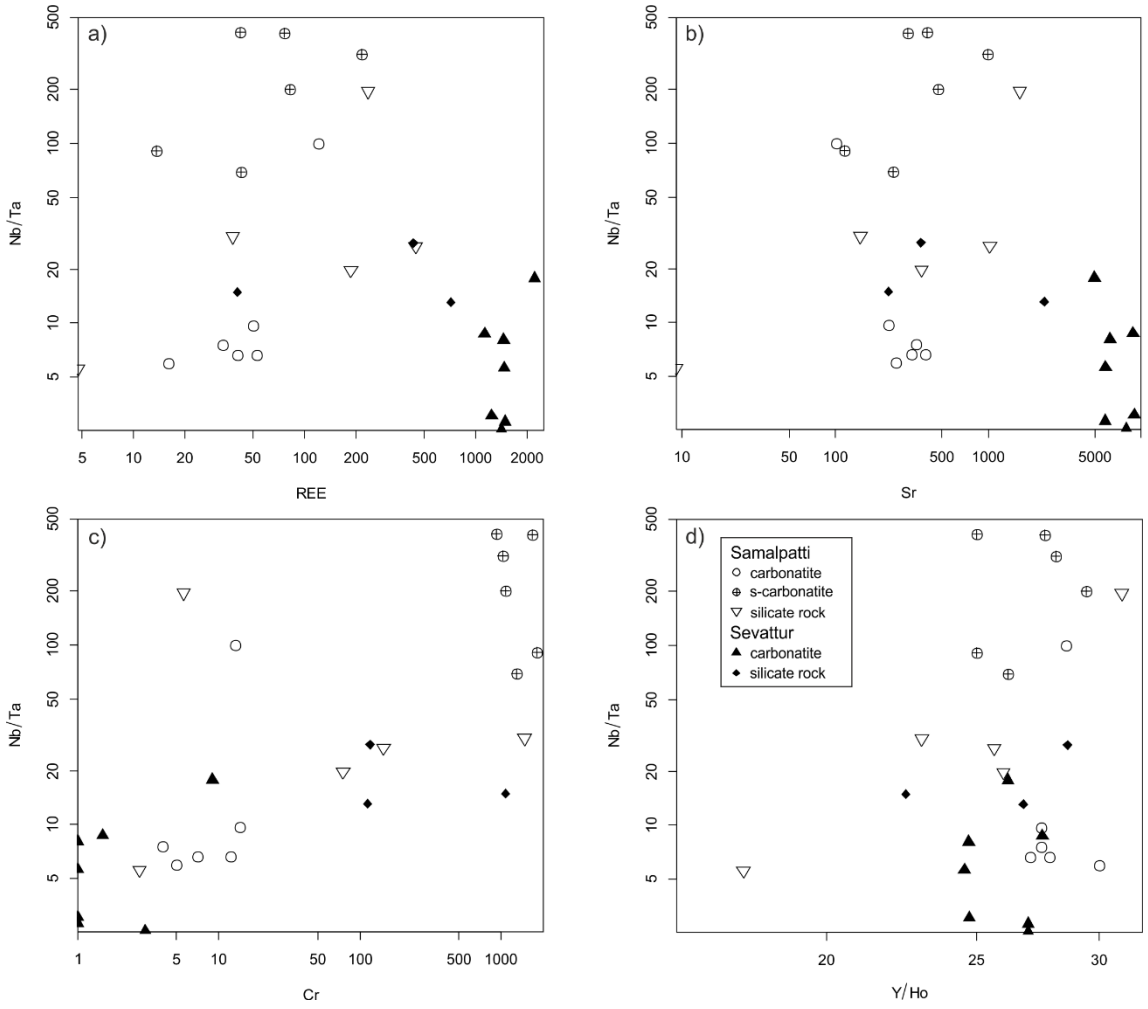

Figure 28. Whole-rock Nb/Ta ratios versus various elements.

5.1.2 The systematics of Y/Ho ratio

Ratios of elements with a similar radius and ionic charge can be an indicator of post-magmatic hydrothermal processes and deviation from the original inventory (Chakhmouradian et al. 2015). The Y/Ho ratio is a measure of decoupling between those two elements in the system and departure of Y/Ho from the chondritic value is an important indicator for hydrothermal reworking (Chakhmouradian et al. 2015). This was well documented in some hydrothermal and volatile-rich hydrothermal systems (e.g., Bühn et al. 2003; Bau and Koschinsky 2009; Chakhmouradian et al. 2013 for examples and possible driving mechanisms). One of these driving mechanisms of different partitioning behavior of Y and Ho in aqueous systems, proposed by Chakhmouradian et al. (2013), is a greater covalence of Ho relative to Y. Moreover, closed system fractionation conditions can be tested using Y/Ho ratios in the whole rock and apatite grains (Brassinnes et al., 2005). To test these alternatives, a detailed evaluation of Y and Ho data for apatite and carbonate minerals was performed.

All analyzed samples (apatite, calcites and dolomites) plot along a linear Y/Ho trend irrespective of their intrinsic lithology (carbonatites, pyroxenites, albite–epidote metasomatic rock). Apatites (Fig. 29a)

are characterized by Y/Ho = 25.6 ± 2.1 (r^2=0.987) whereas Y/Ho = 27.6 ± 1.8 (r^2=0.999) has been found for carbonates (Fig. 29b).

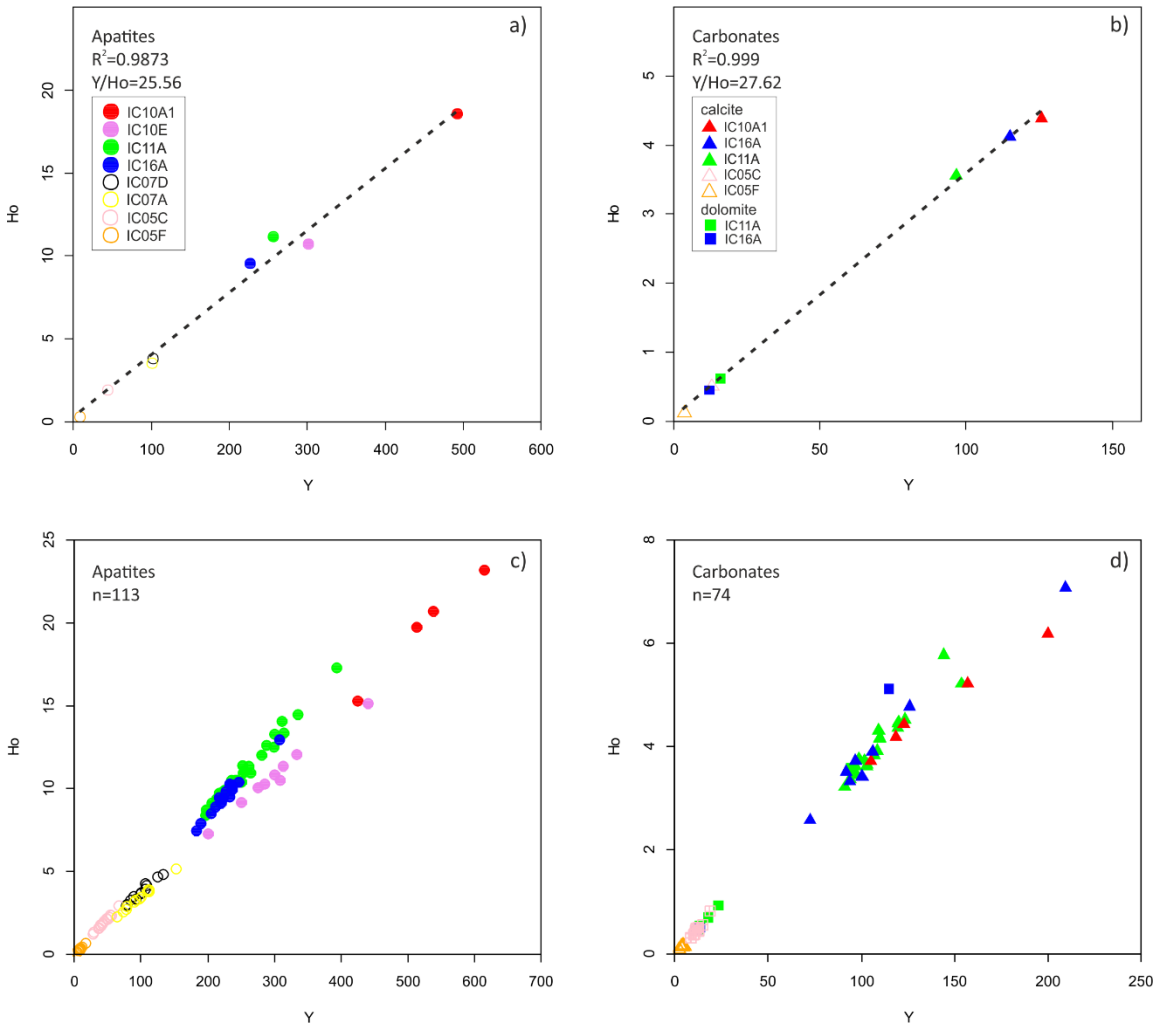

Figure 29. Y/Ho ratios in apatites (a, c) and carbonate minerals (b, d). The upper diagrams represent the average values of selected minerals from each sample, in bottom diagram all measurements are plotted. Trace element concentrations are from LA-ICPMS.

In particular, carbonate Y/Ho ratios are close to the chondritic Y/Ho = 28.8 (McDonough and Sun, 1995) whereas Y/Ho ratios in the apatites are akin to the bulk Solar System ratio (Y/Ho = 25.94), proposed by Pack et al. (2007). Subtle Y/Ho variations are observed for apatites (IC07A: 28.6; IC05C: 22.7) from Samalpatti as well as for apatites from Sevatur (IC11A: 22.9; IC10E: 28). The Y/Ho ratios range from 26.1 (IC05C) to 31.3 (IC05F) for Samalpatti calcites and from 27.1 (IC11A) to 28.6 (IC10A1) for Sevattur calcites. These values broadly overlap with Y/Ho ratios found for two analyzed Sevattur dolomites (26.5 and 25.6, respectively). It is noteworthy that the apatites from IC10A and IC16A show a deviation from this trend reaching higher Ho abundances whereas apatites from IC10E have higher Y abundances, which can be observed only when all values rather than mean values are plotted (Fig. 29c). This does not apply to carbonates since they scatter more than apatites (Fig. 29d).

It is interesting to note that the highest Y/Ho ratio = 31.3 has been measured in calcite from carbonatite IC05F and it deviates from the chondritic value (McDonough and Sun, 1995) and also from the Solar System ratio (Pack et al. 2007). This sample has a relatively primitive REE pattern (Fig. 20) and has been established to represent the primitive end member of the Samalpatti carbonatite suite (Ackerman et al. 2017). On the other hand, its C–O isotope composition attests to massive post-emplacement low-temperature modification (Ackerman et al. 2017). The preliminary K–Ar age data of Rapprich et al. (2017) show younger ages for the syenite (~560–576 Ma for Samalpatti and ~510–540 Ma for Sevattur) coexisting with carbonatite which could serve as a long-lasting heat source and could result in the enhanced levels of hydrothermal activity in both complexes.

Irrespective of the ambiguities related to hydrothermal overprint, all analyzed minerals plot along the well-defined linear trend, which can suggest that they are all cogenetic and come from the same source. Moreover, it may indicate that crystallization of apatite occurred under closed-system conditions and that Y and Ho were not fractionated during the magmatic process (Brassinnes et al., 2005). Because carbonate minerals appear to show similar Y/Ho systematics, the same conclusions also apply to carbonatites. A slight change in Y/Ho ratio could be related to the episodic fractionation of Y-rich phase such as monazite or xenotime. Infrequent monazite grains were occasionally observed in some samples which could incorporate significant amounts of Y compared with REE and Ho, by inference.

5.1.3 Hydrothermal alteration – was there any?

From petrological and mineralogical studies of carbonatites, there are no apparent field evidence for hydrothermal alteration, which would have affected the studied rocks. The sole exception is the albite–epidote metasomatic rock IC07A. From LA-ICPMS and EPMA studies it is clear that this rock underwent extensive hydrothermal alteration, which resulted in depletion of REE in apatite cores compared to rims, and formation of allanite (nominally $(Ce,Ca,Y)_2(Al,Fe^{2+},Fe^{3+})_3(SiO_4)_3(OH)$, which belongs to the epidote supergroup) on the rims of apatite grains (Fig. 30). Apatites from IC07A have trace element concentrations similar to IC07D (pyroxene), only with a marked depletion in LREE which probably is a result of remobilization of LREE and formation of allanite. From these observations IC07A could represent an extensively hydrothermally reworked pyroxenite, originally similar in composition to IC07D.

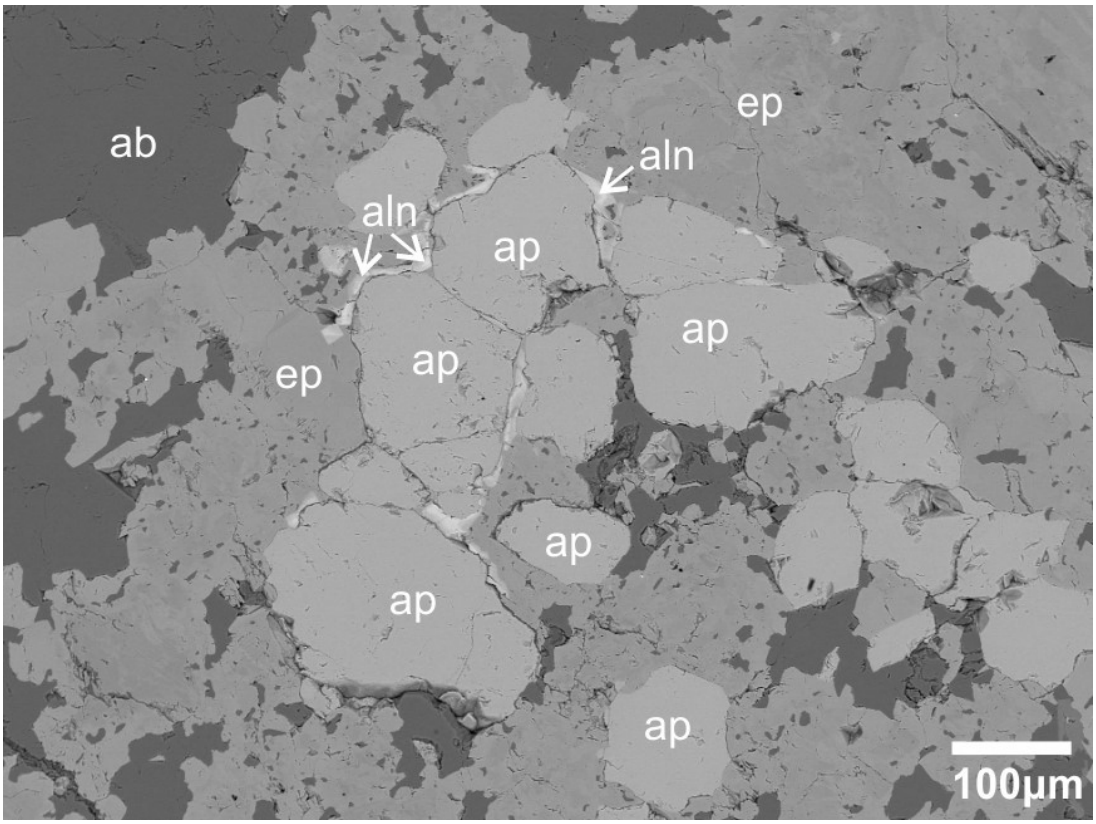

Figure 30. Photo from EPMA of sample IC07A. Abbreviations: ab – albite, aln – allanite, ap – apatite. ep – epidote.

Chakhmouradian et al. (2015) suggested that hydrothermal activity does not produce any unique geochemical fingerprint in carbonatites. Instead, it creates variable geochemical trends, from LREE and LILE enrichments (Turiy Mys, Russia) to HREE enrichment/LILE depletion (Bear Lodge, USA). There is no evidence in thin-sections that calcite or dolomite in carbonatites were hydrothermally reworked. Dolomites from Sevattur are present in the form of exsolutions in calcite but they are enriched in the same elements (i.e. Sr, Sc) as the coexisting calcite. The Y/Ho ratios show little variation in the studied calcites and dolomites (see Section 5.1.2 for more details) and are within the range deconvolved for primary calcite and dolomite at Y/Ho = 22–32 (Chakhmouradian et al. 2015). Hydrothermal alteration would shift Y/Ho ratios to higher values (e.g., 40.4±0.8 for Bear Lodge, Canada; Chakhmouradian et al. 2015). Calcites from sample IC05F have distinctive trace element concentrations and they are generally depleted in LILE and enriched in HFSE. They also have the highest mean Y/Ho = 31.2 from all studied minerals. They are also enriched in U (5.2 ppm), which is among the highest U concentrations ever reported from carbonatitic calcite (e.g., Chakhmouradian et al. 2015). These cumulative observations indicate that calcite in IC05F has been hydrothermally affected (cf. Chakhmouradian et al. 2015), consistent with recent studies (Ackerman et al. 2017; Magna et al. in prep.).

5.2 Distribution coefficients

The distribution coefficients between mineral phases and melt ($D^{mineral/melt}$) were calculated using *in situ* analyses from LA-ICPMS and EPMA. Mineral weight proportions (wt.%) based on mineral densities were calculated from the modal data obtained by TESCAN Integrated Mineral Analyzer (Ackerman et al. 2017). In order to obtain REE contents of the host carbonatite, mineral contribution to the whole-rock REE budget was subtracted from the whole-rock [whole rock (ppm) − (apatite wt.%/100 × apatite REE content (ppm)], following the approach of Brassinnes et al. (2005). The REE are compatible in apatite both in Samalpatti (IC05F) and Sevattur (IC11A, IC16A). Further, distribution coefficients for trace element partitioning between the main rock forming minerals (e.g., apatite, calcite and dolomite) were calculated in order to better understand behavior of the REE in the carbonatitic systems.

The results are listed in Table 16 and plotted in Fig. 31. The distribution coefficients for dolomite calculated here are the first such data available while the only other available data from Dawson and Hinton (2003) were calculated for the distribution of REE between dolomite and apatite or calcite. Their compatibility increases from La to Nd and then decreases steadily to Lu, which is the least compatible REE in these apatites. This produces a convex-upward distribution pattern, similar to D values published by Bühn et al. (2001), Fleet and Pan (1997), Hammouda et al. (2010), and Klemme and Dalpé (2003). The newly obtained D values for the apatite/carbonatite system are are similar to those reported by Fleet and Pan (1997), Brassinnes et al. (2005) and Dawson and Hinton (2003), while they are roughly twice as high as those reported by Chakhmouradian et al. (2017) calculated using a modified Rayleigh fractionation equation. Also, some inconsistencies appear to exist between $D^{apatite/carbonatite}$ values of the latter study compared to other studies, including this work. This is mainly apparent for HREE which do not decrease much in the study of Chakhmouradian et al. (2017). The exact nature of this diversity remains to be investigated.

The newly measured REE in calcite indicate that they are incompatible only from La to Nd, whereas they are compatible from Sm to Lu and HREE are even more compatible than in apatite (Fig. 31). This is in stark contrast to data published by Bühn et al. (2001), where REE in calcite are incompatible. The REE in dolomites appear to be incompatible in both IC11A and IC16A with a steady decrease in incompatibility from La to Lu. The incompatibility of REE in dolomite is consistent with data of Dawson and Hinton (2003), but their data produce a convex-downward pattern with the identical values for La and Lu.

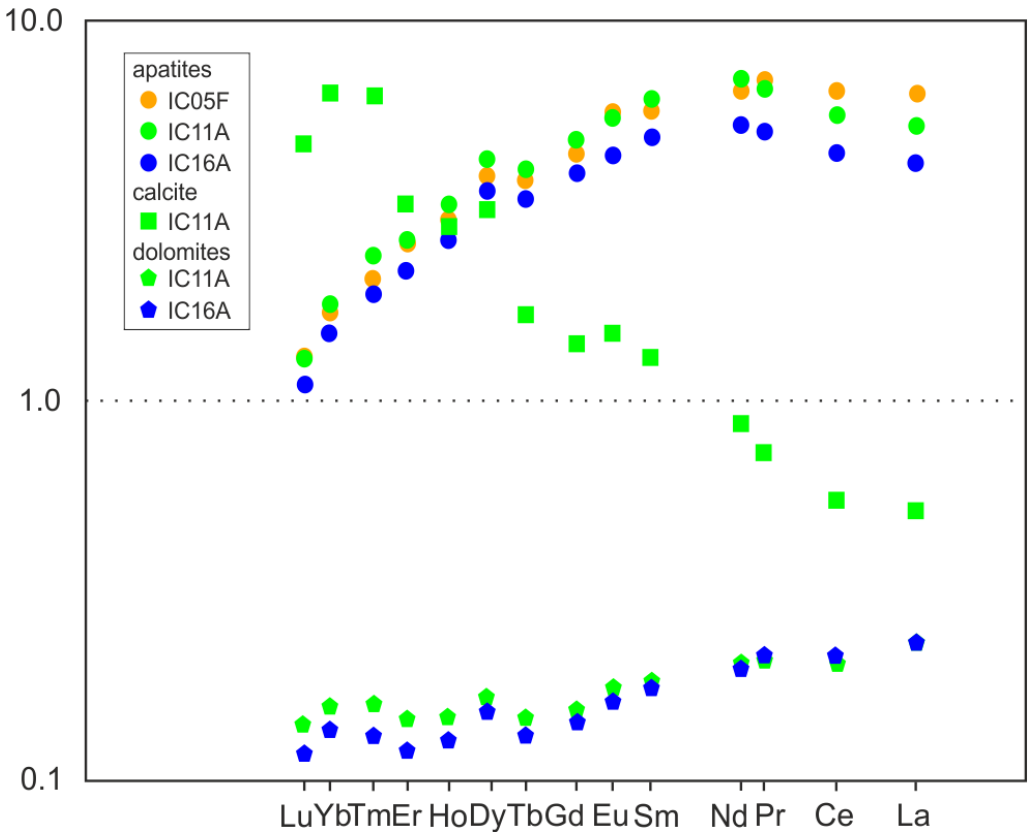

Figure 31. Calculated distribution coefficients (REE) versus cation radii (x axis) in six-fold coordination (from Shannon, 1976).

Table 15. Calculated distribution coefficients of fluorapatite, calcite and dolomite from Samalpatti (IC05F) and Sevattur (IC11A, IC16A). Abbreviations:cc – calcite, dol – dolomite, f-ap – fluorapatite.

	IC05F F-ap	IC11A F-ap	IC16A F-ap	IC11A cc	IC11A dol	IC16A dol
La	6.4	5.3	4.2	0.51	-	0.23
Ce	6.5	5.6	4.5	0.55	0.20	0.21
Pr	7.1	6.6	5.1	0.73	0.21	0.21
Nd	6.6	7.0	5.3	0.88	0.20	0.20
Sm	5.8	6.3	4.9	1.29	0.18	0.18
Eu	5.8	5.6	4.4	1.50	0.18	0.16
Gd	4.5	4.9	4.0	1.43	0.15	0.14
Tb	3.8	4.1	3.4	1.68	0.15	0.13
Dy	3.9	4.4	3.5	3.18	0.17	0.15
Ho	3.0	3.3	2.7	2.87	0.15	0.13
Er	2.6	2.7	2.2	3.31	0.14	0.12
Tm	2.1	2.4	1.9	6.38	0.16	0.13
Yb	1.7	1.8	1.5	6.50	0.16	0.14
Lu	1.3	1.3	1.1	4.76	0.14	0.12

6. CONCLUSIONS

Carbonatites are enigmatic rocks of unclear origin, which represents one of the geological "windows" into the processes occurring in the Earth's mantle. Two studied carbonatite complexes from Tamil Nadu, India Samalpatti and Sevattur display a large variability in both mineralogy and geochemistry. Carbonatites from Sevattur are mineralogically more pristine and they compose mainly from calcite, dolomite, apatite with minor magnetite. Apatite is F-rich (fluorapatite) and contains large amounts of REE. Several Sevattur carbonatites (e.g., IC10A, IC10F) contain REE-rich phase Mckelveyite-(Nd), which is mainly present in calcite in form of micron-size exsolutions. This mineral was not found in samples from Samalpatti. Carbonatites from Samalpatti are more variable than carbonatites from Sevattur; beside calcite and apatite (also F-rich), pyroxene and biotite are also present, resulting in a more variable major element composition. Another difference to Sevattur is the presence of Cr-rich silicocarbonatites containing exotic mineral kosmochlor and Nb-rich titanites, and a larger proportion of amphibole relative to calcite.

The study of selected thin-sections using LA-ICPMS was conducted in order to provide further insights into the distribution of trace elements in apatite, calcite and dolomite. Apatites and carbonate minerals from Sevattur are more enriched in Sr, Ba, REE and have lower concentrations of HFSE than apatites and calcites from Samalpatti. Most strikingly, the REE contents are up to two orders of magnitude higher in apatites and calcites from Sevattur relative to those from Samalpatti.

From the study of thin sections and trace element data in apatites, calcites and dolomites, there is no evidence for extensive hydrothermal alteration for Sevattur. Studied samples display pristine mineralogy with no zoning observed, paralleled by the unchanged ratios of elements with similar geochemical behavior, such as e.g. Y/Ho. Samples from Samalpatti show a different behavior in that they are enriched in HSFE and depleted in REE, Sr and Ba, consistent with published data. One sample (IC07A) indicates extensive post-emplacement history with exsolutions of allanite on the apatite rims, likely formed by hydrothermal activity at later stages of evolution of the complex. High Y/Ho, found for calcite in carbonatite IC05F, could also indicate hydrothermal overprint.

Distribution coefficients for REE between apatite, calcite and dolomite and carbonatite liquid were calculated on the basis of in situ analyses of minerals in carbonatites from both complexes, following the approach of Brassinnes et al. (2005). Distribution coefficients for dolomite calculated here are the first such data available (cf. $D^{dolomite/calcite}$ data of Dawson and Hinton, 2003). The data show a compatible behavior of REE in apatite with maxima found for Nd. The new D values for calcite show a systematic increase from La to Yb and transition from incompatible to compatible behavior broadly at Nd and Sm. For dolomite, bulk REE are incompatible and newly calculated values show a steady decrease from La to Lu.

7. REFERENCES

Ackerman L., Magna T., Rapprich V., Upadhyay D., Krátký O., Čejková B., Erban V., Kochergina Y.V., Hrstka T., 2017. Contrasting petrogenesis of spatially related carbonatites from Samalpatti and Sevattur, Tamil Nadu, India. *Lithos,* 284-285: 257-275.

Bau M., Koschinsky A., 2009. Oxidative scavenging of cerium on hydrous Fe oxide: evidence from the distribution of rare earth elements and yttrium between Fe oxides and Mn oxides in hydrogenetic ferromanganese crusts. *Geochem. J.,* 43:37–47

Blundy J., Dalton J., 2000. Experimental comparison of trace element partitioning between clinopyroxene and melt in carbonate and silicate systems, and implications for mantle metasomatism. *Contrib. Mineral. Petrol.,*139: 356-371.

Blundy J., Wood B., 2003. Partitioning of trace elements between crystals and melts. *Earth Planet. Sci. Lett.,* 210: 383–397.

Boynton W.V., 1984. Cosmochemistry of the rare earth elements; meteorite studies. In: *Rare earth element geochemistry*. Henderson P. (ed.), Elsevier Sci. Publ. Co., Amsterdam. 63-114.

Bragg L., Claringbull G.F., Taylor, W.H. 1965. *Crystal structures of minerals*. Bell and Sons, London.

Brassinnes S., Balaganskaya E., Demaiffe D., 2005. Magmatic evolution of the differentiated ultramafic, alkaline and carbonatite intrusion of Vuoriyarvi (Kola Peninsula, Russia). A LA-ICP-MS study of apatite, *Lithos*, 85: 76-92.

Brooker R.A., Hamilton D.L., 1990. Three-liquid immiscibility and the origin of carbonatites. *Nature,* 346: 459-462.

Brooker R.A., Kjarsgaard B.A., 2011. Silicate-carbonate liquid immiscibility and phase relations in the system SiO_2-Na_2O-Al_2O_3-CaO-CO_2 at 0.1-2.5 GPa with applications to carbonatite genesis. *J. Petrol.,* 52(7-8): 1281- 1305.

Bühn B., 2008. The role of the volatile phase for REE and Y fractionation in low-silica carbonate magmas: implications from natural carbonatites, Namibia. *Mineral. Petrol.,* 92: 453–470.

Bühn B., Schneider G., Dulski P., Rankin A.H., 2003. Fluid-rock interaction during progressive migration of carbonatitic fluids, derived from small-scale trace element and Sr, Pb isotope distribution in hydrothermal fluorite, *Geochim. Cosmochim. Acta*. 67: 4577–4595.

Bühn B., Wall F., Le Bas M.J., 2001. Rare-earth element systematics of carbonatitc fluorapatites, and their significance for carbonatite magma evolution. *Contrib. Mineral. Petrol.,* 141: 572–591.

Chakhmouradian A. R., 2006. High-field-strength elements in carbonatitic rocks: geochemistry, crystal chemistry and significance for constraining the sources of carbonatites. *Chem. Geol,* 235: 138–160.

Chakhmouradian A.R., Böhm C.O., Demény A., Reguir E.P., Hegner E., Creaser R.A., Halden N.M., Yang P. 2009. “Kimberlite” from Wekusko Lake, Manitoba: actually a diamond-indicator-bearing dolomite carbonatite. *Lithos*, 112S: 347–357.

Chakhmouradian A.R., Reguir E.P., Couëslan C., Yang P., 2015. Calcite and dolomite in intrusive carbonatites. II. Trace-element variations. *Mineral. Petrol.,* 110: 361–377 .

Chakhmouradian A.R., Reguir E.P., Zaitsev A.N., Couëslan C., Xu C., Kynicky J., Mumin A.H. & Yang P., 2017. Apatite in carbonatitic rocks: Compositional variation, zoning, element partitioning and petrogenetic significance. *Lithos,* 274-275.

Condie K.C., Allen P., 1984. Origin of Archaean charnockites from southern India. In: Kröner A., Hanson G., Goodwin A.H. (Eds.) *Archaean Geochemistry*. Springer-Verlag, Berlin, pp. 182–203.

Condie K.C., Allen P., Narayana B.L., 1982. Geochemistry of the Archean low to high grade transition zone of southern India. *Contrib. Mineral. Petrol*., 81: 157– 167.

Church A.A., Jones A.P., 1995. Silicate-Carbonate Immiscibility at Oldoinyo-Lengai. *J. Petrol.,* 36(4): 869-889.

Cullers R.L., Medaris G., 1977. Rare earth elements in carbonatite and cogenetic alkaline rocks: Examples from Seabrook Lake and Callander Bay, Ontario. *Contrib. Mineral. Petrol.,* 65(2): 143-153.

Dawson J.B., 1998. Peralkaline nephelinite-natrocarbonatite relationships at Oldoinyo Lengai, Tanzania. *J. Petrol.,* 39(11-12): 2077-2094.

Dawson J.B., Pinkerton H., Norton G.E., Pyle D.M., 1990. Physico-chemical properties of alkali-carbonatite lavas, Tanzania. *Geology,* (18):260-263.

Dawson J., Hinton R., 2003. Trace-element content and partitioning in calcite, dolomite, and apatite in carbonate, Phalaborwa, South Africa, *Min. Mag.,* 67(5): 921-930.

Dempírová L., Šikl J., Kašičková R., Zoulková V., Kříbek B., 2010. The evaluation of precision and relative error of the main components of silicate analyses in Central Laboratory of the Czech Geological Survey. *Zprávy 785 o Geol. výzkumech v roce 2009,* 27: 326–330.

Dobson D.P., Crichton W.A., Vočadlo L., Jones A.P., Wang Y.B., Uchida T., Rivers M., Sutton S.R., Brodholt J.P. 2000. In situ measurement of viscosity of liquids in the Fe-FeS system at high pressures and temperatures. *American Mineral.* 85:1838-1842.

Dobson D.P., Jones A.P., Rabe R., Sekine T., Kurita K., Taniguchi T., Kondo T., Kato T., Shimomura O., Urakawa S. 1996. In-situ measurement of viscosity and density of carbonate melts at high pressure. *Earth. Planet. Sci. Lett.,* 143(1–4), 207–215.

Eby G.N., 1975. Abundance and distribution of rare-earth elements and yttrium in the rocks and minerals of the Oka carbonatite complex, Quebec. *Geochim. Cosmochim. Acta,* 39: 597–620.

Eriksson S.C., Fourie P.J., De Jager D.H., 1985. A cumulate origin for the minerals in clinopyroxenite of the Phalaborwa Complex. *Trans. Geol. Soc. S. Afr.,* 88: 207–214.

Ernst R.E., Srivastava R.K., 2008. India's place in the Proterozoic world: constraints from the large igneous provinces (LIP) record. In: Srivastava R.K., Sivaji Ch., Chalapathi Rao N.V. (Eds.),

Indian Dykes: Geochemistry, Geophysics, and Geochronology. Narosa Publishing House Pvt. Ltd., New Delhi, India, pp. 41–56.

Fleet M.E., Pan Y., 1995. Site preference of rare earth elements in fluorapatite. *American Mineral.,* 80: 329–335.

Fleet M.E., Pan Y., 1997. Rare earth elements in apatite: uptake from H_2O-bearing phosphate fluoride melts and the role of volatile components. *Geochim. Cosmochim. Acta,* 61: 4745–4760.

Fleet M.E., Liu X., Pan Y., 2000. Site preference of rare earth elements in hydroxyapatite [$Ca_{10}(PO_4)_6(OH)_2$]. *J. Solid State Chem.,* 149: 391–398.

Freestone I.C., Hamilton D.L., 1980. The role of liquid immiscibility in the genesis of carbonatites — An experimental study, *Contrib. Mineral. Petrol.,* 73(2):105-117.

French J.E., Haeman L.M., Chacko T., Srivastava R.K., 2008. 1891-1883 Ma Southern BastarCuddapah mafic igneous events, India: a newly recognized large igneous province, *Precamb. Res.,* 160: 308-322

Frondel C., Klein Jr C., 1965. Ureyite, $NaCr_2Si_2O_6$, a new meteoritic pyroxene, *Science*, 149: 742-744.

Gittins J., 1989. The origin and evolution of carbonatite magmas. In: Bell K., (ed,) *Carbonatites: Genesis and Evolution*. Unwin Hyman, London, p 580-600.

Gittins J., Jago B.C., 1998. Differentiation of natrocarbonatite magma at Oldoinyo Lengai volcano, Tanzania. *Mineral. Mag.,* 62: 759-768.

Goldsmith J.R. 1960. Exsolution of dolomite from calcite. *J. Geol,* 68: 103-9.

Gor'kovets V.Ya., Rudashevskii N.S., Rudashevskii V.N., Popov M.G., Antonov A.V., 2013. Indicator minerals of diamond in the lamproitic diatreme, Kostomuksha region, Karelia: Interpretation from mineral and trace element compositions. *Doklady Earth Sciences*, 450: 475-478.

Grady C., 1971. Deep main faults in south India. *J. Geol. Soc. India,* 12: 56– 62.

Gwalani L.G., Rogers K.A., Demény A., Groves D.I., Ramsay R., Beard A., Downes P.J., Eves A., 2010. The Yungul carbonatite dykes associated with the epithermal fluorite deposit at Speewah, Kimberley, Australia: carbon and oxygen isotope constraints on their origin. *Mineral. Petrol.,* 98: 123–141.

Haas J.R., Shock E.L., Sassani D.C., 1995. Rare earth elements in hydrothermal systems: estimates of standard partial modal thermodynamic properties of aqueous complexes of the rare-earth elements at high pressures and temperatures. *Geochim. Cosmochim. Acta*, 59: 4329–4350.

Halama R., Vennemann T., Siebel W., Markl G., 2005. The Gronnedal-Ika carbonatite-syenite complex, South Greenland: carbonatite formation by liquid immiscibility. *J. Petrol.,* 46(1): 191-217.

Harrison T.M., Watson E.B., 1984: The behavior of apatite during crustal anatexis: Equilibrium and kinetic considerations, *Geochim. Cosmochim. Acta*. 48: 1467–1477.

Harmer R.E., Gittins J., 1998. The Case for Primary, Mantle-derived Carbonatite Magma. *J. Petrol.,* 39(11- 12): 1895-1903.

Harmer R.E., Lee C.A., Eglington B.M., 1998. A deep mantle source for carbonatite magmatism; evidence from the nephelinites and carbonatites of the Buhera district, SE Zimbabwe. *Earth. Planet. Sci. Lett.,* 158: 131-142.

Hogarth D., 1977. The pyrochlore group. *American Mineral.,* 62: 430-410.

Hogarth D.D., 1989. Pyrochlore, apatite and amphibole: distinctive minerals in carbonatite. In: Bell K., (ed.) *Carbonatites—Genesis and Evolution*. Unwin Hyman, London, p. 105–148.

Hoskin P.W.O., Kinny P.D., Wyborn D., Chappell B.W., 2000. Identifying accessory mineral saturation during differentiation in granitoid magmas: an integrated approach. *J. Petrol.*, 41: 1365–1396.

Hughes J.M., Cameron M., Crowley K.D., 1989. Structural variations in natural F, OH, and Cl apatites. *American Mineral.,* 74: 870–876.

Hughes J.M., Cameron M., Mariano A.N., 1991. Rare-earth element ordering and structural variations in natural rare-earth-bearing apatites. *American Mineral.,* 76: 1165–1173.

Janoušek V., Farrow C.M., Erban V., 2006. Interpretation of Whole-rock Geochemical Data in Igneous Geochemistry: Introducing Geochemical Data Toolkit (GCDkit). *J. Petrol.,* 47: 1255–1259.

Jochum K.P., Nohl U., Herwig K., Lammel E., Stoll B., Hofmann A.W., 2005. GeoReM: a new geochemical database for reference materials and isotopic standards. *Geostand, Geoanal. Res.,* 29: 87–133.

Jochum K.P., Weis U., Stoll,B., Kuzmin D., Yang Q., Raczek I., Jacob D.E., Stracke A., Birbaum K., Frick D.A., Günther D., Enzweiler J., 2011: Determination of Reference Values for NIST SRM 610–617 Glasses Following ISO Guidelines. *Geostand, Geoanal. Res.,* 35: 397–429.

Jones A.P., Genge M., Carmody L., 2013. Carbonatite melts and carbonatites. *Rev. Mineral. Geochem.,* 75: 289-322.

Kaminsky F., 2012. Mineralogy of the lower mantle: A review of 'super-deep' mineral inclusions in diamond. *Earth. Sci. Rev.,* 110: 127-147.

Kaminsky F., Wirth R., Schreiber A., Thomas R., 2009, Nyerereite and nahcolite inclusions in diamond: evidence for lower-mantle carbonatitic magmas. *Mineral. Mag.,* 73(5): 797-816.

Kjarsgaard B., Hamilton D.L., 1988. Liquid immiscibility and the origin of alkali-poor carbonatites, *Mineral. Mag.,* 52: 43-55.

Kjarsgaard B., Hamilton D.L., 1989. The genesis of carbonatites by immiscibility. In: Bell K. (ed.) *Carbonatites—Genesis and Evolution*. Unwin Hyman, London, p. 388-404.

Kjarsgaard B., Peterson T., 1991. Nephelinite-carbonatite liquid immiscibility at Shombole volcano, East Africa: Petrographic and experimental evidence. *Mineral. Petrol.,* 43(4): 293-314.

Klemme S., Dalpe C., 2003. Trace element partitioning between apatite and carbonatite melt. *American Mineral.,* 88: 639-646.

Klemme S., Vanderlaan S.R., Foley S.F., Gunther D., 1995. Experimentally Determined Trace and Minor Element Partitioning between Clinopyroxene and Carbonatite Melt under Upper-Mantle Conditions. *Earth Planet. Sci. Lett.,* 133(3-4): 439-448.

Krafft M., Keller J., 1989. Temperature measurements in carbonatite lava lakes and flows from Oldoinyo Lengai, Tanzania. *Science,* 245(4914): 168-170.

Le Bas M.J., 1987. Nephelinites and carbonatites. *Geol. Soc. London Special Pub.,* 30(1): 53-83.

Le Bas M.J., 1989. Diversification of carbonatite. In: Bell K. (Ed.) *Carbonatites: Genesis and Evolution*. Unwin Hyman, London, pp. 428– 445.

Le Bas M.J., Handley C., 1979. Variation in apatite composition in ijolitic and carbonatitic igneous rocks. *Nature,* 279: 54– 56.

Le Maitre R.W., 2002. *Igneous Rocks: A Classification and Glossary of Terms.* Cambridge University Press, Cambridge, UK.

Lee W.J., Wyllie P.J., 1997. Liquid immiscibility between nephelinite and carbonatite from 1.0 to 2.5 GPa compared with mantle melt compositions. *Contrib. Mineral. Petrol.,* 127(1):1-16.

Long K.R., Van Gosen B.S., Foley N.K., Cordier D., 2010. The principal rare earth elements deposits of the United States—A summary of domestic deposits and a global perspective: U.S. Geological Survey Scientific Investigations Report, *2010 - 5220*, 96 p

Mackie P.E., Young R.A., 1973. Location of Nd dopant in fluorapatite, $Ca_5(PO_4)_3F$:Nd. *J. Appl. Crystallogr.,* 6: 26–31.

Masaki Y., Yuka H., Naoko N., Hirogo K., 2005. Rb-Sr, Sm-Nd ages of the Phalaborwa Carbonatite Complex, South Africa, *Polar. Geosci.,* 18: 101-113.

McDonough W. F., and Sun S.- s., 1995. " The composition of the Earth", *Chem. Geol.,* 120: 223–253.

Migdisov A.A., Williams-Jones A.E., Normand C., Wood S.A., 2008. A spectrophotometric study of samarium (III) speciation in chloride solutions at elevated temperatures. *Geochim. Cosmochim. Acta*, 72: 1611–1625.

Moralev V.M., Voronovski S.N., Borodin L.S., 1975. New findings about the age of carbonatites and syenites from southern India. *USSR Acad. Sci.* 222: 46–48.

Morogan V., 1989. Mass transfer and REE mobility during fenitization at Alnö, Sweden. *Contrib. Mineral. Petrol.,* 103: 25–34.

Mysen B.O., 1983. The structure of silicate melts. *Annu. Rev. Earth. Planet. Sci.,* 11(1): 75-97.

Nelson D.R., Chivas A.R., Chappell B.W., McCulloch M.T., 1988. Geochemical and isotopic systematics in carbonatites and implications for the evolution of ocean-island sources. *Geochim. Cosmochim. Acta,* 52: 1- 17.

Norman M.D., Pearson N.J., Sharma A., Griffin W.L., 1996. Quantitative analysis of trace elements in geological materials by laser ablation ICPMS: instrumental operating conditions and calibration values of NIST glasses. *Geostand. Newsl.,* 20(2): 247–261.

Oppenheimer C., 1998. Satellite observation of active carbonatite volcanism at Ol Doinyo Lengai, Tanzania. *Int. J. Remote Sensing,* 19(1): 55-64.

Pack A., Russell S.S., Shelley J.M.G., van Zuilen M., 2007. Geo- and cosmochemistry of the twin elements yttrium and holmium. *Geochim. Cosmochim. Acta,* 71: 4592-4608.

Pandit M.K., Sial A.N., Sukumaran G.B., Pimentael A.K., Ramasamy A.K., Ferreira V.P., 2002. Depleted and enriched mantle sources for Palaeo- and Neoproterozoic carbonatites of southern India: Sr, Nd, C-0 isotopic and geochemical constraints. *Chem. Geol.,* 189: 69-89.

Patchett J.P., Kuovo O., Hedge C.E., Tatsumoto M., 1982. Evolution of continental crust and mantle heterogeneity: Evidence from Hf isotopes. *Contrib. Mineral. Petrol.,* 78(3): 279-297.

Peucat J.J., Mahabaleshwar B., Jayananda,M., 1993. Age of younger tonalitic magmatism and granulitic metamorphism in the south Indian transition zone (Krishnagiri area): comparison with old Peninsular gneisses from the Gorur– Hassan area. *J. Metamorph. Geol.,* 11: 879– 888.

Puustinen K., 1972. Richterite and actinolite from the Siilinjarvi carbonatite complex, Finland. *Bull. Geol. Soc. Finland.,* 44: 83-86.

Qing H., Mountjoy E.W., 1994. Formation of coarsely crystalline, hydrothermal dolomite reservoirs in the Presqu'ile Barrier, Western Canada Sedimentary Basin. *AAPG Bulletin,* 78(1): 55-77.

Rapprich V., Pécskay Z., Magna T, Míková J., (2017). Age disparity for spatially related Sevattur and Samalpatti carbonatite complexes. Abstract in *Goldschmidt2017*.

Rosenthal A., Yaxley G.M., Green D.H., Hermann J., Kovacs I., Spandler C. 2014. Continuous eclogite melting and variable refertilisation in upwelling heterogeneous mantle. *Sci. Rep.,* 4

Rudnick R.L., and Gao S., 2003. Composition of the Continental Crust. In: Holland H.D., Turekian, K.K. (ed.) *Treatise on Geochemistry*. 3rd ed., Elsevier, Amsterdam, 1-64.

Schleicher H., Kramm U., Pernicka E., Schidlowski M., Schmidt F., Subramanian V., Todt W., Viladkar S., 1998. Enriched subcontinental upper mantle beneath southern India: evidence from Pb, Nd, Sr and C–O isotopic studies on Tamil Nadu carbonatites. *J. Petrol.,* 39: 1765–1785.

Shannon R.D., 1976. Revised effective ionic radii and systematic studies of inter atomic distances in halides and chalcogenides. *Acta Crystal.,* 32: 751–767.

Stoppa F., Jones A., Sharygin V., 2009. Nyerereite from carbonatite rocks at Vulture volcano: implications for mantle metasomatism and petrogenesis of alkali carbonate melts. *Cent. Euro. J. Geosci.,* 1(2): 131-151.

Streckeisen A., 1980. Classification and nomenclature of volcanic rocks, lamprophyres, carbonatites and melilitic rocks. IUGS Subcomission on the Systematics of Igneous Rocks. *Geol. Rundsch.,* 69: 194-207.

Subramanian V., Viladkar S.G., Upendran R., 1978. Carbonatite alkali complex of Samalpatti, Dharmapuri district, Tamil Nadu. *J. Geol. Soc. India*, 19: 206–216.

Sweeney R.J., 1994. Carbonatite melt compositions in the Earth's mantle. *Earth. Planet. Sci. Lett.,* 128(3-4): 259-270.

Treiman A.H., Schedl A. 1983. Properties of carbonatite magma and processes in carbonatite magma chambers. *J. Geol.,* 91(4): 437-447.

Veizer J., Bell K., Jansen S.L., 1992. Temporal distribution of carbonatites. *Geology,* 20: 1147-1149.

Verplanck P.L., Van Gosen B.S., Seal R.R, McCafferty, A.E., 2014. A deposit model for carbonatite and peralkaline intrusion-related rare earth element deposits: U.S. Geological Survey Scientific Investigations Report. *2010–5070-J*, 58 p,

Viladkar S.G., Bismayer U., 2014. U-rich pyrochlore from Sevathur carbonatites, Tamil Nadu. *J. Geol. Soc. India,* 83: 147-154.

Wall F., Zaitsev A.N., 2004. Rare earth minerals in Kola carbonatites. In: Wall F., Zaitsev A.N. (ed..) *Phoscorites and Carbonatites from Mantle to Mine: the Key Example of the Kola Alkaline Province.* Volume. 10. Mineralogical Society Series. Mineralogical Society London, pp. 341–373.

Wallace M.E., Green D.H., 1988. An experimental determination of primary carbonatite magma composition. *Nature,* 335: 343-346.

Watson E.B., Green T.H., 1981, Apatite/liquid partition coefficients for the rare-earth elements and strontium. *Earth Planet. Sci. Lett.,*56: 405– 421.

Williams-Jones A.E., Samson I.M., Olivo G.R., 2000. The genesis of hydrothermal fluorite-REE deposits in the Gallinas Mountains, New Mexico. *Econ. Geol.,* 95: 327–342.

Wolff J.A., 1994. Physical properties of carbonatite magmas inferred from molten salt data, and application to extraction patterns from carbonatite–silicate magma chambers. *Geol. Mag.,* 131: 145–153.

Wood S.A., 1990. The aqueous geochemistry of the rare-earth elements and yttrium, 1. Review of available low-temperature data for inorganic complexes and the inorganic REE speciation of nature waters. *Chem. Geol.,* 82: 159–186.

Woolley A.R., Church A.A., 2005. Extrusive carbonatites: A brief review. *Lithos,* 85(1-4): 1-14.

Woolley A.R., Kjarsgaard B.A., 2008. *Carbonatite occurrences of the world: map and database*. Geological Survey of Canada Open File # 5796, 28 p

Yi-Nok N.G., Guang-Hai S.H.I., Santosh M., 2016. Titanite-bearing omphacitite from the Jade Tract, Myanmar: Interpretation from mineral and trace element compositions. *J. Asian Earth Sci.,* 117: 1-12.

Ying J., Zhou X., Zhang H., 2004. Geochemical and isotopic investigation of the Laiwu–Zibo carbonatites from western Shandong Province, China, and implications for their petrogenesis and enriched mantle source. *Lithos,* 75(3-4): 413-426.

Internet

https://en.wikipedia.org/wiki/Rare_earth_element, 3. 5. 2017